ANKARA UNIVERSITY
GRADUATE SCHOOL OF NATURAL AND APPLIED SCIENCES

MASTER'S THESIS

INVESTIGATION OF THE CORROSION BEHAVIOR OF METAL ELECTRODES USED IN MICROBIAL FUEL CELL FOR GREEN ENERGY PRODUCTION

Mohammed Khamees Fayyadh ALALWANI

DEPARTMENT OF ENERGY ENGINEERING

ANKARA
2022

ÖZET

Yüksek Lisans Tezi

YEŞİL ENERJİ ÜRETİMİ İÇİN MİKROBİYAL YAKIT HÜCRESİNDE KULLANILAN METAL ELEKTROTLARIN KOROZYON DAVRANIŞLARININ İNCELENMESİ

Mohammed Khamees Fayyadh ALALWANI

Ankara Üniversitesi
Fen Bilimleri Enstitüsü
Enerji Mühendisliği Anabilim Dalı

Danışman: Doç. Dr. Özcan KÖYSÜREN

Elektrot malzemesi, mikrobiyal yakıt hücrelerinde (MFC'ler) üretilen elektrik miktarında önemli bir rol oynar. MFC'lerde kullanılan metal elektrotlar, hücre veriminin düşmesine yol açan biyolojik korozyona ve konsantrasyon hücresi korozyonuna maruz kalır. Bu çalışmada, seçilen üç elektrot malzemesinin, paslanmaz çelik, bakır ve çinkonun farklı çalışma koşulları altındaki korozyon davranışı araştırılmış ve tartışılmıştır. Bu çalışmada saccharomyces cerevisiae, mikroorganizma (MO) olarak ve sodyum asetat ise substrat olarak anot bölümüne eklenmiştir. MO konsantrasyonu, katot bölümünün havalandırılması ve katot bölümündeki akış hızı gibi farklı çalışma parametrelerinin bu elektrotların korozyon hızı (CR) üzerindeki etkisi incelenmiştir. Elektrotların korozyon davranışını ve üretilen akımın davranışını anlamak için elektrotun potansiyeli farklı koşullar için ölçülmüştür. Hem anot bölmesinde hem de katot bölmesinde elektrotların en yüksek CR'sinin anot bölmesinde artan MO konsantrasyonu ile arttığı tespit edildi. Paslanmaz çelik, araştırılan tüm çalışma parametreleri aralığı için en düşük korozyon oranını sergiledi ve ardından bakır geldi. İncelenen tüm koşullarda korozyon hızının çok yüksek olması ve üretilen akımın çoğunun korozyondan kaynaklanması nedeniyle çinko elektrotun MFC'de elektrot olarak zayıf olduğu tespit edildi. Ek olarak, bu çalışma, su bölmesindeki hava pompalaması ve çalkalamanın, üretilen akımda ve her iki bölmedeki elektrotların CR'sinde kayda değer bir artışa neden olduğunu göstermiştir.

Mayıs 2022, 91 sayfa

Anahtar Kelimeler: MFC (Mikrobiyal yakıt hücresi), elektrot malzemesi, korozyon, anaerobik mikroorganizma, akış hızı, havalandırma

ABSTRACT

Master‘s Thesis

INVESTIGATION OF THE CORROSION BEHAVIOR OF METAL ELECTRODES USED IN MICROBIAL FUEL CELL FOR GREEN ENERGY PRODUCTION

Mohammed Khamees Fayyadh ALALWANI

Ankara University
The Graduate School of Natural and Applied Sciences
Department of Energy Engineering

Supervisor: Assoc. Prof. Dr. Özcan KÖYSÜREN

The electrodes material plays an important role in the amount of electricity produced in microbial fuel cells (MFCs). Metal electrodes used in MFCs are subject to biological corrosion and concentration cell corrosion which leads to decrease the efficiency of the cell. In the present work, the corrosion behavior of three selected electrode materials, stainless steel, copper, and zinc under different operating conditions was investigated and discussed. The microorganism (MO) used in this study was Saccharomyces cerevisiae in the anode chamber with sodium acetate as a substrate. The effect of different operating parameters on the corrosion rate (CR) of these electrodes were studied such as: MO concentration, aeration of cathode chamber, and flow velocity in cathode chamber. The potential of the electrode was measured for different conditions to understand the corrosion behavior of electrodes and the behavior of produced current. It was found that the highest CR of the electrodes in both anode compartment and cathode compartment increases with increasing MO concentration in anode compartment. The stainless steel exhibited the lowest corrosion rate for the whole investigated range of operating parameters followed by copper. The zinc electrode was found to be poor as an electrode in MFC as its corrosion rate was very high in all conditions investigated and most of the produced current is due to the corrosion. In addition, this study showed that the air pumping and agitation in water compartment causes an appreciable increase in the produced current and in the CR of the electrodes in both compartments.

May 2022, 91 pages

Keywords: MFC (Microbial fuel cell), electrode material, corrosion, microorganism, agitation velocity, aeration

ACKNOWLEDGEMENTS

I would like to acknowledge and give my warmest thanks to my supervisor Dr. Özcan KÖYSÜREN who made this work possible. His guidance and full trust during the research work and the writing of the thesis. I'm so grateful you were my supervisor.

I would like to thank the Energy Engineering Department staff /Ankara University for providing me with the Graduate Assistantship throughout my graduate studies

Special thanks to Iraq ministry of Environment, Dr. Jassim Al Falahi and my colleagues in the ministry. Because you are partners of success, partners of achievement.

I am grateful to you Dr. Basim O. Hasan for the time and effort you spent with me.

I express my deep love and sincere appreciation to my family, in particular dearest to my heart my mother, and wife, for their helping and supporting during the long research period. I am really lucky to have such a family. This work is dedicated to them.

I am thankful as well to all my friends, especially my best friends Cevat, Gökhan, Büşra and Fatima, whose gave me so much hope, support, and advice

Mohammed Khamees Fayyadh ALALWANI
Ankara, May 2022

LIST OF CONTENTS

NOTATIONS AND ABBREVIATIONS

A	Area
C	Concentration of microorganisms
CR	Corrosion rate
E	Electrode potential
g/l	grams per liter
gmd	Corrosion rate unit $g/m^2.day$
h	Mass transfer coefficient
I	Current density
J	Mass flux
N	Agitation speeds
T	Temperature
T	Time

Abbreviations

AC	Activated Carbon
AEM	Atomic Exchange Membrane
bulk	Bulk solution region
CEM	Cations Exchange Membrane
CE	Current efficiency
COD	Chemical Oxygen Demand
Cu	Copper
DCMFC	Double Chamber Microbial Fuel Cell
DO	Dissolved Oxygen
GAS	Granular Activated Carbon
GFB	Reticulated vitreous carbon
GG	Guar Gum
GR	Graphite
RVC	Graphene Bioelectronics
Mass	Mass transfer
MO	Microorganisms
O2	Oxygen
SCMFC	Single-chambered microbial fuel cell
SS	Stainless Steel
ww	West water
Zn	Zinc
o	Equilibrium state

LIST OF TABLES

LIST OF FIGURES

1. INTRODUCTION

Household and commercial energy consumption has increased as the global population develops. Roughly, 80 percent of world energy supplies depend on current situations. Non-renewable fossil fuels are easily exhausting. Crude oil, natural gas and liquid fuel reserves were estimated to last 60, 120, and 60 years, respectively, at current consumption rates (Buyanov et al. 2011). Another problem with fossil fuel consumption is greenhouse gas emissions (GHGs). Microbial fuel cells (MFCs) have recently been intensively researched in many academic laboratories as a potential bioenergy production technology from organic carbon sources such as wastewater, sludge and others (Zhou et al. 2014, Rhoads et al. 2005). The MFCs convert the energy stored in the chemical structures of organic materials into electrical energy through the catalyst electrically active bacteria reactions (biocatalysis). MFCs generate bioelectricity directly in the process of degrading organic matter in wastewater instead of a biofuel (Zhou 2014, Rahimnejad 2015, Logan and Regan 2006). The performance of MFC is depending on the electrode materials, electrode potential, microorganism concentration and substrate concentration. These factors influence the microbial metabolism, and thus the formation and composition of biofilms. Microbial biofilms use a number of electron exchange pathways to create electrochemical interactions with metal surfaces. Direct mechanisms involve adsorbed bio compounds enzymes, which catalyze the cathodic reduction of oxygen for aerobic biocorrosion or the proton/water reduction in anaerobic processes (Bergel et al. 2005). Microscopic organisms serve as catalysts in MFCs, turning chemical energy into electrical energy effectively through biological electrochemical reactions (Deval et al. 2017). According to Jack et al. (1992), microorganisms were accountable for 34% of localized corrosion at an oil company. In the 1950s, it was estimated that the yearly cost of microorganism influence corrosion (MIC)-related material properties repair and upkeep in different kinds of delivery in the United States would be around $0.5-2 billion. Booth (1964) estimated that MIC was accountable for 50% of pipe corrosive environment in the United Kingdom. Microbial impacts are thought to be responsible for roughly 20% of all corrosive environment to metallic surfaces.

Microorganism influence corrosion (MIC) is the result of a microbiologically induced change that promotes the formation or preservation of physiochemical interactions that would not normally occur under essentially similar circumstances. It is important to remember that in essence, these microorganisms' procedures need not act in solitude, but instead in live show with electrochemistry forces inside the particular setting. The metal degradation is recognized as biocorrosion, or microbially-influenced corrosion (Little and Wanger 1994, Usher 2014). Southern Africa's national electricity company has identified MIC of steel material in coolant rivers and streams in virtually most of its power plants, supplying 90% of the total electricity generation.

The electrodes material has a significant impact on the electrochemical performance of MFCs. As a result, electrode testing is crucial in this industry. The fundamental and particular characteristics of MFC electrodes materials are numerous. Electrochemical solid terminal materials ought to have high reactivity, biocompatibility, chemical stability, dimensional stability, and also safely effective or caustic in particular (Mashkour and Rahimnejad 2015). Metal electrodes are widely investigated to serve as electrodes in MFC (Hamed et al. 2020, Nurettin 2017). Despite the several advantages of metal electrode such as high electrical conductivity, high mechanical properties, availability and cost-effective prices, the important limitation is the corrosion. The formation biofilm and the formed compounds due to the bacterial activity affects the electric current generated and the corrosion rate of metal electrode in MFCs.

The microbial fuel cell (MFC) is mainly a concentration cell in which a part of the current produced between the two terminals of the same electrode material is due to the potential difference and may be due to the corrosion. Despite the use of same electrode material in the two compartments of MFC, a potential difference arises due to the establishment of concentration cell effect. The corrosion in concentration cells has been investigated by several author such as Ali and Hasan (2020), and Ahmad (2006).

In MFC, the presence of microorganism and substrate and the produced compounds due to bacterial activity increases the concentration cell effect which leads to increase the

current produced. The potential difference between the two terminals may cause an enhanced corrosion of the electrode in the compartment of high potential that leads to decrease the MFC efficiency. The rate of corrosion of the electrode is dependent also on the electrochemical properties of that electrode.

Amongst all metals, stainless steel, copper and zinc have been recently proposed as a suggested electrode for MFC operation. In fact, most studies used these materials does not pay enough attention to the corrosion problem of such metals in MFC environment in both compartments. The conditions in both compartments are different and can becomes considerably corrosive due to the formation of corrosive compounds in anode compartment and due to the aeration and flow in cathode compartment to increase the cell efficiency. The electrical connection between the two electrodes in MFC causes the corrosion phenomena to become more complicated due to mutual effect of electrode on each other. Although the corrosion phenomenon in MFC has a significant effect, studies concerning this issue are limited in literature. Most of the literature focuses on the maximization of the produced current without evaluation of the consequences on the electrode corrosion often. Some studies used two different materials as electrode in MFC without evaluation of the galvanic effect that is responsible about the production of important part of the cell current. Accordingly, studying the corrosion behavior of the commonly used metals electrode in microbial fuel cell under different operating conditions is of a scientific and practical significance for recommending the successful metals for this application.

1.1 Objectives of the Study

The major objectives of this work are:

1- Studying the corrosion behavior of some selected metals that are used as electrode material in MFC; which are stainless steel, copper, and zinc.
2- Studying the effect of different operating parameters such as the microorganism concentration in anode compartment, aeration in cathode, and flow velocity on the corrosion rate and on the MFC current of these metals.

2. LITERATURE SURVEY

2.1 The Concept of a Microbial Fuel Fell (MFC):

The MFC is one of the most promising technologies for producing biological energy (Drapcho et al. 2008, Zhang et al. 2019). MFCs have become one of the most prominent technologies for generating clean green energy in current history (Mohan and Chandrasekhar 2011, Pant et al. 2012). MFC, which utilizes organic and inorganic waste to create power, is one of the environmentally friendly technologies that has expanded gradually over the previous few decades (Mohan et al. 2014). A MFC is a bio-electrochemical reactor containing microorganisms that create energy by oxidizing organic or inorganic molecules (Logan 2006, Mook 2012).

Microbial fuel cells use an extremely active catalytic process to transform the stored energy in the molecular structure or organic compounds into electrical energy (biocatalysis). MFCs are a form of biofuel cell made up of solutions, electrode, biofuels, biomaterials and other things. Microbial fuel cells also employ proton-conducting membranes (or salt bridges). In microbial fuel cells, inert electrochemical solid terminals such as graphite, carbon compounds and platinum are typically utilized (Çek 2016). MFC generates electricity using bacteria's metabolic energy, acting as a bioprocess for the organic oxidation and inorganic compounds as well as the creation of electrons and protons. Figure 2.1 depicts a typical MFC in its simplest form. The reactions (Eq. 2.1-2.3) are presented with acetic acid as the anode substrates and oxygen (O_2) as the terminal electron for the cathode (Kalia and Kumar 2017).

$$\text{Anodic reaction : } CH_3COOH + H_2O \rightarrow 2CO_2 + 8H^+ + 8e^- \quad (2.1)$$

$$\text{Cathodic reaction : } 8H^+ + 8e^- + 2O_2 \rightarrow 4H_2O \quad (2.2)$$

$$\text{Overall reaction : } CH_3COOH + 2O_2 \rightarrow 2H_2O + 2CO_2 \quad (2.3)$$

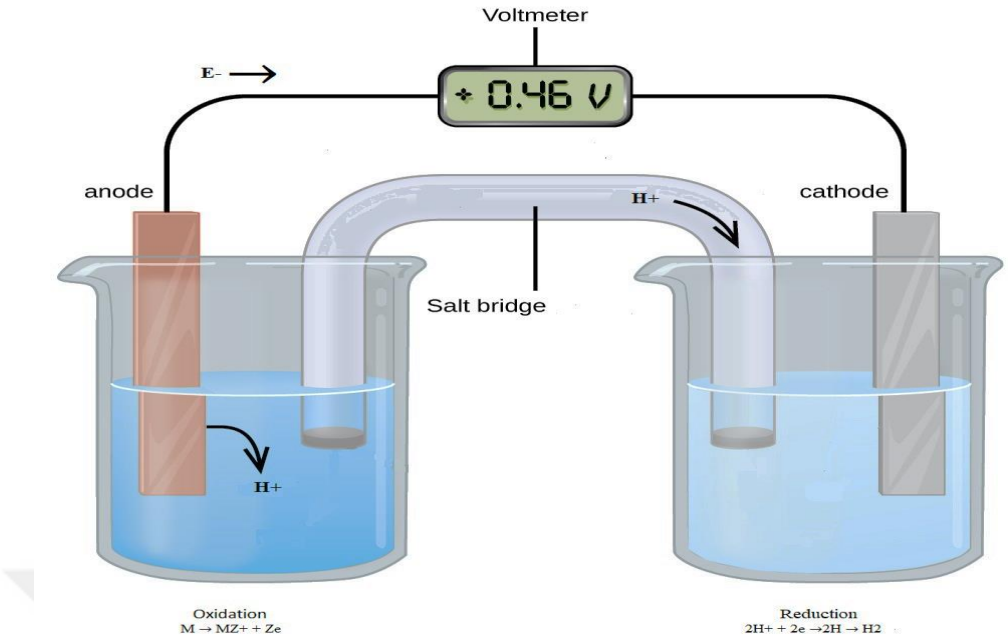

Figure 2.1 The layout of a simple MFC (Gerdon 2020)

In the anode compartment (anode reaction), microorganism respiration oxidizes the acetate substrate to carbon dioxide, releasing protons and electrons (Equation 2.1). During this reaction, electron intermediates are generated. It is then sent to the cathode compartment via an external integrated circuit. Kim et al. (2007) analyzed that each transferred electron is the result of the corresponding protons passing through the proton permeable membrane and difusde into the cathode compartment, maintaining the charge neutrality of the cathode compartment. The electrons are known to be a useful product from the oxidation reaction at the anode compartment, which travels through the conductors to the cathode compartment and forms water at the cathode electrode. Also, as shown in the formula, protons react with electrons and oxygen to form water molecules (cathodic reaction) (Equation 2.2). These protons travel to the cathode chamber through the membranes connected to both the cathode and anode chambers. Membranes allow protons (H^+) to pass through, but at the same time do not allow electrons to pass through. Therefore, the presence of oxygen in the cathodic reaction is important for the completion of the reaction. Interestingly, the flow of electrons from the positive electrode to the negative electrode through an external circuit is involved in the generation of energy.

2.2 Basic Concept of Bio-Catalytic Energy Production and the Mechanisms of Electron Transfer

Energy-rich molecules, such as glucose, are metabolized by living cells, and energy is gained through following oxidation and reduction reactions (Eq. 2.4 and 2.5). To assist to metabolize the substrate, enzymes in the cell minimize the activation energy (Christgen et al. 2011).

$$C_6H_{12}O_6 + 6H_2O \rightarrow 6CO_2 + 24H^+ + 24e^- \qquad E_0 = 0.014 \quad V\ (SHE) \qquad (2.4)$$

$$6O_2 + 24H^+ + 24e^- \rightarrow 12H_2O \qquad E_0 = 1.23 \quad V\ (SHE) \qquad (2.5)$$

Logan and Regan (2006) stated that microorganisms can produce electrons by three methods:

I. Exogenous mediators (those that are produced outside of the cell) include small amounts of potassium to work properly, thionine's and neutral red.

II. Adopting bacteria's own mediators

III. Electron transfer directly from respiration enzymes (cytochromes) to the electrodes. Microorganisms are used to generate power in MFCs.

MFCs generate electric power by the use of microbes. Organisms that transmit electrons to the anodic electrode are called electrode-reduction microorganisms. While the micro-organism oxidizes organic materials or substrate into CO_2. The organisms can transfer electrons through a mediator particle in the electrolyte, directly through enzymes in their outer membrane, or through external circuit or pili that coat the outer surface of the bacterium (Clark and Pazdernik 2009).

Figure 2.2 reveals the microbial fuel cell theory, direct electron transfer and then nanowire structure from a bacterium to a working electrode. Electron paths from bacteria to the positive electrode have been posited as conduction (direct) or facilitation (Figure 2.2) (Torres et al. 2010). Like recommended in chemical methods, mediators are produced by the microbial community (Rahimnejad et al. 2015). The charged particles produced in Eq. 2.4 are transferred to the anode as a final electron acceptor. An open circuit is then used to send them to the cathodic electrode. A conductive polymeric matrix

and conductive nanostructured wire for close interaction with the anode are two other options (Kato Marcus 2007, Sengodu 2015). In recent times, MFC research has mainly focused on some issues such as MFC type anode, cathode, and membrane (Table 2.1). Municipal/domestic industry effluents are the most common substrates used. MFCs can be upscaled for treating wastewater by layering and/or using an altered electrode, as discussed in the preceding sections. Before manufacturing wastewaters were introduced, a current rating cons. of 1.25 A/m^2 and a removal efficiency of 35 percent were achieved when utilized in conjunction with another sewage treatment unit, such as an anaerobic fermentation (AD) unit with a 45 m^3 spending area (Wang et al. 2020).

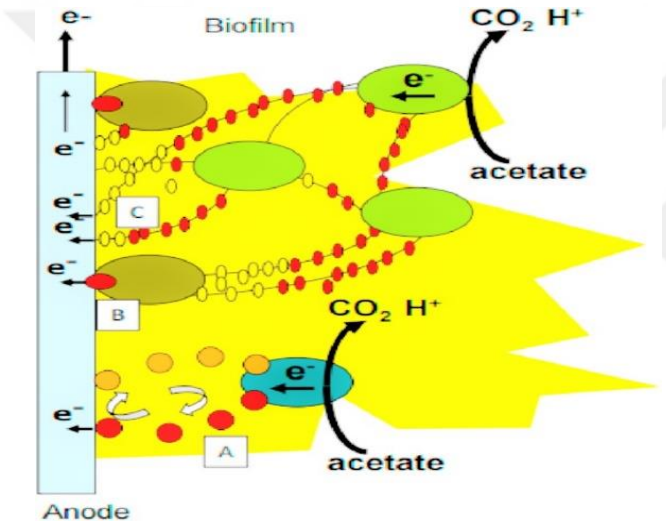

Figure 2.2 Basic concepts of MFC prevailing (a) the mediated, (b) direct and (c) electron transfer and nanowires (Mohan 2014)

Table 2.1 Summary of MFC studies in the last five years (2016–2020)

	Reactor Type	Substrate	Anode (Number)	Cathode (Number)	Membrane	References
1	Movable, 1.5 m^3 (Primary clarifier-DCMFC-Secondary clarifier)	Primary effluent	GFB (8)	Bio-GFB (7), Anode effluent	Dynamic (microbial) membrane	(He et al. 2019)

Table 2.1 Summary of MFC studies in the last five years (2016–2020) (continue)

2	DCMFC, 64 units, 1000 L	Municipal ww	RVC	RVC, Groundwater	VANA-Dion	(Blatter et al. 2021)
3	DCMFC, 50 units, 1000 L	Municipal ww	GAC	GAC, Artificial catholyte	CEM	(Liang et al., 2018)
4	SCMFC, 6 units, 720 L	Sanitary sewage	C felt	CoZnFeO or SnCu/C felt	Clayware	(Das et al. 2020)
5	Submergible MFC, 255 L	Municipal ww	GFB (10)	SS-AC (16, VitoCORE®)	Glass fiber separator	(Hiegemanneet al. 2019)
6	DCMFC, 96 units, 200 L	Primary effluent	CFB	C cloth/N-AC, Aerobic effluent	CEM	(Ge at al. 2016)
7	SCMFC, 12 units, 110 L	Swine ww	GFB (20)	Gas diffusion cathode	None	(Babanova et al. 2020)
8	SCMFC, 85 L	Domestic ww	GFB (22)	SS-AC (15, VitoCORE®)	Glass fiber separator	(Rossi et al. 2019)
9	DCMFC, 72 L	Synthetic ww	GAC/Ti mesh	GAC/Ti mesh, Desalination effluent	CEM	(Wu et al. 2016)
10	DCMFC, 6 units, 60 L,	Swine manure	GG	GR, Ammonium	AEM	(Vilajeliu-Pons et al. 2017)
			SS	SS, Ammonium	AEM	(Vilajeliu-Pons et al. 2017)
11	SCMFC, 45 L	Primary effluent	GFB (8)	Pt/C cloth/SS (2)	None	(Hiegemann et al. 2016)
12	SCMFC, 40 units, 16 L	Municipal ww	C felt	Pb/C cloth	CEM	(Estrada-Arriaga et al. 2018)
13	DCMFC, 2 units, 20 L	Brewery ww	Modified C cloth	Modified C cloth	Nano-filtration membrane	(Lu et al. 2017)

2.3 The Anode and Cathode Compartment

A typical MFCs design consists of two chambers: one is the anode chamber (anaerobic) and the other is the cathode chamber (aerobic). The anode chamber that contains active bacteria oxidize the substrate to produced protons and electrons, and transport the

electrons to form a biofilm on the anode electrode surface (Kim et al. 2008). These electrons pass through the external circuit to reach the cathode, while positive charged particles pass through the electrolyte and transfer through the salt bridge to reach the cathode. When protons pass to the cathode chamber, they combine with negative charged electrons and oxygen to form water with help of a catalyst (Liu and Logan 2004). The dynamical membranes and simmered anolyte constructed of graphite fiber brushes were used by He et al. (2019) to build low-cost bio-cathodes with microbiological biofilm growth. A multi-panel air electrode has been patented by Bouwman et al. (2020), which allows many smaller cathodes to be linked together through a uniform sheet of metal. Rossi et al. (2019) tested this inter air cathode for purifying household sewage in an 85 L single-chambered microbial fuel cell (SCMFC). With a 22-graphite fiber brushing as the anode and fiber glass as that of the separator, a peak power efficiency of 0.605 W/m^3 was achieved, with chemical oxygen demand (COD) elimination of 80% and current efficiency (CE) of 27%. A 255 L MFC sample with the same electrode unit has also been examined.

2.4 The Corrosion and Forms of Corrosion Attack in MFCs

Corrosion is an electrochemical process because it involves the transfer of electrons between the surface of metal and the aqueous electrolyte solution (Zvandasara et al. 2010). Corrosion is caused by the natural tendency of most metals to return to their natural state (Melchers 2005, Norsworthy 2014). Metal corrosion in an electrolytic environment is an electrochemical process associated with the corresponding oxidation and reduction reactions (Darowicki et al. 2001). Current flows from the high potential electrode to the low potential electrode. As a result, the system experiences two reactions at the same time. Oxidation is the process that occurs when electrons are emitted from a surface of electrode called the anode. The emitted electrons are used in other circuits in the circuit shown in the Figure 2.3.

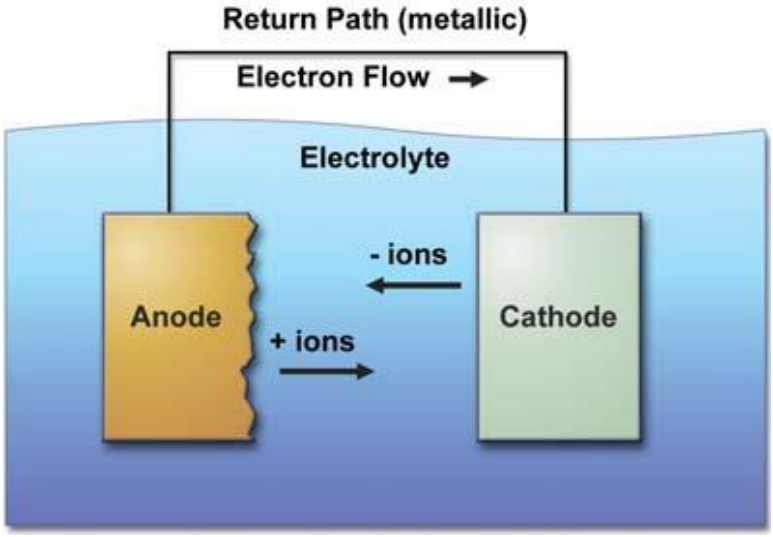

Figure 2.3 The corrosion cell (Richard 2021)

The steel corrosion would be considered as an electro-chemical technique which happens in stages. First attack happens at anodic electrode region on the surface, where ferrous ions go into electrolyte. Electrons are released from the anodic region and pass through the external circuit to the nearby cathodic region on the surface where they combine with O_2 and H_2O to form OH^- ions. The OH^- ions react with the ferrous ions from the anodic electrode to produce iron hydroxide, which has high tendency to react with ambient air to produce hydrated iron oxide, red corrosion surface. The overall reaction is shown by the following expression (Robert et al. 2003, Revie 2011):

Steel + oxygen + water = rust

This electrochemical process (corrosion) leads to loss of material properties, causes economic loss, compromises safety, and causes environmental problems (Hussein 2006, Roberge 2019). MFC has several corrosion attacks, which can be categorized based on what corroded metal is found on the surface. Mere visual inspection can result in any form. The naked eye is generally sufficient but zooming may or may not be useful.

2.4.1 Biological corrosion

The degradation of metal or non-metal objects due to the presence of microorganisms is known as biological corrosion. This pitting corrosion is frequently caused by bacteria clinging to metal surfaces inside the shape of biofilm. Corrosion can be caused by

organisms producing oxidizing chemicals, which are mainly metabolism products or indirect consequences of metabolic products acting on the metal. An electrochemical reaction causes a metal in liquid to ionize.

$$M \rightarrow M^{Z+} + Ze^{-} \quad (2.6)$$

Electrons removal by one or more mechanisms causes the reaction to proceed to corrosion:

$$2H^{+} + 2e^{-} \rightarrow 2H \rightarrow H_2 \quad (2.7)$$

$$H_20 + 1/20_2 + 2e^{-} \rightarrow 2(OH)^{-} \quad (2.8)$$

The oxidizers in these reactions are hydrogen ions and oxygen. Microbial development or higher microorganisms may also contribute to or trigger corrosion by creating differential concentrations of depolarizing agents, differential oxygen, or chemical concentration cells. Certain anaerobic microorganisms that can activate and use hydrocarbons can eliminate hydrogen (electrons) from metal substrates, speeding up the process (Eq. 2.7). Interaction by organisms with the creation or destruction of natural or applied protective layers, as well as the degradation of corrosion protection in closed systems, might all have a part in the outcome corrosion rate. Various organic and inorganic acids are among the most corrosive compounds created by bacteria. What is important to promote corrosion is mainly produced under aerobic parameters (Iverson 2008). These currents are important for the corrosion of many metals when they are dirty or very heavy to activate metabolic processes in which microorganisms can generate currents due to fluctuations in the cons. of oxygen or ions on the metal electrochemical interface border. These potential differences cause the metal to be corroded in the subterranean oxygen-poor anodic region, where electrons combine with oxygen and water to form hydroxyl ions (Miller et al. 2016). Organisms that are susceptible to oxidation have been found not only in anodes, where electrons are transmitted from microbes to terminals, but in cathodes, where protons are consumed by bacteria (Bergel et al. 2005). The indirect involvement of aerobic microorganisms in metal corrosion is well understood (Figure 2.4a) (Hamilton 2003, Beech and Sunner 2004,). Exopolysaccharides produce a biofilm on the metal substrate (EPS). At the anode, zerovalent Fe is oxidized, and electrons are transported to the cathode, reducing EPS bound Fe^{3+} to Fe^{2+}. Chemically or biochemically, Fe^{2+} is oxidized to Fe^{3+}, reducing oxygen (Beech and Sunner 2004). Sulfate-reducing bacteria, mostly species in the genus

Desulfovibrio (Kakooei et al. 2012, Mand et al. 2014), employ sulfate as an acceptor and minerals as an electron carrier in anaerobic MIC circumstances. According to one theory, electrons are transferred directly from corrosion occurring metals to microbial species (as depicted in Figure 2.4b) (Venzlaff et al. 2013). Other bacteria, such as anaerobic chemolithotrophic homoacetogenic form a biofilm on which sulfate reducing microbes cause corrosion. (Mand et al. 2014) Metals, on the other hand, are employed as electron donors. According to one theory, electrons are transported directly from corrosion occurring metals into bacterial cells (as depicted in Figure 2.4b) (Venzlaff et al. 2013). Other bacteria, including anaerobic heterotrophs homoacetogens like Acetobacterium woodii, establish a biofilm on the corroding electrode with the sulfate-reducing bacteria (Mand et al., 2014). Desulfovibrio organisms cannot develop chemolithotrophically, therefore the homoacetogens feed acetate to the sulfate-reducing bacteria. As a result, knowledge obtained in the field of MIC might be used to advance cathode construction for MFCs and conversely (Erable et al. 2012).

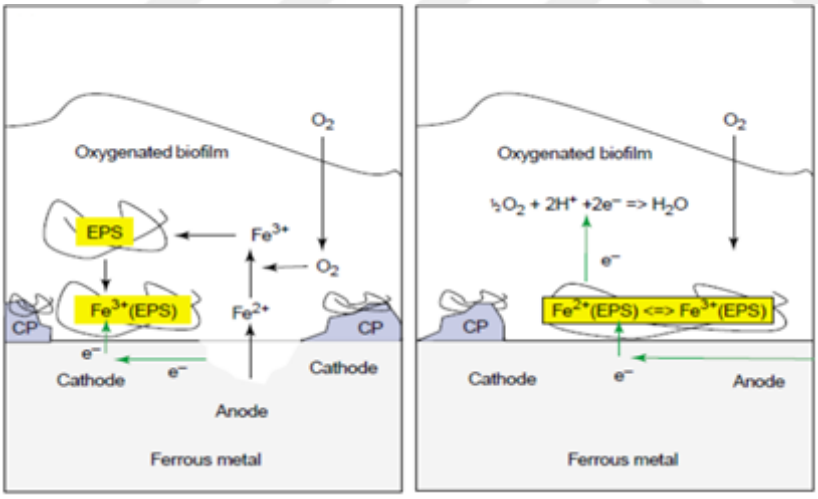

Figure 2.4 a) Showing of iron corrosion under aerobic states (Beech and Sunner, 2004)

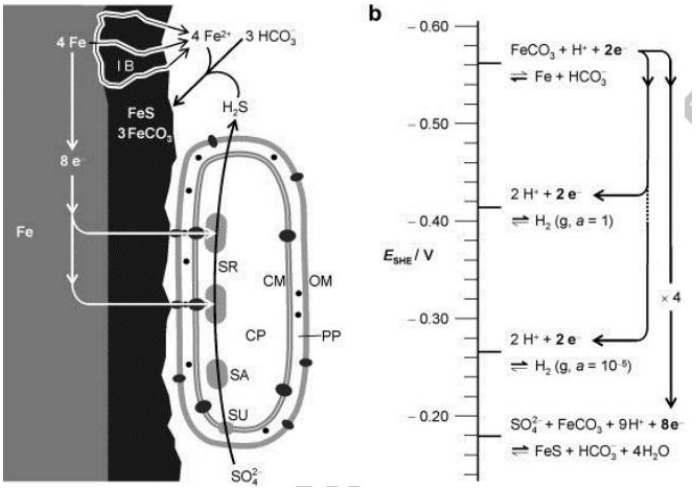

b) Sulfate-reducing bacterium MIC presenting electron transfer from zero-valent electrode to the bacterial domain through equilibrium redox development of the mechanisms (Venzlaff et al. 2013)

2.4.2 General corrosion

This kind of corrosion is one of the most popular corrosion forms happened on most metal electrode at a constant rate and often predictable. All homogeneous metals are subject to such general attacks when there is no potential difference between any two points on the electrode. Uniform corrosion is a chemical or electrochemical reaction used to characterize this attack, which happens on specific area of electrode surface or on the whole electrode surface. The metal becomes thinner and ultimately fails (Revie and Uhlig 2008, Fontana and Greene 2018). Uniform corrosion can be common in active dissolution in acids, oxidation and tarnishing, anodic oxidation and passivity, atmospheric and immersed corrosion in certain cases (Revie and Uhlig 2011).

2.4.3 Concentration cell corrosion

This sort of corrosion occurs between same metal immersed in different electrolytes with different corrosive species concentrations. The difference in potential forces the metal to develop cathodic and anodic zones. The electrical circuit (a conduit for electron movement) is completed by the metal surface and the electrolyte solution, allowing

current to flow and electrochemical corrosion to proceed (Ali and Hasan 2020). Concentration cell corrosion can be classified into two categories:

1- Metal Ion Concentration Cells: In the presence of water, a high concentration of metal ions in microorganism compartment and a low concentration of metal ions in water compartment. This difference in concentration of metal ions will create difference in electrical potential. The portion of metal in contact with low metal ion concentration will be cathodic, while the area in contact with high metal ion concentration will be anodic and corroded.
2- Oxygen Concentration Cells: A water solution in contact with the metal surface will normally contain dissolved oxygen. When there is a difference in dissolved oxygen concentration between microorganism compartment (anode) and water compartment (cathode), corrosion will occur at the area of low-oxygen concentration (anode).

Concentration Cells (Galvanic cells) are commonly seen in subterranean constructions like as buried pipelines for crude oils, where the water layer that settles at the bottom of the tank has high concentration of salt, causing cons. cell deterioration between both the tank walls and the tank base. The potential difference is caused by changes in the dissolved content of corrosive components in the fluids found at the bottom of the storage facilities, resulting in cathodic and anodic zones (Ahmad 2006, Heidersbach 2018).

2.5 Parameters Impacting on MFC Electrodes Corrosion Rate

The accumulation of resulted biological contaminates in the biofilm (oxidized intermediates or protons) would be prevented where oxidation parameters can be changed, and the metabolism of the biofilm stops (Clauwaert et al. 2007). For the suitable operation of the MFC, both protons and electrons need to move freely from the anode to the cathode at the highest feasible rates. Diffusion alone may not be sufficient to reach acceptable levels of current and cell potential. A sharp decrease in proton transport can decrease the pH of anode below 5 making it unfavorable for bacterial growing and more corrosive. To solve this problem, turbulent parameters can be introduced into both electrode by either vibration or recycling of raw materials (Rozendal et al. 2008). However, energy is spent, which reduces the overall efficiency of the system (Clauwaert

et al. 2008). The rate of corrosion is subjected for various parameters in microbial fuel cell. The various parameters depend mainly upon major mechanisms: physical, chemical, and biological as illustrated in Figure 2.5 (Muhammad et al. 2018).

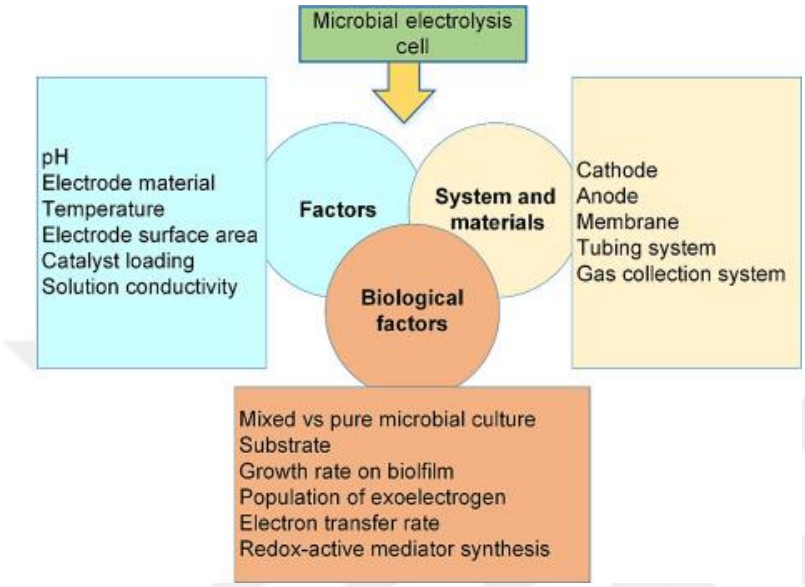

Figure 2.5 The effective parameters on MIC corrosion (Muhammed et al. 2018)

2.5.1 Effect of microorganism

Biofilms are bacterial populations that attach to metallic or even non-metallic electrochemical interface borders (Hall Stoodley et al. 2004). Adherent cells are bacteria that are embedded in biofilms, whereas planktonic cells are germs that are floating in bulk fluid (Donlan 2002, Veerachamy 2014). Microorganisms without stems can break out from the biofilm and colonize new territory (Costerton 2007). Microorganisms release extracellular polymer substances (EPS), such as nucleic acids, polysaccharides, and proteins to create biofilms (Usher et al. 2014). Corrosion that is impacted by microbiology is caused by microbial activity (Little and Lee 2014, Liu et al. 2018). In the vast majority of cases, biofilms are regarded to be the principal source of microbiologically caused corrosion (Xu et al. 2017). Due to bacteriologically impacted corrosion (MIC), aluminum alloy is not damaged by pitting corrosion (Dai et al. 2016). Bacteria create organic acids, which can cause corrosion to carbon steel. Other metals, such as zinc, have been observed to be corroded by these acids (Juzeli et al. 2007, Qu et al. 2017). Microorganisms are

already known to cause biocorrosion due to organic acid production which increases the acidity beneath biofilm communities (Xu et al. 2016). The pH underlying the biofilm may be lower than that of the bulk liquid. Vroom et al. (1999) observed that the acidity values of two nearby locations in the same biofilm might range by 2 or more. Proton impact is thermochemically beneficial when combined with oxidization at low enough pH. The organic acids are generally weak acids. At the same pH, acids, which have the ability to buffer protons, are significantly more invasive than strong acids like sulfuric (Kryachko and Hemmingsen 2017).

2.5.2 Effect of electrode materials

In terms of electron transport, resistance to corrosion, and electrolytic efficiency, choosing the proper electrochemical electrode is critical for MFC performance. Scaling power generation using various types of carbon paper, carbon steel, copper and stainless steel has been the subject of significant research (Govind 2015). The latest trend in MFC research work is to choose the low-cost electrode material, high corrosion resistant and high current density. Furthermore, the negative electrode must possess catalytic characteristics for the reduction of oxygen (Logan 2010). The anode and cathode materials must have the following features: Porosity and electrode area: The electrode of the terminals drastically limits the MFC's output power. The electrode resistance is equivalent to the ohm losses. Increasing the specific electrode area while maintaining the volume constant is the simplest technique to decrease losses and improve MFC efficiency. Furthermore, the huge electrode area gives more sites for reactions, which improves the electrode's reaction rate (Wang et al. 2011, Rismani-Yazdi 2008). Permeability, on the other hand, lowers the material's conductivity. Electrical Conductivity: After traveling through to the anode, electrons generated by microorganisms most typically flow via external circuits. The electrochemical solid terminal material's excellent electrical conductivity adds to the electron flow's low impedance. At around the same time, in order to enable electron transfer, the interface impedance must be low. Ionic conductivity is also required at the cathode to support the three-phase border reaction (Natarajan and Van Nguyen 2004). Stability and long-term viability: Microbial fuel cells' reducing, and oxidizing environments can induce material

expansion and degradation. Large electrode irregularity can boost the material's endurance while also raising the risk of cross-contamination, lowering MFC's long-term effectiveness. As a result, in both acidic and basic environments, the electrochemical solid terminal material must be robust and stable. Cost and accessibility: For fuel cells, the cost of electrocatalysts has a substantial influence on the capital cost. In order for MFC to be commercialized, materials must be inexpensive, durable, and easily available. Platinum, for example, is both costly and unsustainable. In the future, precious metal-free alternatives, such as composites, may be used to replace precious metals in electrode. Furthermore, the anode material utilized must be biocompatible. Bacterial adhesion is increased by using biocompatible materials, which extends the life of MFC.

2.5.3 Effect of dissolved oxygen concentration (DO)

Most electrolytes that come into contact with the air (natural water and synthetic solutions in flask) will have dissolved oxygen. The quantity of oxygen that water can hold is affected by the temperature, saltiness, and water pressure. As the temperature rises, the absorption of gases drops (colder water holds more oxygen). With increased salinity, gas viscosity decreases (freshwater holds more oxygen than does saltwater). With altitude, both pressure gradient and percentage of oxygen saturation will change. Finally, when pressure decreases, gas solubility diminishes. As a result of the reduction in relative pressure, the amount of oxygen dissolved (DO) and consumed in water reduces as altitude rises. The DO can oxidize dissolved substances into inorganic salts and ruin the protective hydrogen coating that develops on many minerals (Revie and Uhlig 2011). Due to such unsteady system features of the structure as i - building up of passivation layer on the electrode, ii - development of exterior roughness, iii - changing physical properties characteristics of the corrosion products and iv - changing mechanics of flow, transfer phenomena under operation flood are very complicated in corrosion processes in which dispersed oxygen acts as a depolarizer (Mahato et al. 1980).

2.5.4 Effect of flow velocity

Due to the flow impacts on both oxidation and reduction processes, velocity of the fluid is among the most critical characteristics to examine throughout metal corrosion (Musa et al. 2011). The relative mobility between the metal electrodes and the corrosion occurring environment can affect the corrosion process in a variety of ways. The heat and mass transfer of reagents toward as well as from the interface of the corrosion occurring metal can be increased as a result of this relative movement, leading to an increase in the corrosion rate. As a result, the impact of flow on corrosion of metals is a crucial factor to consider when designing and utilizing industrial machinery. As previously stated, speed has the greatest impact on base mass transfer. The substrate mass transfer is mostly affected by velocity. As previously stated, the mass transfer equations for the anode side and the kinetics equations are the same for both configurations. The only difference in the mass transfer equations for the cathode side is that the cathode compartment equation is substituted by Eq (2.9). In this configuration, natural convection carries oxygen from the environment to the bulk. As a result, the oxygen flux is calculated as follows (Vania et al., 2018):

$$N_{O_2} = h_{mass}\left(C_{O_2}^{o} - C_{O_2}^{bulk}\right) \tag{2.9}$$

The transmission of motion from such an agitator to the liquid is required for agitated mixing of liquids. The functioning of an impeller placed on a shaft driven motor may be separated into two categories (Coker 2007):

1. When shearing stresses transmit momentum in a plane perpendicular to the streamwise direction. Spinning disc and conical agitators are included in this category.
2. Normal stresses transmit momentum in a flow direction that is parallel towards the streamlines. Agitators in this domain include paddles, propeller, and turbocharged mixers.

Wagh (2017) investigated the impact of agitation speed on MFC efficiency. The results showed that raising agitation speed increased fuel cell's efficiency. Because the voltage is formed by the diffusion of particles induced by microbes, the dispersion situation is

eliminated by agitation or agitating the solution. The higher the agitation speed, the more exterior power is consumed, which is not good. With increased agitation speeds, the air movement inside the electrolyte creates additional challenges. Hamed et al. (2020) discovered that increased agitation speeds first increase overall power density by raising the agitating speed of a certain value. By expanding the amount of bubble shards in the bulk solution, raising the agitation speed creates more electronic resistance inside the electrolyte. Baday et al. (2017) discovered that raising agitation of the bulk solution increases the corrosion rate. This demonstrates that when agitating is conducted off with no gas sparging, the influence of the mixing rate upon that erosion rate is more evident. The contradictory impacts of the exhaust stream on the system's hydraulics explain this. The rising of the gas has diminished the strength of liquid turbulence caused by the impellers on the bottom half of the vessel, as well as the flow regime has shifted from radially to longitudinal (Vasconcelos et al. 1995).

2.6 Literature Review

The effect of dissolved oxygen concentration (DO) on MFC performance for electricity production was investigated by **Tao et al. (2014)**. In fed-batch mode, the two cylindrical chamber MFCs were used. Anode was carbon paper, while cathode was carbon cloth containing (Pt). The solution in the blown glass bottle was oxygenated with an air pump, and the airflow was balanced with a rotameter for air flow. The cathode received four airflow doses of 3.5, 2.8, 2.5, and 2.0 mg/l, respectively. The cathode electrolyte was recirculated at a rate of around 20 mL/min between the cathode chamber and the glass container. The anode and cathode chambers were inoculated with a mixture of anaerobic and aerobic sludge. Under a 3.5 mg/l air flowrate, the maximum output voltage is 521 mV (Tao et al. 2014).

Ogugbue et al. (2015) used a dual-chambered (anaerobic and aerobic) fuel cell to generate power from swine effluent. Copper electrodes, in instance, generated far more power than carbon (graphite) electrodes. The power generated by the microbial fuel cell with copper electrodes increased from an initial output of 12.81 watts to a peak of 251.54 watts and then decreased to 57.57 watts after an eight-week trial. In addition, power

output in the graphite electrode microbial fuel cell followed a similar pattern, growing from 2.52 W to 52.26 W before dropping to 8.448 W at the end of eight weeks (Ogugbue et al. 2015).

According to **Aghababaie et al. (2015),** copper was not an ideal material for anode due to its microbial toxicity. Although carbon was a superior electrochemical solid terminal material for bacterial adhesion, it had a lower conductivity for converting electrons. Foam, linen, carbon felt, fibers, and paper are some of the materials available. Copper anodes provide low power (2 mW/m^2) when compared with stainless steel (12 mW/m^2) or carbon cloth (CC) (880 mW/m^2) anodes due to the greater specific electrode area of CC compared to the metal mesh. Graphite rods or plates are more multilateral in nature since they are easy to handle, inexpensive, and have a definite electrode area. When compared with other electrochemical solid terminal materials, CCs have a higher porosity and mechanical strength (Aghababaie et al. 2015).

Javed et al. (2016) illustrated the numerous mechanisms suggested for MIC of copper alloys, as well as microbe tolerance to copper ions and their influence on future microbial corrosion. Sulphate-reducing bacteria have been shown to cause localized and/or inter-granular degradation of copper-nickel alloys in many of recent research. According to the study, copper-based alloys really aren't resistant to microbial populations and the resulting MIC. When exposed to seawater, alloying elements have indeed been known to suffer from localized corrosion. Both biotic and abiotic mechanisms have been used to explain the type of corrosive environments on these alloys (Javed et al. 2016).

Dual chamber MFC was utilized by **Oliveira et al. (2016)**. A graphite brush was used to collect the electron-transferring bacteria in the anode chamber, while a simple carbon paper impregnated with Pt (platinum) was used as the cathode electrode in the cathode chamber. In the anode and cathode chambers, wastewater was employed as an inoculum. The effect of hydrodynamic conditions on MFC performance was determined using various rotational speeds in the cathode chamber. The varied Reynolds numbers of rotational speeds (0, 2236, 11152, 22317 and 33469) were tried. For a 22317 Reynolds

number of rotational speed, a higher power density of 37.3 mW/m^2 was reached (Oliveira et al. 2016).

Harshitha et al. (2019) employed graphite electrodes in a two-chamber MFC. The substrate is cow dung compost, while the anode inoculum is municipal sludge mixed with drain water. The operating period (days) and temperature are two variables that have a significant impact on voltage generation. On the second day, a maximum of 223 mV of voltage was created, which then progressively fell to 220 mV on the fourth day. At working temperatures of 30–35°C, the better voltage output of 215 mV was obtained. Alkalinity (pH of 8) that promotes the growth of organic matter and hence affects the MFC's effectiveness (Harshitha et al. 2019).

Liu et al. (2019) studied the corrosion mechanisms of carbon steel underneath deposit in the addition of the sulphate reduction bacterial (SRB) Desulfotomaculum nigricans employing electrode morphology, losing weight, and electromechanical testing. According to the findings, SRB under deposit greatly exacerbated both overall and localized corrosion. According to the losing weight data, the rate of material deterioration in the presence of SRB was nearly 6 times that of the control. The greatest corrosion pit depth in the presence of SRB was nearly 7.7 times that of controls. That both anodic and cathodic processes were considerably enhanced by SRB. Significant corrosion process occurred as a result of a galvanic action produced by the heterogeneity biofilm in the presence of SRB (Liu et al. 2019).

Khouzani et al. (2019) discovered a significant microbiologically driven collapse in the elbow of a sub electrode amine pipeline. The investigators performed a comprehensive examination into a significant MIC-related collapse in a subterranean amine pipeline, which included intensive microstructural studies, corroded products/biofilm studies, and causative bacteria monitoring. Conclusions were drawn using data from visual observation, transmission electron microscopy (TEM) and Power X-ray spectrometry (EDS)/X-Ray Diffraction (XRD) experiments. The presence of pathogenic microorganisms, notably salt microbes, which play a vital role in corrosion, was also

evaluated. The failure in this example was found to be caused by salt bacterial (SRB), a well-known significant group of microorganisms engaged in microbiological corrosion (Khouzani et al. 2019).

The impact of operating factors on MFC performance was investigated by **Gadkari et al. (2020).** A total of four single-chamber membranelles air-cathode MFCs were built. They experimented with different working temperatures ranging from 20 to 40℃, and found a 4.5 percent drop in maximum power density at 40℃ compared to 34℃. The effect of electrode spacing was also investigated. The spacing ranged from one centimeter to four centimeters. The optimal power density rises as the distance between the two electrodes is reduced. The present work delivers the investigation of the impact on various parameters: electrodes metal type, the presence and absence of air pumping, the yeast concentration and the agitation speed. The electrochemical characteristics of microbial fuel cell and corrosion rate are obtained through the current study (Gadkari et al. 2020).

3. EXPERIMENTAL WORK

3.1 Microbial Fuel Cell (MFC) Configuration

The electrochemical cell constructed in this work was a double chamber microbial fuel cell (MFC) operates in a batch mode under the aeration. The experimental set up is shown schematically and photographically in Figures 3.1 and 3.2, respectively. Three different electrode materials were used which were stainless steel (SS), copper (Cu), and Zinc (Zn). The electrode was placed in the middle of a solution containing different concentrations of microorganism (MO) which was yeast (Saccharomyces cerevisiae) and sodium chloride 0.1 N to facilitate the electrons transfer in the circuit. This compartment is the MO compartment which also contains a substrate of 2g/l. The other compartment (water compartment) also contained 0.1 N NaCl. The two solutions were connected with a salt bridge containing saturated salt solution of 0.4N NaCl used to transfer the ions between the microorganism (MO) compartments and water compartment. The electrodes were connected by external copper wire to transfer electricity and complete the circuit. The temperature was kept constant at 30ºC using a water bath. Air pump was used to pump the air into water chamber at a rate of 2.51 l/min. A mechanical agitator was used for agitating the solution with different stirring speeds in the water chamber.

The experimental work includes 4 parts:

1. Studying the effect of microorganism concentration (3, 6, and 10 g/l) on the corrosion rate, cell current and electrode potentials.
2. Examination the effect of increasing the dissolved oxygen (DO) concentration by air pumping into the water (cathode) chamber on the corrosion rate and electrode potentials in MO compartment and in water compartment.
3. Investigating the effect of agitation velocity on corrosion rate, current and electrode potentials by agitating the solutions with different speeds; 150, 300 and 450 rpm.
4. Studying the joint effect of various agitation velocity (150, 300 and 450 rpm) with air pumping in water chamber on corrosion rate, cell current and potentials of electrodes.

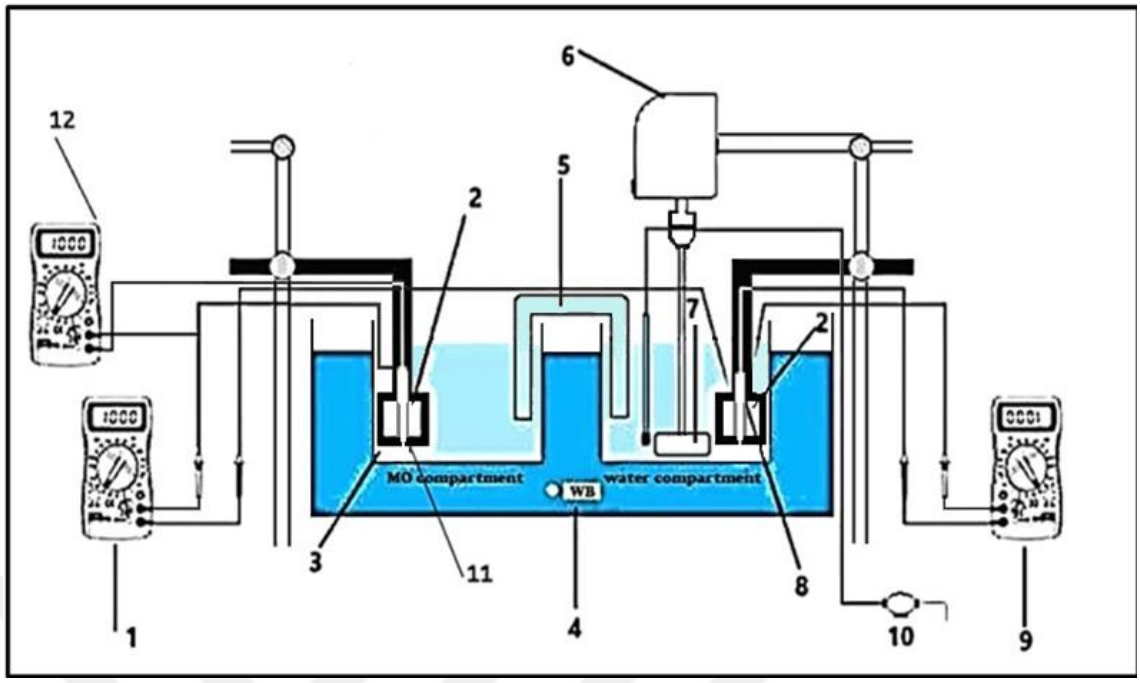

Figure 3.1 Sketch diagram of the MFC unit: (1) Ampere meter, (2) Electrodes, (3) Beaker, (4) Water bath, (5) Salt bridge, (6) Stirrer, (7) Impeller, (8) Saturated calomel electrode in MO solution side, (9) Voltmeter, (10) Air pump, (11) Saturated calomel electrode in water solution side, and (12) Voltmeter

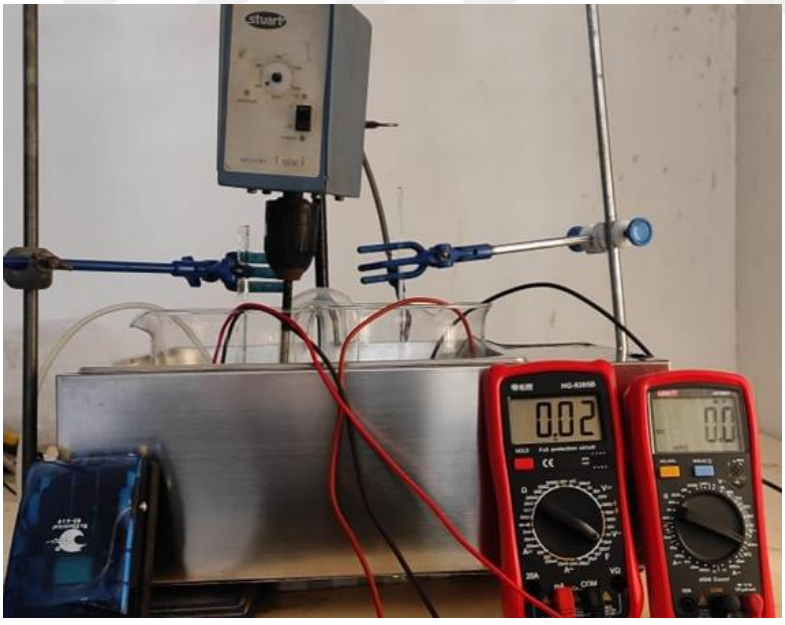

Figure 3.2 Photograph of the experimental cell.

3.2 Materials

3.2.1 Electrode materials

Three electrode materials were used: stainless steel, copper and zinc, as an electrode for bio-electricity production in MFC to study their corrosion behavior. These materials were selected because of their use in literature for MFC electrode. Figure 3.3 shows photos of the 3 electrodes used. The dimensions of each electrode were 50 × 50 mm. One face was exposed to the solution, while the other was taped shut.

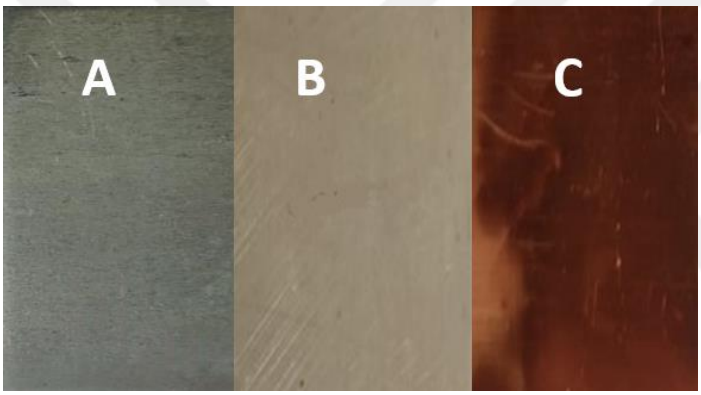

Figure 3.3 Three electrodes, (a) zinc (Zn), (b) stainless steel (SS) and (c) copper (Cu)

3.2.2 Organic substrate

Sodium acetate (product code 20236 K02, China) with a concentration of 2 g/l is used as a substrate to enhance microorganism fuel cells energy generation.

3.3 Experimental Apparatus

The experimental apparatus comprised:

1. Water bath: CIC model (India) with a temperature controller to keep the temperature constant within ±1.5 °C. All experiments were carried out at constant temperature of 30°C.

2. Beakers: two beakers of 2 liters made of Pyrex were placed in the test solution served as anode and cathode compartments.
3. Electronic Balance: (KERN& Sohn, GmbH, Germany) It can measure weights that range up to 200g, with the precision of 0.1mg. This was used to weigh the electrodes before and after the experiment in weight loss experiments.
4. Desiccator: (Hubei, China) made of Pyrex to keep the electrodes away from moisture using highly active silica gel.
5. Thermometer: The device, which can operate in the range of -10°C to 50°C, was used to measure the solution temperature.
6. Reference Electrode: It was a standard calomel electrode (SCE) (model ME-SC900, United Kingdom), used to measure the potentials of each electrode in each chamber (Figure 3.4a). The tip of the reference electrode was placed at about 2 mm from the electrode surface.
7. Salt bridge: Made of Pyrex for ensuring the electrical connection between the two compartments. Its inner diameter is 1.3 mm (Figure 3.4b).
8. Mechanical stirrer: type SS10 manufactured by Stuart (UK) to provide flow velocity for the solution in water compartment (which is the cathode compartment) with a range of 0 to 2000 rpm. The stirrer is equipped with an impeller of two blades with the dimensions of 30 mm height, 15 mm width and 2 mm thickness as shown in Figure 3.5c.
9. Air pump: It pumps the air with a flow rate of 2.5 l/ min. In MFC, air supply is used to increase the oxygen concentration in the cathode compartment which enhances the produced current (Figure 3.4e).
10. Digital pH Meter: type (VantaKool, diliss, China) that measures the pH value of the sample ±0.3 at temperature in a range of 0°C - 50°C.
11. Dissolved Oxygen Meter: Senso Direct 200 model used to calculate the concentration of dissolved oxygen in a unit (mg/l) (Figure 3.4f).
12. VICTOR VC97 Digital Voltmeter: to measure the potential in V.
13. VICTOR VC97 Digital Multimeter: to measure the current in mA.
14. Glass holder: to hold electrodes in the solution as shown in Figure 3.4d.
15. Accessories: connection wires, stands and clamps.

16. Microscope: (MML 1200, KRUSS, Germany) used to take photographs of each electrode at 500x zooming (Figure 3.5).

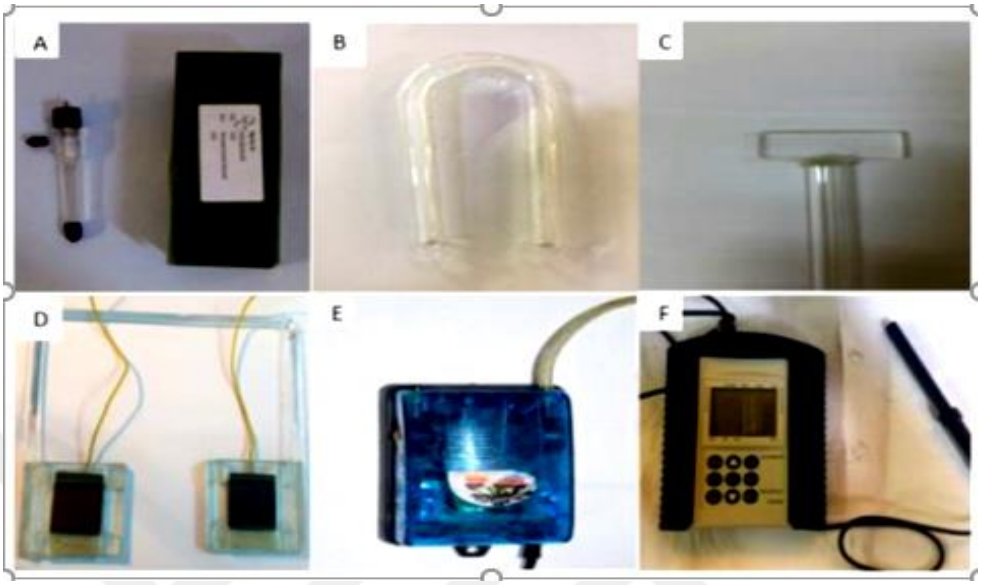

Figure 3.4 (a) Calomel electrode, (b) Desiccator, (c) Salt bridge, (d) stirrer paddle, (e) Air pumping and (f) Dissolve Oxygen meter

Figure 3.5 Microscope used to take photographs

3.4 Experimental Procedure

3.4.1 Electrodes corrosion rate measurement (weight loss)

Before each run, the electrode specimen was washed with tap water with brushing by plastic brush, followed by distilled water, dried with a clean cloth. Then it was dried by using a furnace at about 80ºC for 5 minutes (Mahato et al. 1980). The desiccator containing high activity silica gel was used for keeping the specimen until use. Then the specimens were weighed to the 4^{th} decimal of gram (w1) by using digital balance. One face of the electrodes was completely insulated by tape and the electrodes were placed in the middle of the compartments. The, Sodium acetate salt of 2 g/l, used as a substrate to enhance MFC energy generation, and sodium chloride of 0.1 N, used to facilitate the electrons transfer in the circuit, were added into the anodic compartment which containing yeast (Saccharomyces cerevisiae, MO). The MO chamber is the anode chamber because most of the reactions in this chamber are oxidation reaction (Potter 2011).

The other compartment, containing water with NaCl, is the cathode chamber that include the cathodic reactions especially oxygen reduction reaction. The two solutions were connected with a salt bridge containing saturated salt solution used to transfer the ions between the microorganism (MO) compartment and the water compartment. The electrodes are connected by external copper wire to transfer electricity and complete the circuit. The temperature was kept constant at 30°C by using a water bath. At the end of weight loss experiments (different MO concentration, flow velocity, and air pumping and agitating in cathode compartment) the electrodes were cleaned according to a standard procedure. The specimen after the corrosion test was cleaned by water with brushing by plastic brush, then rinsed with distilled water and acetone, respectively. Then was placed in oven at 80ºC for 5 minutes and kept in desiccator until it cools and then weighted (w2). So that the corrosion rate (CR) can be determined using the Equation 3.1:

$$CR = \Delta W/A \times \mathrm{T} \tag{3.1}$$

where Δw is weight loss (gram), A is area (m^2), and T is time (day).

3.4.2 Current density and potential measurements

Before each test, the two beakers were washed with distilled water at the start of each run. The temperature of the solution was double-checked using a thermometer. The electrodes were then immersed in both compartments, and the electrical circuit was completed by connecting the electrodes, ammeter, voltmeter, and placing the salt bridge. The electrodes were held in the solutions by connecting them to a glass board. The yeast microorganism was then added to one compartment and mixed gently and left for 15 minutes to let it grow and adapt to the temperature and the surrounding environment. Sodium acetate (2 g/l) substrate was added. Bacteria grew in aerobic conditions in the anodic compartment. The produced current and the electrode's potentials after adding the yeast microorganism (Saccharomyces cerevisiae) were recorded with time for three hours.

It is to be confirmed that the electrode material is the same in each compartment. In the measurement of closed circuit (working MFC), potential of the electrodes was measured with time. The measurements of the electrode potentials were performed by using two saturated calomel electrodes. The Lugging capillaries were positioned at 2 mm from the surface of the electrodes. The experimental runs were carried out twice or more for checking reproducibility and accuracy. Air was pumped into the water compartment at a rate of 2.5 l/min. The dissolved oxygen (DO) was measured under different operating conditions. A mechanical agitator (stirrer) was used to provide the required rotational speed.

3.4.3 Microscopic tests of electrodes corrosion

After each experiment, the electrodes cleaned according to standard procedure and microscopic images of corroded electrodes were taken for different conditions.

4. RESULTS AND DISCUSSION

This chapter presents the experimental results and discussion for the corrosion of three different electrode materials (copper, stainless steel, zinc) for the whole investigated ranges of microorganism concentration, air pumping, agitation velocity, and conjoint effect of air pumping with agitation velocities in cathode compartment of microbial fuel cell (MFC). The results are presented and discussed in this chapter as the corrosion of electrodes under running conditions of energy generation for a range of operating conditions.

4.1 Corrosion of Copper Electrode in MFC

4.1.1 Effect of MO concentration

Table 4.1a shows the MO concentration effect on the corrosion rate (CR) of copper electrodes in anode and cathode chambers at T= 30°C and 2 g/l sodium acetate as a substrate. In anode chamber when increasing the MO concentration from 3 to 10 g/l, the corrosion rate of electrodes increases from 2.11 to 6.34 gmd (about 200% increase). This increase in the corrosion rate of electrode is due to biological corrosion. Corrosion is caused by organisms producing oxidizing or depolarizing agents, which are mainly metabolic products or indirect products of metabolic products acting on the metal. The microbes release carbon dioxide gas (CO_2) as a result of the process of respiration and food fermentation (as seen in Table 4.1b). Thus carbonic acid H_2CO_3, corrosive to metals, can be produced and increasing the MO concentration led to the solution in anode chamber to be more acidic (Eqs 4.1 and 4.2) (Revankar 2016):

$$CH_3COOH + H_2O \rightarrow 2CO_2 + 8H^+ + 8e^- \quad (4.1)$$

$$CO_2 + H_2O \rightarrow H_2CO_3 \quad (4.2)$$

In addition, the microbes work on corrosion due to the chemicals resulting from the metabolic processes of yeast, as this microorganism increases the acidity of the MO solution as shown in Table 4.1b. Thus, the biofilm formation on metal surface, and this biofilm works to collect chemicals under it, causing corrosion (Revie and Uhlig 2011). This chemical attack the electrode surface by oxidizing the copper as in Equation 4.3:

$$Cu \rightarrow Cu^{2+} + 2e^{-} \quad (4.3)$$

In cathode chamber it is notable that the corrosion rate of copper electrode in water compartment (Cathode chamber) increases too from 0.19-2.88 gmd by increasing the MO concentration in anode chamber from 3-10 g/l. The reason is the chemical and electrochemical process in MFCs. In the cathode chamber, the reduction of O_2 is main cathodic reaction as in Eqs. 2.7–2.8.

$$2H^{+} + 2e^{-} \rightarrow 2H \rightarrow H_2 \quad (2.7)$$

$$H_2O + 1/2O_2 + 2e^{-} \rightarrow 2(OH)^{-} \quad (2.8)$$

Electrons are released from anode chamber and pass through the external circuit to the cathode chamber where they combine with O_2 and H_2O to form OH^- ions. The OH^- ions react with the copper ions from the cathode electrode by uniform corrosion to produce copper hydroxide, which has high tendency to react with ambient air (O_2) to produce hydrated copper oxide, which means that increasing CR in the anode compartment causes an increase in the CR in cathode compartment. Another reason, when two electrodes are immersed in an electrolyte, one of which acts as an anode (high potential force because of bacteria activity) and the other as a cathode. Moving an electric current between them in the electrolyte solution, the potential difference force of electrodes in the solution works to corrode the anode as one of the poles of the concentration cell corrosion (Ali and Hasan 2020). Moreover, it is clear that the corrosion rate of copper electrodes in anode chamber at different MO concentrations is more than in cathode chamber. First reason is the biological corrosion in anode chamber. When the pH is less than 4.0, the oxide film dissolves instead of a being accumulated on the surface of electrode to create a layer. The surface of electrode is in direct contact with the acid solution without the protective oxide film the corrosion reaction continues at a faster rate than it does at higher pH values (Gedeon 2011) (Table 4.1b). Second reason is the potential difference of electrodes (Figure 4.1). As well as Figure 4.1 shows that the potential becomes more negative with time until reaching the steady state value. This decrease is ascribed to biofilm formation and corrosion product layer on the electrode surface.

Table 4.1 a) The MO concentration effect on the corrosion rate of copper electrodes in anode and cathode chambers

MO Concentration	Cu corrosion rate in anode chamber gmd	Cu corrosion rate in cathode chamber gmd
Yeast 3 g/l	2.11	0.19
Yeast 6 g/l	3.46	2.21
Yeast 10 g/l	5.34	2.88

b) The values of pH at T=30°C and 2 g/l sodium acetate in anode compartment

MO Concentration	MO compartment	Water compartment (0.1 N NaCl solution)
Yeast 3 g/l	4.1	6.3
Yeast 6 g/l	3.9	6.2
Yeast 10 g/l	3.5	6.2

Figures 4.2 and 4.3 show the MO concentration effect on the potential of cupper electrode versus time immersed in the MO solution at T= 30°C. When increasing the MO concentration from 3-10 g/l, the potential shift in anode chamber to a more positive value. On another hand, increasing MO concentration from 3 to10 g/l shifts the potential (cathode chamber) slightly to a more positive value. The reason is that the increased concentration of microorganisms leads to increasing in oxidation process, and an increase the thickness of biofilms that is formed on the electrode surface and the MO compartment solution becomes more acidic (Table 4.1b). Increase acidity of the MO solution increase the electrode potential of MO chamber (Figure 4.2) (Revie and Uhlig 2000). This is accompanied by an increase in current density as shown in Figure 4.4. In fact, this current might be partly due to the microbial activity and partly due to corrosion of the electrodes.

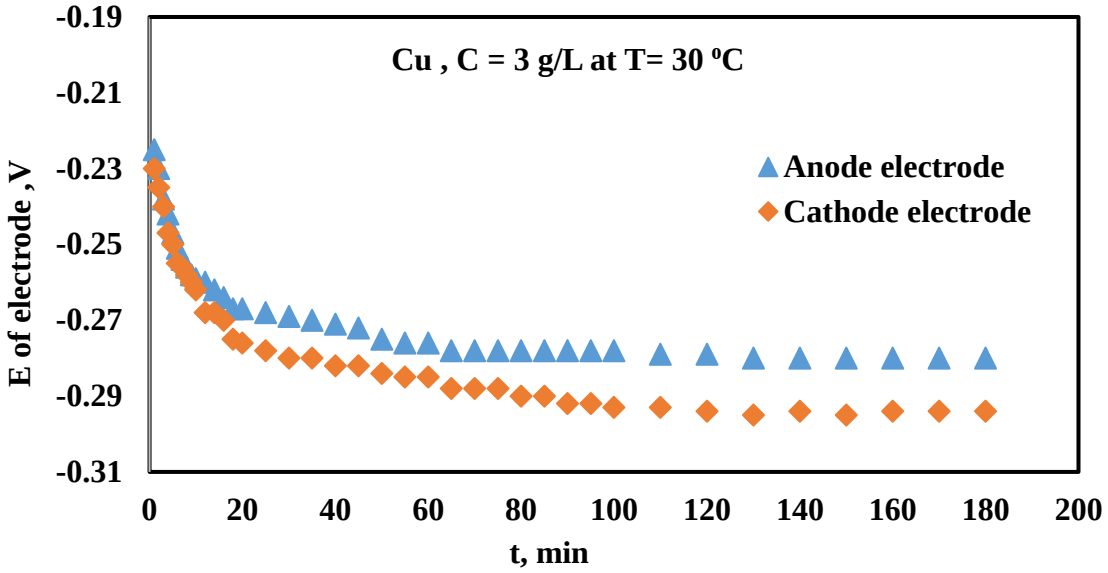

Figure 4.1 Comparison between the potential of anode and cathode electrodes

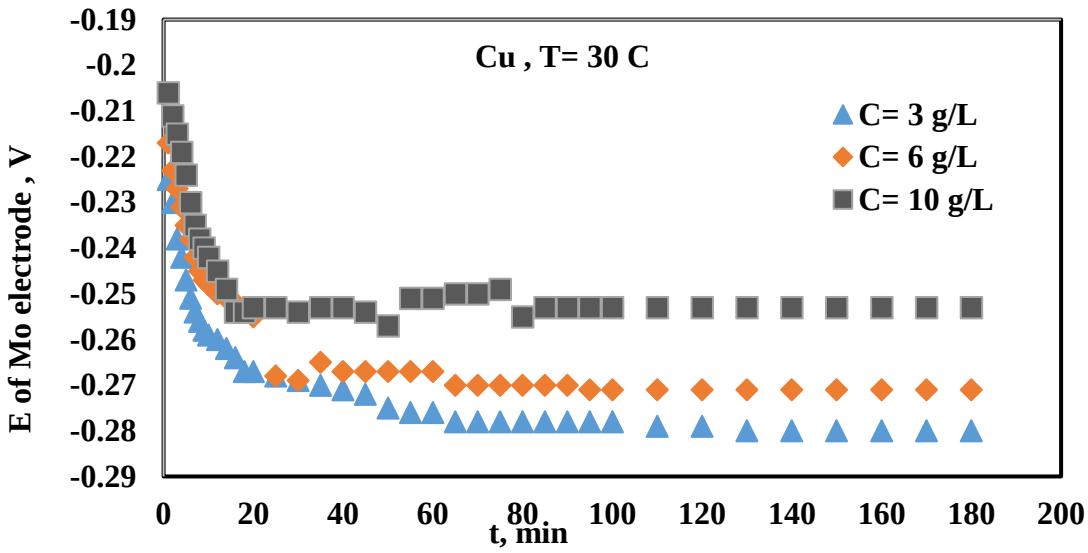

Figure 4.2 Effect of different MO concentrations on copper electrode potential in anode chamber

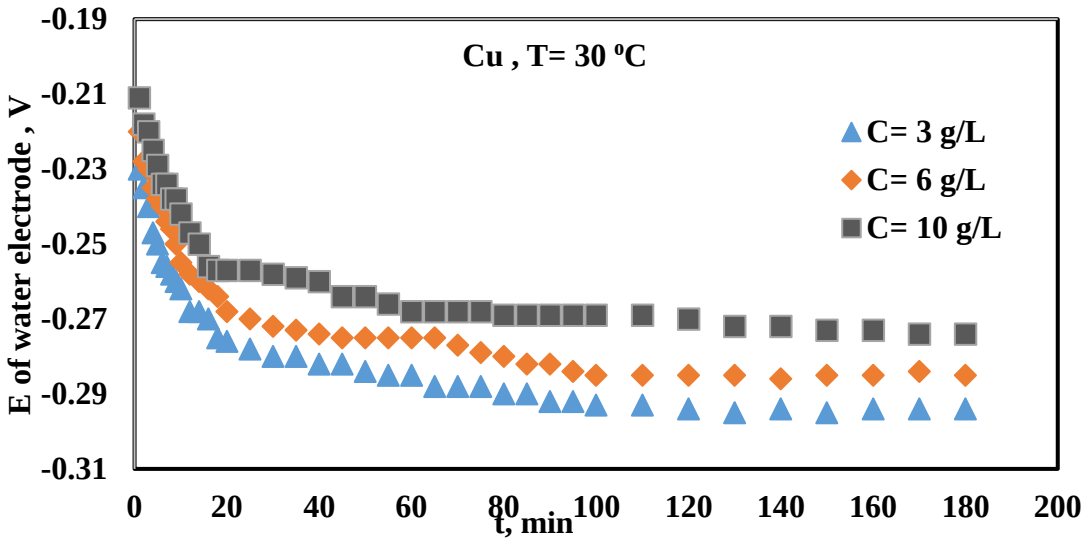

Figure 4.3 Effect of different MO concentrations on copper electrode potential in cathode chamber

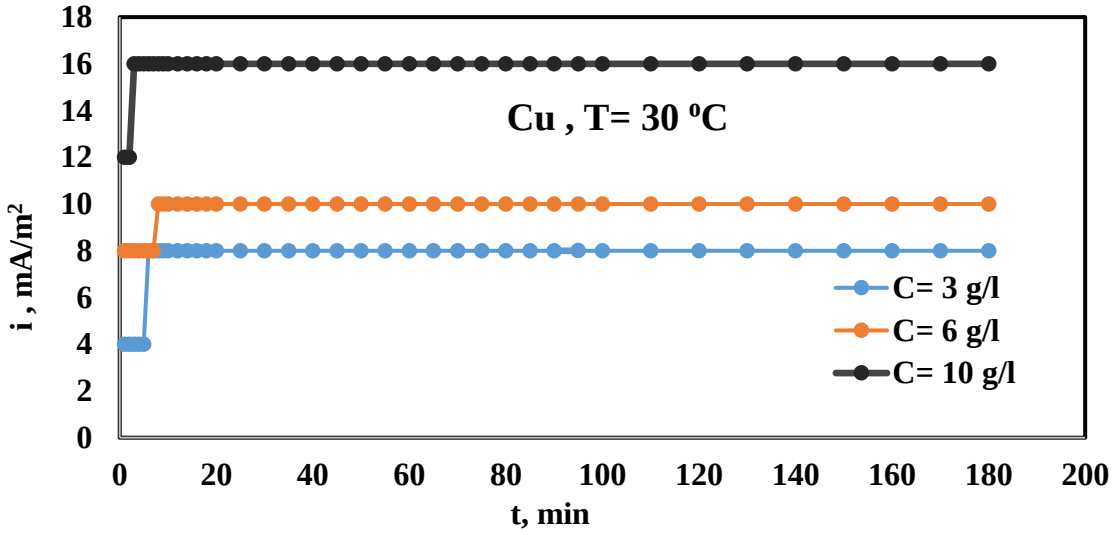

Figure 4.4 The current density versus time for copper at different concentrations of MO

Figure 4.5a-c show microscopic images of the electrode surfaces before and after the experiment for different MO concentrations. Those images confirm that increasing MO concentration increases the corrosion for both electrodes as they are galvanic couple.

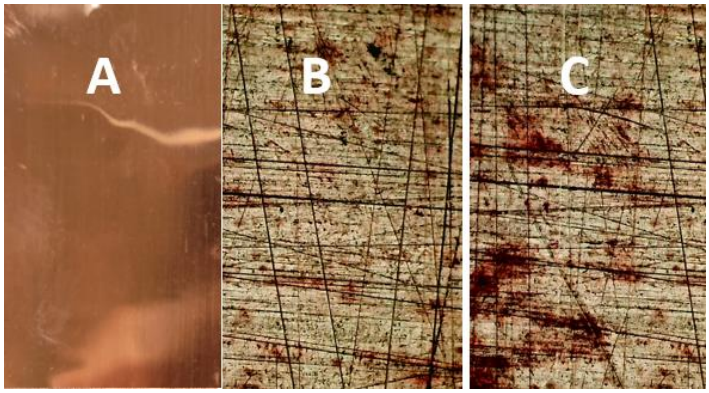

Figure 4.5 a) Microscopic images of (a) clear copper electrode, (b) corroded copper electrode in water compartment, (c) corroded copper electrode in MO compartment at C= 3 g/l (500x zoom)

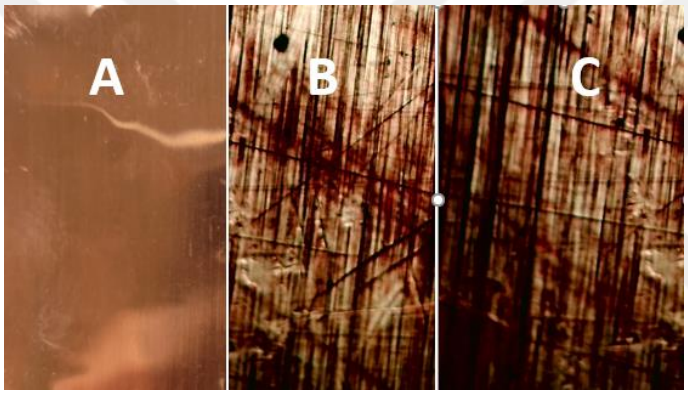

b) Microscopic images of (a) clear copper electrode, (b) corroded copper electrode in water compartment, (c) corroded copper electrode in MO compartment C= 6 g/l with the magnification is 500x

c) Microscopic images (a) clear copper electrode, (b) corroded copper electrode in water compartment, (c) corroded coper electrode in MO compartment at C= 10 g/l (500x zoom)

4.1.2 Effect of air pumping

Table 4.2 shows the air pumping effect into water chamber at a rate of 2.5 l/min at different MO concentrations on the corrosion rate of copper electrodes at 30ºC. Increasing yeast concentration led to increases in the corrosion rate of the two compartment (anode and cathode) electrodes. Comparing Table 4.2 with Table 4.1 indicates that when pumping the air in water compartment, the corrosion rate of copper in that compartment increases appreciably compared to the case of without air pumping. The corrosion rate of copper in (MO) anode compartment increase slightly compared to the case of no air. This phenomenon can be interpreted as follows: when the air is pumped into the cathode chamber, the oxygen concentration in this chamber increases (as shown in Table 4.3), leading to increase in the corrosion rate because oxygen is a strong oxidizer to the metal (Revie and Uhlig 2011). The air pumping led to increase the CR of anode electrode as they galvanically linked.

Table 4.2 Effect of air pumping at different MO concentrations on the corrosion rate of copper electrodes

MO Concentration	Cu corrosion rate in anode chamber gmd	Cu corrosion rate in cathode chamber with aeration gmd
Yeast 3 g/l	2.21	0.76
Yeast 6 g/l	3.88	2.30
Yeast 10 g/l	6.19	3.65

Table 4.3 Measured concentration of dissolved oxygen at 30°C, with the sodium acetate concentration of 2 g/l, yeast 3-6 g/l in anode compartment, and air pumping speed 2.5 l/min in cathode compartment

Component	The concentration of dissolved oxygen (mg/l)
Distilled water + 0.1 N NaCl (salt)	6.1
Distilled water + 3 g/l yeast + sodium acetate	2.4
Distilled water + 6 g/l yeast + sodium acetate	2.1
Distilled water + salt + air pumping	7.2

Figure 4.6 shows the air pumping (aeration) effect into the water compartment (cathode compartment) on the potential of both copper electrodes (anode and cathode compartments) versus time at concentration of MO of 3 g/l. The results show that the addition of air into the water compartment has shift the potential of electrodes to more positive. The reasons are subject to several considerations such as increased O_2 concentration in both chambers and the joint effect of biofilm and bubbles on the anode surface (Table 4.3).

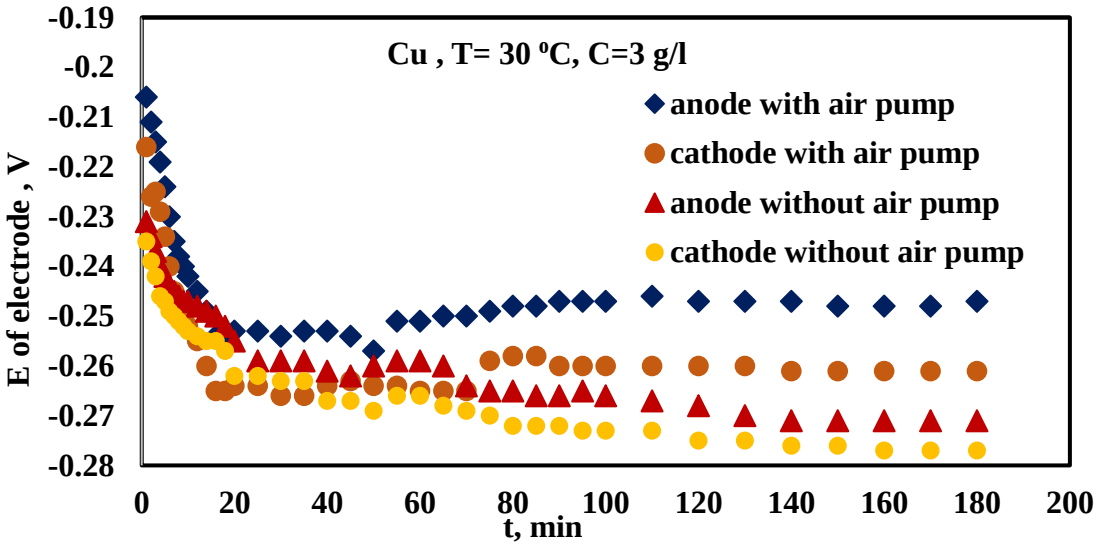

Figure 4.6 Electrode potential vs. time in the presence and absence of air pumping in water (cathode) chamber for 3g/l MO concentration

Figure 4.7a-b shows the aeration effect in the water chamber on the galvanic current density between copper electrodes for different concentrations of microorganism 3-10 g/l. These results reveal that the aeration into the water compartment works to increase the current output. This is because it increases the dissolved oxygen concentration in the water compartment (Table 4.3), which reacts with the proton H^+ transported through the salt bridge resulted from bacteria oxidation. Increased bacteria oxidation leads to an increase in corrosion rate of copper electrode in anode chamber that causes an increasing corrosion rate of copper electrode in cathode chamber too as it is galvanically coupled with anode chamber. Another reason for increasing the produced current is that when pumping the air in the water chamber, the oxygen concentration increases leading to an increase in the potential of the cathode (as shown in Figure 4.6) which results in the

increased potential difference between cathode and anode (Salam et. al. 2020, Ali and Hasan 2020) which enhances the MO oxidation and thus the current and corrosion rate increases by galvanic action as show in Figures 4.8 and 4.9. When there is no aeration, the current is low and when aerating the cathode chamber, the current increases. This large increase of current clearly indicate the increase in corrosion rate of at least on the terminal, which is the anode (Table 4.2). By direct contact, electroactive bacteria can move electrons to an electrode due to the presence of redox-active proteins (Drapcho et al. 2008, Kumar 2015).

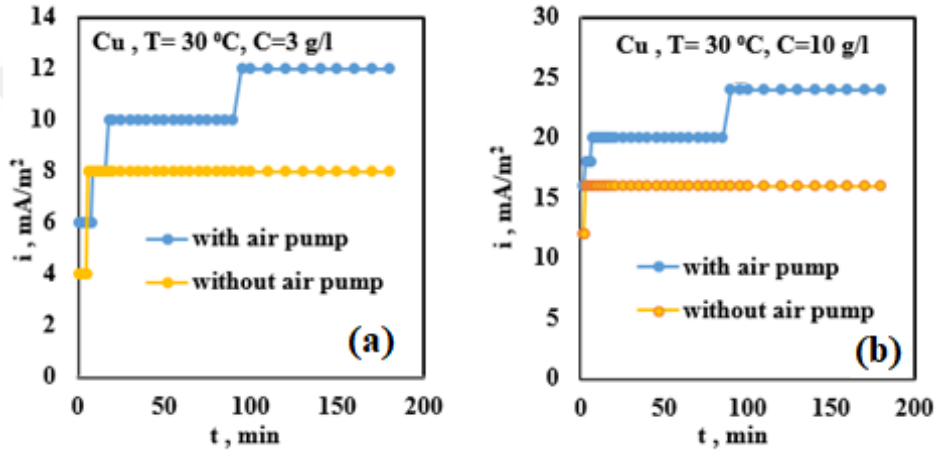

Figure 4.7 Current density vs. time for copper electrode in the presence of air pumping in the water chamber and the effect of the MO concentration at (a) 3 g/l, (b) 10 g/l

The current produced in the MO compartment is a result of two contributions. Part of it comes from the corrosion of metals in the two terminals which is the scope of the present work. The second part comes from the oxidation reactions occurring in the cell due the microorganism activity. The exact or rough estimation of bio-current which is produced from MO activity needs to carry out experiments with highly noble metals that do not corrode. This is beyond the scope of present work and can be investigated in future research. Definitely, part of this current is a result of the electrodes corrosion in the two compartments as indicated by the weight loss of each electrode. Figure 4.8 and 4.9 show microscopic images of copper electrodes in different conditions. The copper electrode in both compartments is subjected to a clear corrosion attack leading to a clear defect of the surface morphology.

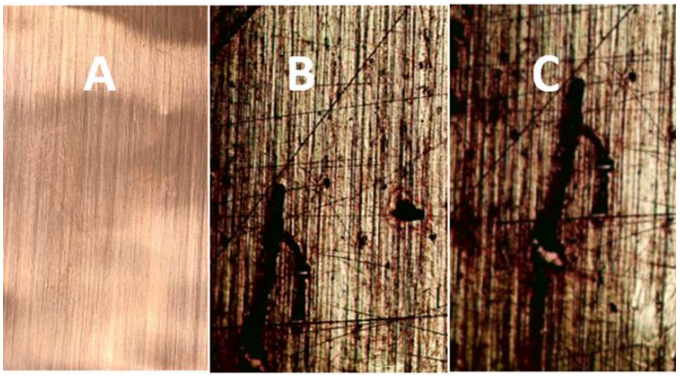

Figure 4.8 Microscopic images of electrodes under air pumping into water compartment, (a) clear copper electrode, (b) corroded copper electrode in water compartment, (c) corroded copper electrode in MO compartment at C= 3 g/l (500x zoom)

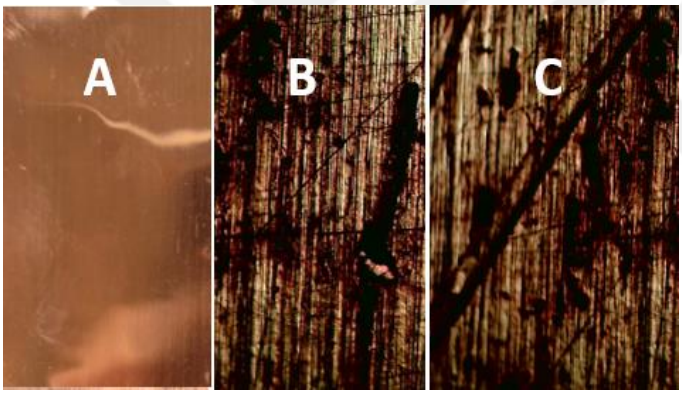

Figure 4.9 Microscopic images of electrodes under air pumping into water compartment, (a) clear copper electrode, (b) corroded copper electrode in water compartment, (c) corroded copper electrode in MO compartment at C= 10 g/l (500x zoom)

4.1.3 Effect of flow velocity

Table 4.4 shows the agitation velocity effect in the water chamber on the corrosion rate of copper electrodes in the two compartments. It can be seen that increasing agitation velocity from 150 to 450 rpm increases the corrosion rate of the two electrodes for the range of MO concentration of 3-10 g/l. This is because of the increase of oxygen transport from the solution bulk to the electrode surface (cathode) in the water compartment (Table 4.5). Oxygen works to increase the corrosion rate of cathode

electrodes, thus increasing CR of cathode electrodes increases the corrosion rate (CR) of anode electrodes as they are galvanically coupled. In general, the flow velocity in cathode chamber enhances the corrosion rate of both MO electrode and water electrode due to the effect of flow induced corrosion. This finding agrees with previous works of different authors (Hasan 2014, Ali and Hasan 2020).

Table 4.4 The effect of agitation velocities in the water compartment on the corrosion rate of two compartments for copper electrodes

MO Concentration	Speed in cathode chamber, rpm	Cu corrosion rate in anode chamber, gmd	Cu corrosion rate in cathode chamber, gmd
Yeast 3 g/l	150	5.19	2.30
	300	6.57	3.38
	450	8.65	4.61
Yeast 6 g/l	150	1.15	1.92
	300	5	4.42
	450	5.76	4.80
Yeast 10 g/l	150	1.6	1.9
	300	2.30	2.11
	450	4.23	2.30

Figure 4.10a shows stirring speed effect in the water compartment on the cell current density. Increasing speed results in an increase in current density but at high speed (450 rpm) a slight decline in current density occurs. The increase in the cell current density with increasing flow velocity in cathode compartment is ascribed to the increased oxygen arrival to the electrode surface which enhancing the oxygen reduction reaction. This increase in the reaction results in an increase of the corrosion rate of both electrodes in MO and water chambers. At high speed (450 rpm), air bubbles were formed on the surface of cathode electrode (Figure 4.10b). The air bubbles on copper electrode surface shifts the potential to more negative due to the resistance polarization and the current decreases in case of 450 rpm compared to 300 rpm because the air bubbles increase the electrical resistance around the electrode. Also, it can be seen that the increase in the agitation speed (450 rpm) resulted in an increase of O_2 transfer into the anode compartment.

Figure 4.11 shows potential trends in both compartments with time for different agitation speeds. The potential of both electrodes (anode and cathode) shift to more positive because increasing the dissolved oxygen concentration in both compartments (Table 4.4). The increasing electrodes potential means increasing CR of electrodes.

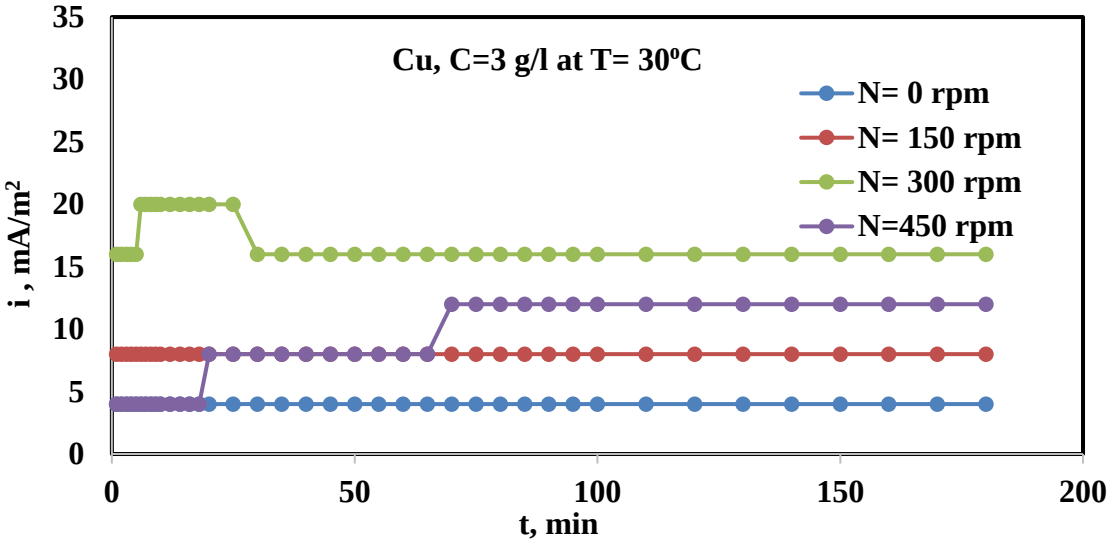

Figure 4.10 a) The current density for copper electrode at different agitation velocities in water chamber at MO concentration of 3 g/l

b) The photograph showing air bubbles on the copper electrode (cathode) at N= 450 rpm

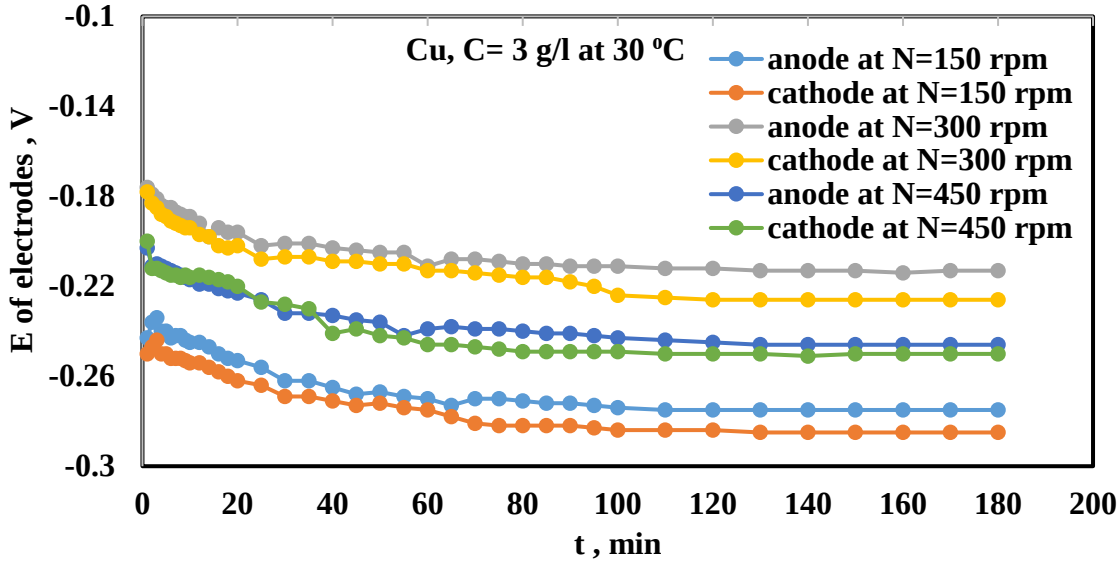

Figure 4.11 The effect of different agitation velocities into water compartment on copper electrodes potential for water and MO compartments at C=3 g/l.

Table 4.5 lists the measured dissolved oxygen concentration in MO (anode) and water (cathode) chambers. When the compartment is open to the atmosphere, increasing the agitation speed, causes transport of oxygen from atmosphere to the water chamber. Then, the O_2 transfers from water chamber to the MO chamber via the salt bridge. This increase of O_2 concentration in both chambers may affect the corrosion rate by affecting the microbe's activity and oxidation reactions.

Table 4.5 Measured dissolved oxygen (DO) concentration in both compartments at different agitation velocities, at C = 3 g/l and T= 30ºC

Agitation velocity (rpm)	DO concentration in MO chamber mg/l	DO concentration in water chamber mg/l
0	2.4	6.1
150	2.5	6.4
300	2.9	6.9
450	3.1	7.1

Figures 4.12 show microscopic images of electrodes after the cathode compartment has been exposed to the agitation velocity of 450 rpm. According to these images, CR in anode electrode is more than in cathode electrode.

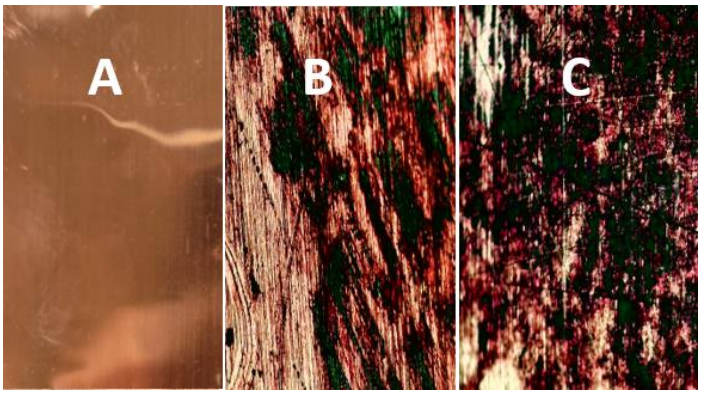

Figure 4.12 Microscopic images of (a) clear copper electrode, (b) corroded copper electrode in water compartment, (c) corroded MO compartment electrode, at C= 3 g/l, 450 rpm agitation velocity and the magnification of 500x

4.1.3 Effect of air pumping 2.51 l/min and flow velocity

Table 4.6 shows the effect of agitation velocity, 150, 300 and 450 rpm, respectively, and 2.51 l/min of air pumping in the water compartment on corrosion rate of electrodes at different MO concentrations. It is notable that at 3 g/l MO concentration, increasing agitation velocity between 150-450 rpm with 2.51 l/min of air pumping in the water compartment, the corrosion rate of copper electrodes increases because of increasing turbulence of the solution and this turbulence of solutions may remove the protective films (copper oxide).

Figure 4.13 shows effect of agitation velocities and pumping in the water compartment on current density at the MO concentration of 3 g/l. These results show that an increase in the agitation speed leads to an increase in current because of the increase in the potential difference. It is indicated that there is no decrease in current density even at high velocity. The disturbances within the solution remove the corrosion layer that is formed on the copper electrodes surface, so the current density continues to increase even at high speed. The steady-state current density values are 8, 10, 12, and 16 mA/m^2 at 0, 150, 300 and 450 rpm, respectively.

Figure 4.14 shows microscopic images of electrodes at 450 rpm agitation velocity and air pumping into the water compartment, at 3 g/l MO concentration, and T= 30°C. It is clear that the corrosion on the anode electrode surface is more than the corrosion on the cathode electrode surface.

Table 4.6 The effect of air pumping 2.51 l/min and different agitation velocities in water compartment on the corrosion rate of copper electrodes in two compartments at different MO concentrations

MO Concentration	Speed, rpm in cathode chamber	Cu corrosion rate in anode chamber gmd	Cu corrosion rate in cathode chamber gmd
Yeast 3 g/l	150	2.69	1.15
	300	3.65	3.07
	450	5.96	5.19
Yeast 6 g/l	150	2.5	2.3
	300	5.38	2.11
	450	5.57	3.84
Yeast 10 g/l	150	2.8	2.4
	300	5.19	4.03
	450	6.3	4.92

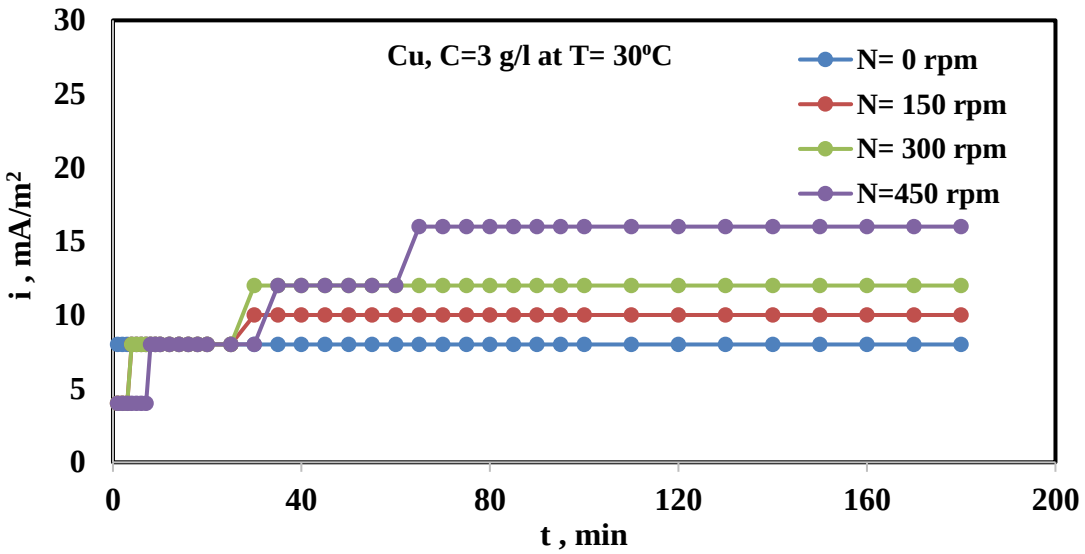

Figure 4.13 Current densities vs. time for copper electrode for air pumping and different agitation velocity at MO concentration of 3 g/l

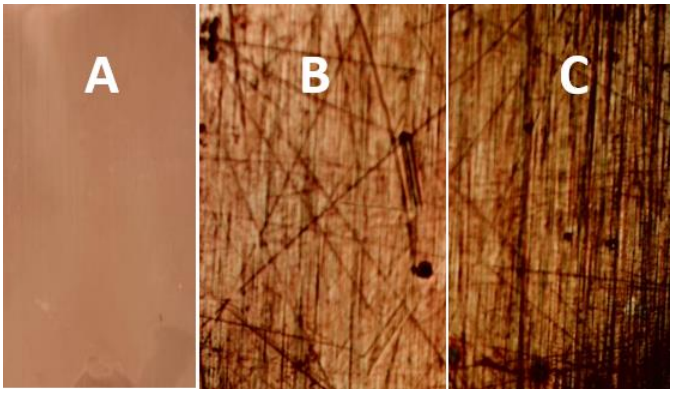

Figure 4.14 Microscopic images of (a) clear copper electrode, (b) corroded copper electrode in water compartment, (c) corroded copper electrode in MO compartment, at C= 3 g/l, 450 rpm agitation velocity and air pumping into the water compartment (500x zoom)

4.2 Corrosion of Stainless Steel (316) Electrode in MFC

4.2.1 Effect of MO concentration

Table 4.7 presents the corrosion rate of stainless steel (SS) in both MO (anode) chamber and water (cathode) chamber for different MO concentrations at 30ºC and 2g/l sodium acetate. It is obvious that the CR of SS increases with increasing the MO concentration. At 3 g/l of MO concentration, the corrosion rate of electrodes is zero. The cell current density at this concentration is also zero as shown in Figure 4.15. This can be ascribed to the fact that the bacteria form a thin biofilm on SS electrode surface which produces a negligible amount of current on stainless steel electrode surface. Figure 4.16 shows a little defect of the SS surface at 3 g/l. This indicates the high corrosion resistance of SS in the MO solutions. Increasing the MO concentration to 6 and 10 g/l causes a clear generation of current as in Figure 4.17 and a noticeable corrosion rate of SS (as in Table 4.7). The amount of electroactive biofilm produced on the electrode surface determines the increase in electrochemical performance (Yuvraj et al. 2017). Stainless steel contains metallic components that enhance bacteria metabolism and so facilitate biocorrosion (Lopes et al. 2006). Another reason is that the potential difference between the electrodes is very low as shown in Figure 4.18. The small potential difference between SS electrodes in both chambers plays an importance role for low produced current values. This is attributed to

the electrochemical properties of SS, which is high from corrosion standpoint and low from biological current production standpoint.

The increase in the produced current with increasing the MO concentration is ascribed to the increase in the thickness of biofilm on anode surface of SS. Biofilms have long been recognized as powerful microbial corrosion catalysts because they catalyze the reduction of dissolved oxygen on stainless steel (Equation 4.4) (Bergel et al. 2005, Scotto and Lai 2016):

$$O_2 + 2H_2O + 2Me \rightarrow 2Me(OH)_2 \quad (4.4)$$

where Me is the metal atom. The underlying alloy's oxidation provides the electrons taken from the substance by the cathodic process (Hamilton 2003). The first impact is an increase in free corrosion potential (potential ennoblement), which causes the oxide layer that shields stainless steel from corrosion to be disrupted. The disruption of the biofilm may increase the possibility of corrosion (Erable 2012) (Figures 4.16-4.17).

Table 4.7 The effect of MO concentrations on the corrosion rate of stainless-steel electrodes

MO Concentration	**SS corrosion rate in anode chamber gmd**	**SS corrosion rate in cathode chamber gmd**
Yeast 3 g/l	0	0
Yeast 6 g/l	1.5	0.23
Yeast 10 g/l	3.65	1.53

Figure 4.15 illustrates the MO concentration effect on current density. The increase in concentration from 6-10 g/l resulted in an improvement in MFC performance with the increase in the current density produced. At 3 g/l a current density was zero because the potential difference between electrodes is too low as show in Figure 4.18. The maximum steady-state current density is 4 mA/m^2 at 6 g/l and 10 g/l. This behavior is dependent on the surface morphology, adhesion properties and electrochemical properties of stainless steel which affects the formation of the biofilm. Also, there is an increase in current density and a decrease in potential in the first half-hour of the run followed by a state of stability. This depends on the activity of microorganisms, the efficiency in the

transmission of electrons to the electrodes, and conductivity of the electrode and of solution. Hisham et al. (2013) deduced that the sudden drop and rise in performance of MFC might be due to the biofilm formed on the conductor surface, which has completely detached itself from the conductor. To replace the previous deteriorated biofilm, a new one is created. The energy produced on such electrode is dependent on the electrochemical behavior of this metal, and adhesion of biofilm on this metal and its thickness (Salam et al. 2020). Images (Figure 4.16) indicate slight corrosion for bacterial concentration of 3 g/l, while Figure 4.17 indicates appreciable corrosion in 10 g/l MO concentration which support the CR values in Table 4.7.

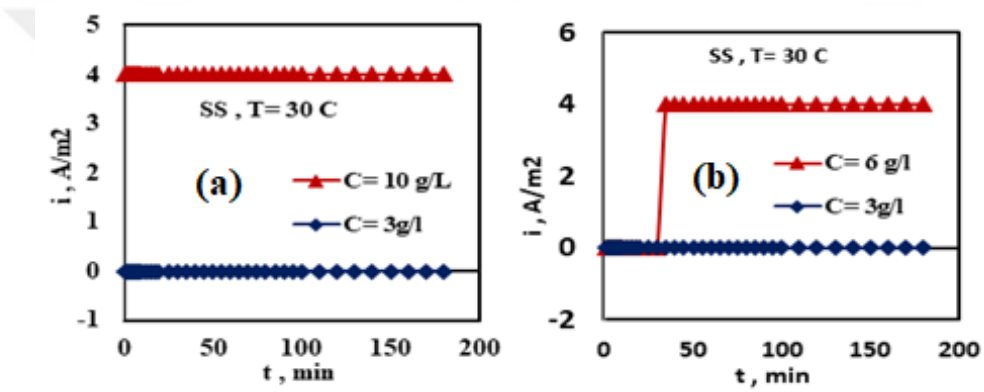

Figure 4.15 Current vs. time graphs of SS electrodes at (a) 3 g/l and 10 g/l, (b) 3 g/l and 6 g/l MO concentrations

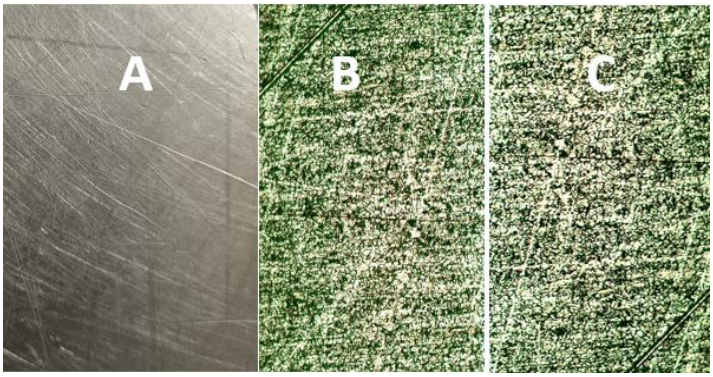

Figure 4.1**6** Microscopy image of (a) clear stainless-steel electrode, (b) corroded SS electrode in water compartment, (c) corroded SS electrode in MO compartment, at C= 3 g/l (500x zoom)

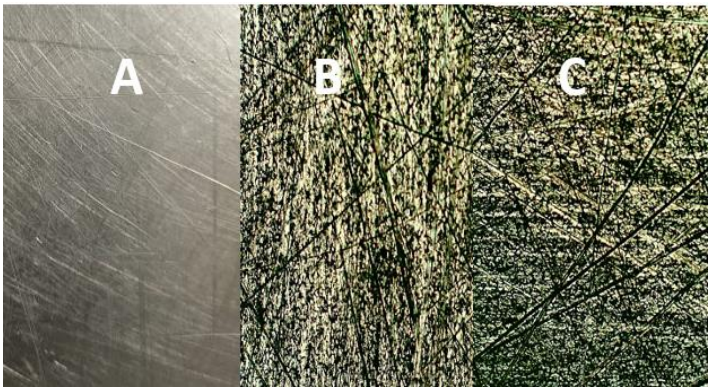

Figure 4.17 Microscopy image of (a) clear stainless-steel electrode, (b) corroded SS electrode in water compartment, (c) corroded SS electrode in MO compartment, at C= 10 g/l (500x zoom)

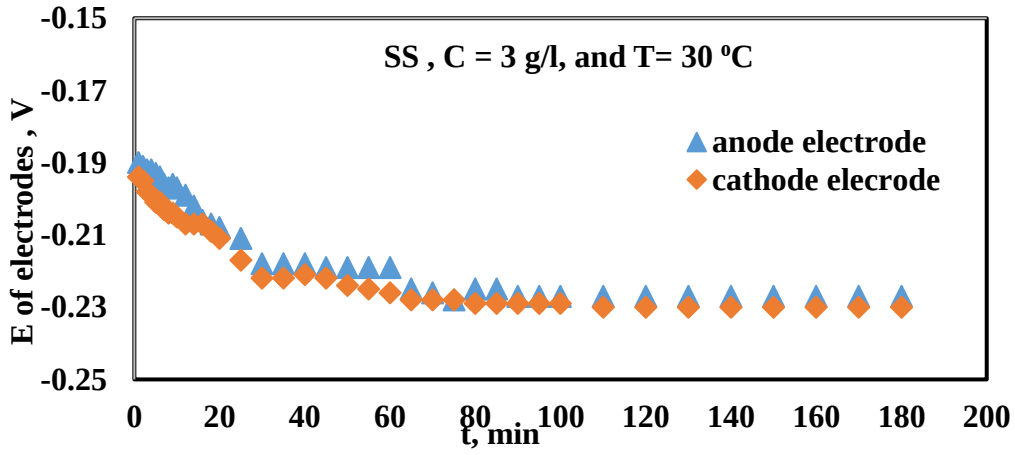

Figure 4.18 Electrode potentials vs. time for anode and cathode electrodes at MO concentration of 3 g/l

4.2.2 Effect of air pumping

Table 4.8 presents the corrosion rate (CR) of SS in MFC under the effect of air pumping in the water chamber for different MO concentrations. Comparing Table 4.8 with 4.7 indicates that the air pumping in cathode chamber causes an increase in the corrosion rate of SS in both chambers. The increased oxygen concentration in the aerated chamber enhances the oxidation of SS and reduction reaction of O_2 on SS surface which increases the CR of both terminals. The reason is the aeration of water compartment increases the dissolved oxygen in cathode (as shown in Table 4.3) which causes an increased corrosion

rate in cathode electrode and that lead to an increase in the CR at anode electrode as they are galvanically coupled.

Table 4.8 The effect of air pumping 2.51 l/min in cathode chamber at different MO concentrations on the corrosion rate of stainless-steel electrodes

MO Concentration	SS corrosion rate in anode chamber gmd	SS corrosion rate in cathode chamber gmd
Yeast 3 g/l	0.19	0.17
Yeast 6 g/l	2.29	1.31
Yeast 10 g/l	5.57	4.61

Figure 4.19 shows the comparison between the potential of stainless-steel electrodes in anode chamber and cathode chamber in the presence and absence of aeration in the water compartment versus time at 3 g/l MO concentration. It is clear that no difference between potential of electrodes (anode and cathode) in the presence and absence of aeration in the water compartment. This explains why the current density is zero and the CR is low for this concentration. The zero current indicate that the oxidation and reduction reaction in both chambers are very little or absent.

Figures 4.20 and 4.21 show air pumping effect in the water compartment on the potential of the MO electrode at 6 g/l and 10 g/l concentrations of MO, respectively. It can be seen that there is an increase in the potential of SS in the MO solution due to aeration of the water compartment. It is indicated that the tendency of the MO electrode towards the positive direction can be due to the passage of oxygen across the salt bridge that affects the active bacteria shifting the potential to more positive. Another reason for the potential shift is that the presence of air in the water compartment increases the potential at this compartment which in turn increases the potential in the MO compartment due to the galvanic effect based on the concept of mixed potential theory (Table 4.3) (Revie and Uhlig 2011).

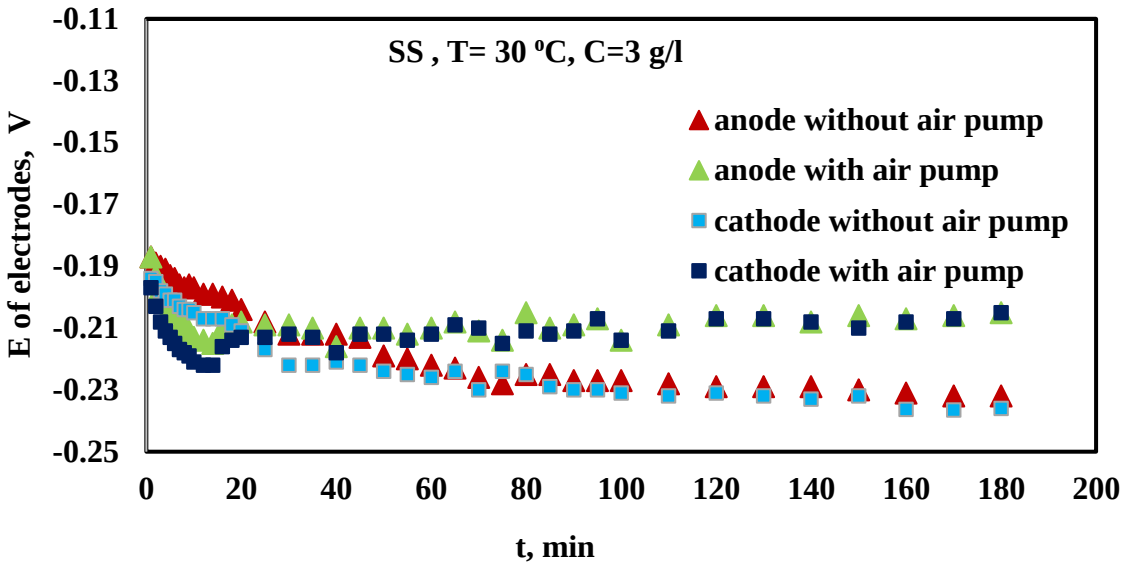

Figure 4.19 Comparison between the potential of SS electrodes in anode and cathode compartments (with and without air pumping into the water compartment) at 3 g/l MO concentration

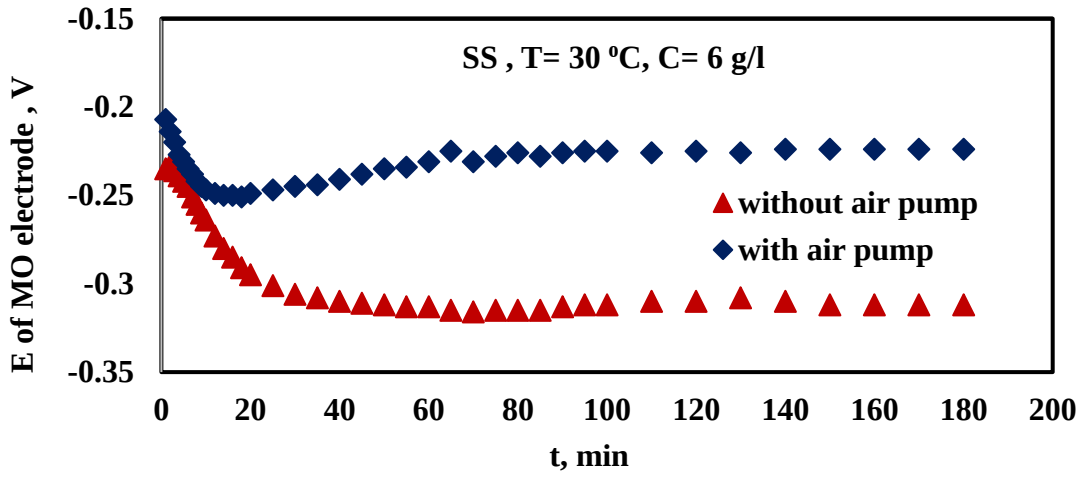

Figure 4.20 Electrode potential versus time for SS electrode in the MO chamber in the presence and absence of aeration for 6 g/l MO concentration

Figures 4.22 and 4.23 show the effect of air pumping into the water compartment on the current density at different MO concentrations of 6-10 g/l. The presence of air increases the currents by average percentages of 100% and 80% for MO concentrations of 6, and 10 g/l, respectively.

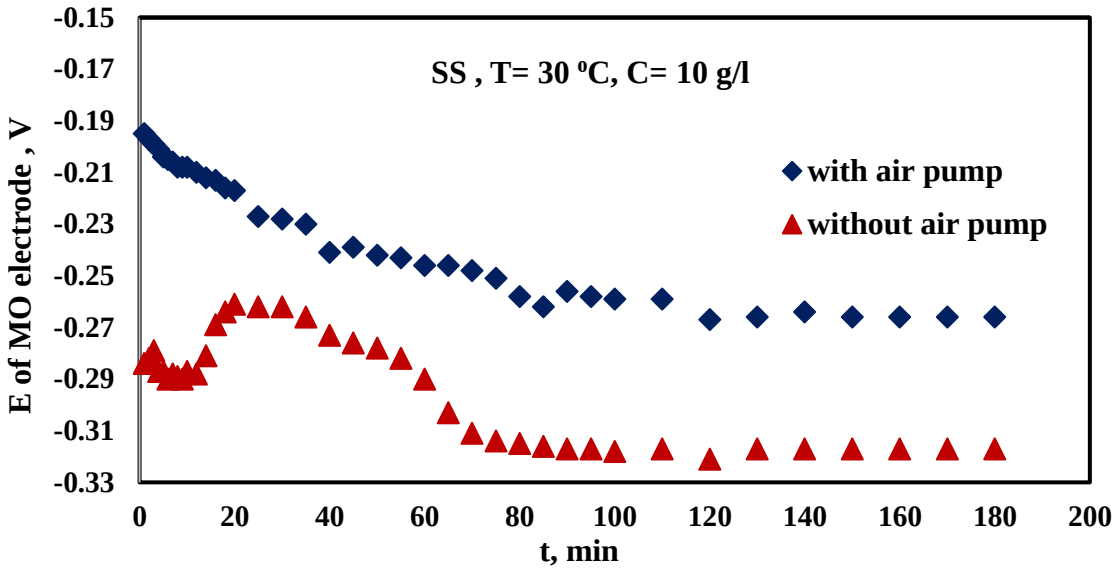

Figure 4.21 The potential versus time for SS electrode in the MO chamber in the presence and absence of aeration for 10 g/l MO concentration

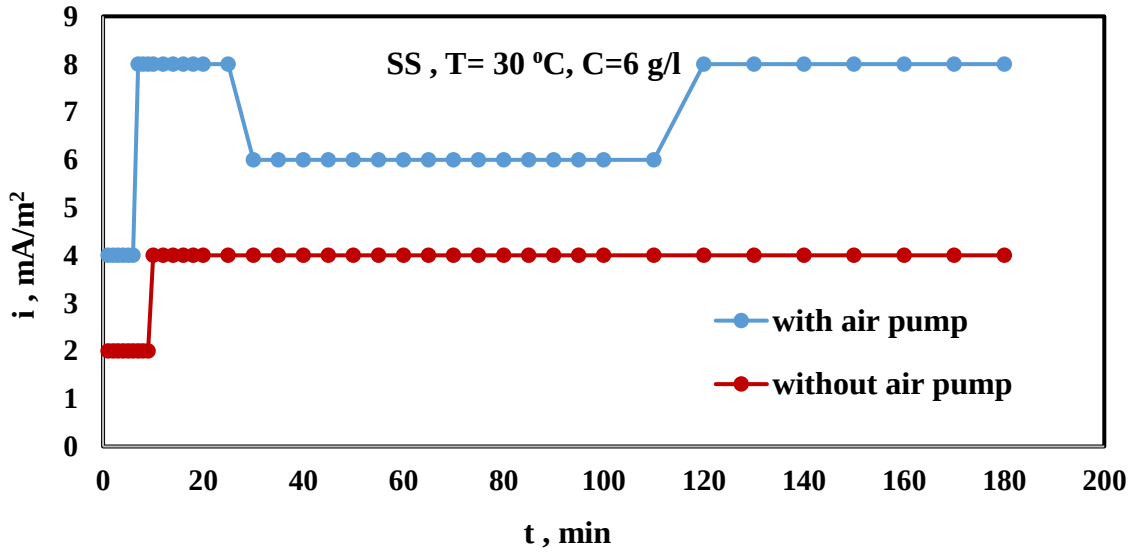

Figure 4.22 Effect of presence and absence of aeration into the water chamber on current density for stainless steel electrode at 6 g/l MO solution

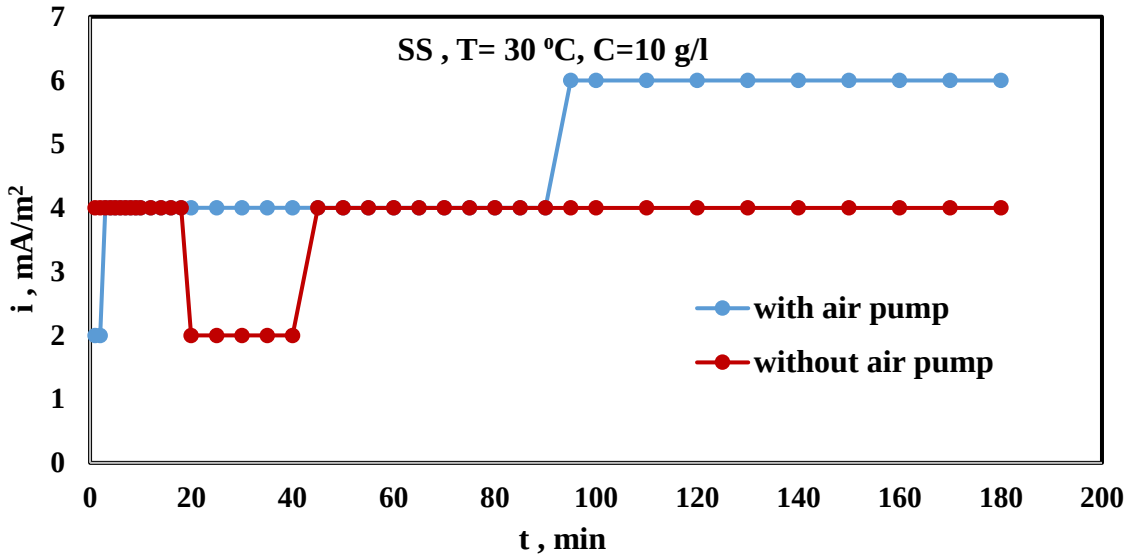

Figure 4.23 The current density in the presence and absence of aeration into the cathode chamber for stainless steel electrode at 10 g/l MO solution

4.2.3 Effect of flow velocity

Table 4.9 shows the effect of agitation velocities into the water compartment on the corrosion rate of stainless-steel electrodes of both compartments at 30ºC and 2g/l of sodium acetate. The result shows that increasing agitation velocities in the water compartment at 3-10 g/l MO concentration increases the corrosion rate of electrodes in cathode chamber. The reason is increasing dissolved oxygen concentration in the water chamber by speed increases. The corrosion of stainless-steel increases by an increase in the concentration of dissolved oxygen (Gong et al. 2020) (Table 4.5). For the anode electrode, bacteria may form a thin biofilm on stainless-steel surface. This thin biofilm has small effect on corrosion of electrode because of stainless steel corrosion resistance.

At MO concentrations of 6 g/l to 10 g/l, the corrosion rate in cathode chamber increases by increasing agitation velocities. The reason was explained previously (Cu electrode). Figure 4.26 shows the optical microscope images of stainless-steel electrodes at 450 rpm agitation velocity in the water compartment at C= 6 g/l and T= 30°C. The corrosion in the anode compartment is more than in cathode compartment.

Table 4.9 The effect of agitation velocities in the water compartment on the corrosion rate of stainless-steel electrodes

MO Concentration	Speed, rpm in cathode chamber	SS corrosion rate in anode chamber gmd	SS corrosion rate in cathode chamber gmd
Yeast 3 g/l	150	0	0
	300	0.28	0.32
	450	0.31	0.36
Yeast 6 g/l	150	1.5	1.2
	300	1.96	0.92
	450	2.2	1.3
Yeast 10 g/l	150	1.3	0.92
	300	2.2	1.83
	450	3.1	2.23

Figure 4.24 shows the effect of the different agitation velocity in the water compartment on the potential of SS in anode at 6 g/l MO concentration. This figure shows that increasing agitation velocity shifts the potential to more positive. This is due to the increased arrival of O_2 to the surface by convective transport from the solution bulk (Ferolis 1979, Slaiman et al. 2010, Ali and Hasan 2020).

Figure 4.25 illustrates the effect of agitation velocities in the water compartment at 6 g/l MO concentration on the produced current. There is a rise in the current density in the first half hour of run with increasing agitation velocity until the current density reaches a steady state at 4 mA/m^2. Increasing the dissolved oxygen concentration in MO compartment is not favorable for increasing MFC performance as has been pointed out by Karmakar et al. (2010).

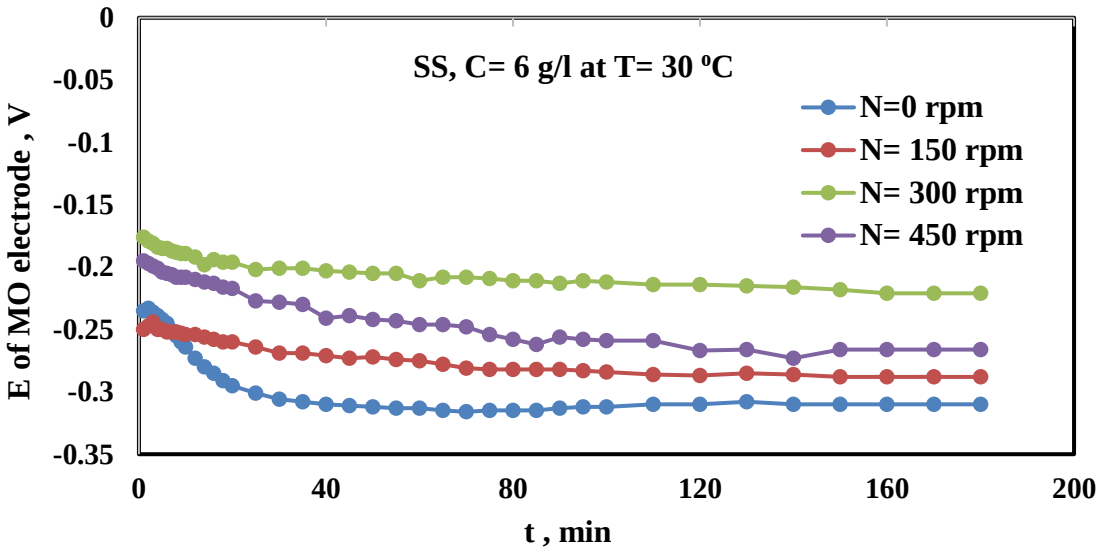

Figure 4.24 The effect of different agitation velocities into the water solution on the potential of SS electrode in the MO compartment at C=6 g/l

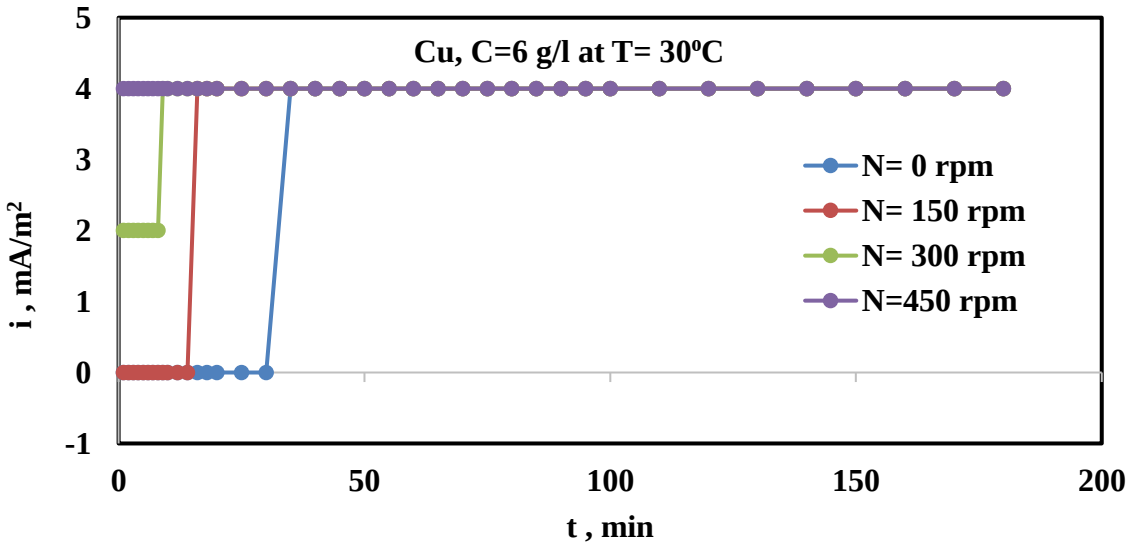

Figure 4.25 Effect of agitation velocities in the water compartment at 6 g/l MO concentration on the produced current

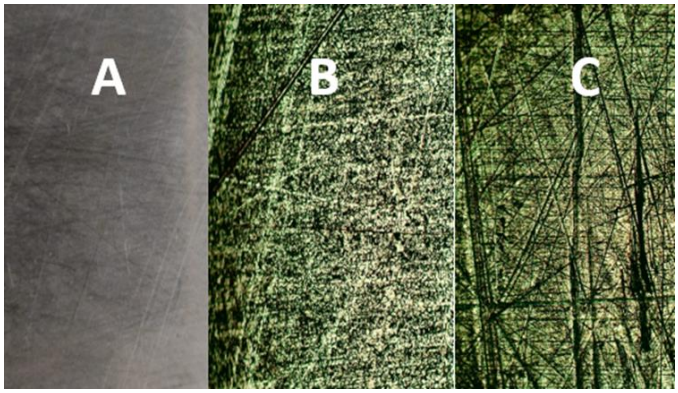

Figure 4.26 Microscopic image of (a) clear stainless-steel electrode, (b) corroded SS electrode of the water compartment, (c) corroded SS electrode of the MO compartment in the presence of agitation in the water compartment at C= 6 g/l (500x zoom)

4.2.4 Effect of pumping of air 2.51 l/m and flow velocity

Table 4.10 shows the effect of different agitation velocity and pumping of air 2.51 l/min into water compartment on the corrosion rate of SS electrodes in both cathode and anode chamber at different MO concentration, 2 g/l sodium acetate and T= 30°C. The results show that at 3 g/l MO concentration, increasing agitation speed and pumping of air into cathode compartment leads to increase corrosion rate of electrodes in the water compartment. The reason is increasing agitation velocity and air pumping remove passive layer on the surface of electrode. Stainless steel (316) is an iron-chromium alloy in which the chromium forms a thin coating of oxide on the steel's surface, known as the "passive" layer, which inhibits surface corrosion (Kim and Yu 2013). Hence, the removal of this layer causes increasing the corrosion rate. At 6 and 10 g/l MO concentration, increasing agitation velocities at 2.51 l/min of air pumping into the cathode chamber led to an increase in the CR value of both electrodes as show in Figure 4.30. Increasing agitator speed at air pumping in the water compartment has no effect on the potential of electrodes at C= 3 g/l. In this MO concentration of 3 g/l, the current density is zero because there is no potential difference between electrodes. The reason explained previously in the effect of air pumping for SS electrode.

Table 4.10 The effect of different agitation velocity at air pumping of 2.51 l/min into the water compartment on the corrosion rate of SS electrodes in both cathode and anode chamber at different MO concentrations

MO Concentration	Speed, rpm in cathode chamber	SS corrosion rate in anode chamber gmd	SS corrosion rate in cathode chamber gmd
Yeast 3 g/l	150	0.38	0.56
	300	0.51	0.92
	450	0.31	0.52
Yeast 6 g/l	150	5.76	2.88
	300	6.92	3.84
	450	7.43	4.21
Yeast 10 g/l	150	2.7	1.62
	300	3.46	3.07
	450	4.5	4.01

Figures 4.27 and 4.28 show the effect of the aeration (2.51 l/min) and different agitation velocity into the water compartment on the potential of anode and cathode electrodes at 6 g/l MO concentration. Those figures show that the potential of the MO electrode is more negative since DO is transferred from the water solution to the MO solution through the salt bridge and the potential of MO solution is sensitive to traces of O_2, which can weaken the MO activity (Bennetto et al. 1983). On the other hand, the SS electrode potential in the water solution is more positive.

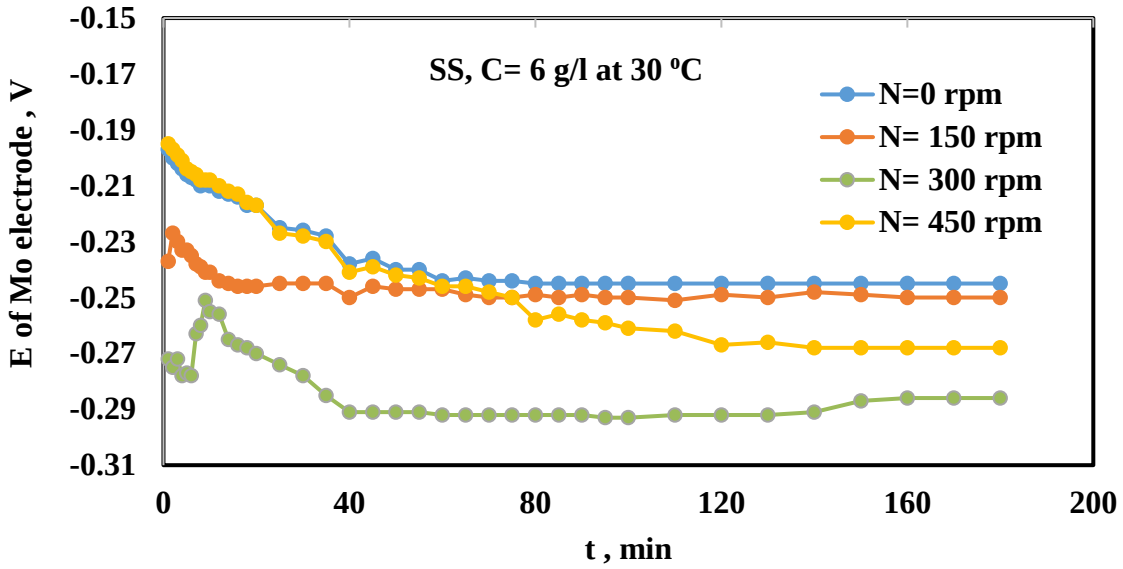

Figure 4.27 The effect of different agitation velocity at 2.51 l/min of air pumping into the water compartment on the SS electrode potential in MO compartment at 6 g/l MO solution

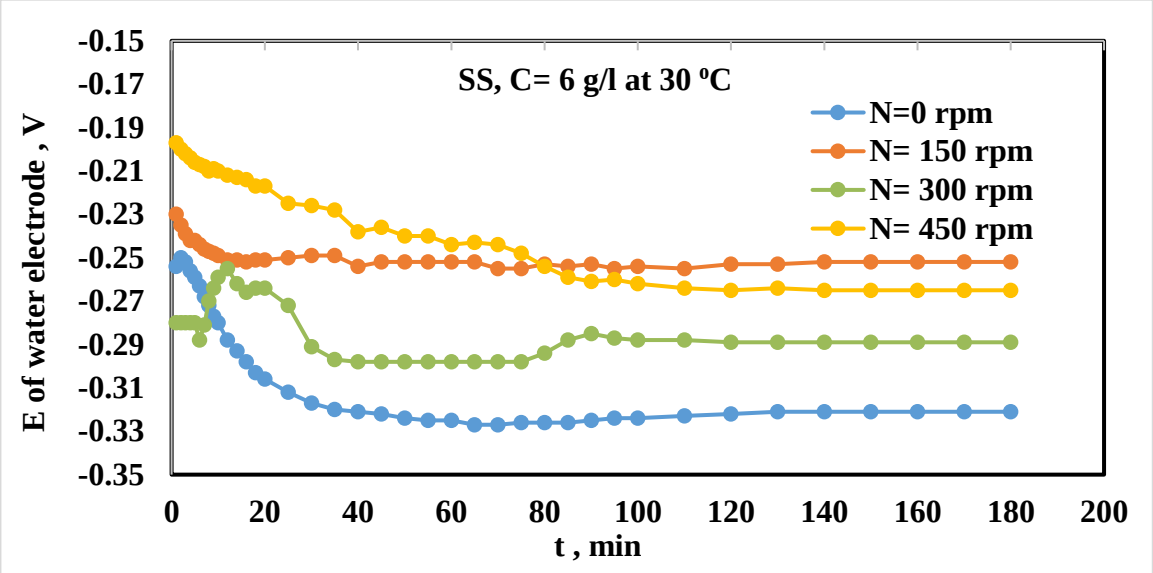

Figure 4.28 Effect of air pumping (2.51 l/min) and different agitation velocity into the water chamber on SS electrode potential in water solution at C= 6 g/l

Figure 4.29 exhibits the current density graph of the SS electrode in different agitation speeds at 2.51 l/min of air pumping into the water compartment at MO concentration of 6 g/l. As a general trend, increasing the agitation speed causes an increase in the cell current due to the increased O_2 reduction on the metals surface (Salam et. al. 2020).

Conspicuously that for all speeds the current increases with time to reach steady state value. It is notable that agitation at 300 rpm with air pumping gives high current density due to the increased O_2 concentration by aeration and O_2 transport to the electrode surface by stirring. For high speed (450 rpm) the presence of the air pumping reduces the current produced below 300 rpm. This is thought that the fact that the sever dispersion of air bubbles in the solution which arrives to the electrode surface reducing the electrical conductivity resulting in lower current flow in the cell as shown in Table 4.10b.

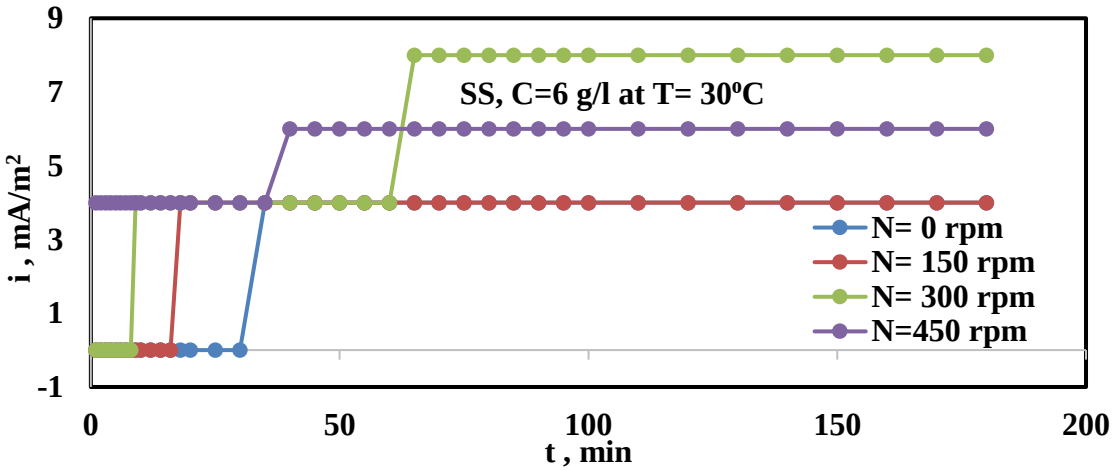

Figure 4.29 The current vs. time behavior of SS electrode for different agitation speeds at 2.5 l/min of air pumping into the water chamber at 6 g/l MO concentration

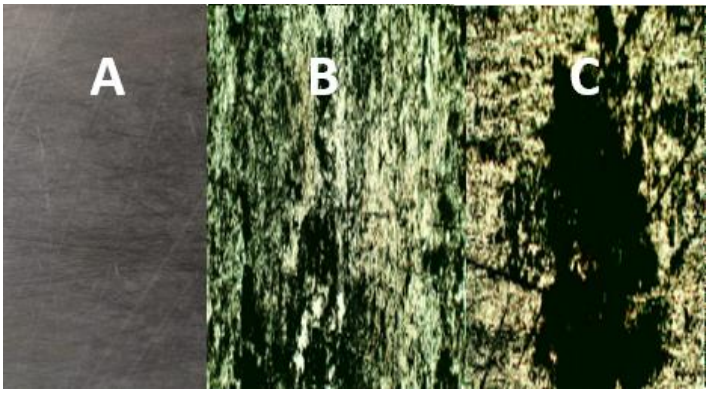

Figure 4.30 Microscopic image of (a) clear stainless-steel electrode, (b) corroded SS electrode of water compartment, (c) corroded SS electrode in MO compartment at agitation velocity and air pumping in water compartment at C= 6g/l (500x zoom)

4.3 Corrosion of Zinc Electrode in MFC

4.3.1 Effect of MO concentration

Table 4.11 shows the bacteria concentration effect on the corrosion rate of Zn electrodes in both anode and cathode chambers. When increasing the MO concentration from 3-10 g/l in anode chamber, the corrosion rate of Zn electrodes increases appreciably from 5.57 to 34.42 gmd (6.1 times). This increase is the highest when compared with SS and Cu electrodes. According to Zuo (2007) and Jia (2019), corrosion is either accelerated or slowed when a bacterial biofilm forms on zinc surface. Zinc is easily affected by bacteria and is easily covered by biofilm. Furthermore, the bacteria's (biofilm) attachment to the zinc has accelerated corrosion (Yu et al 2014). It is notable that the CR of zinc electrode in anode (MO) chamber is less than that of CR value in cathode (water) chamber as shown in Table 4.11.

Table 4.11 Bacteria concentration effect on the corrosion rate of zinc electrodes in both cathode and anode compartments

MO Concentration	Zn corrosion rate in anode chamber	Zn corrosion rate in cathode chamber
Yeast 3 g/l	5.57	16.92
Yeast 6 g/l	14.80	20.19
Yeast 10 g/	15.42	38.42

The higher corrosion rate in water chamber can be explained based on the potential values in Fig.4.31. It can be seen that the Zn electrode in MO chamber is more negative than that in water chamber. This causes higher corrosion rate in water chamber due to higher potential. This means that the presence of MO biofilm on Zn reduced the potential, and the metabolism might cause a production of some ions that leads to shift the potential to more negative which means less corrosion. The presence of biofilm may reduce the arrival of O_2 to the anode surface partially which causes the CR of the anode to be less than the CR of the cathode. The ions of zinc that formed on the surface of electrode through the corrosion of electrodes may be toxic to bacteria. Galvan et al (2018) reported that zinc oxide nanoparticles are toxic to the baker's yeast, Saccharomyces cerevisiae.

Dead bacteria deposit on the surface of zinc electrode (because of surface roughness) and prevent oxygen from reaching zinc surface, which leads to reduced corrosion on the anode electrode. Accordingly, in the MFC cell, increasing MO concentrations in one chamber causes an appreciable increase in the corrosion rate of both coupled electrodes.

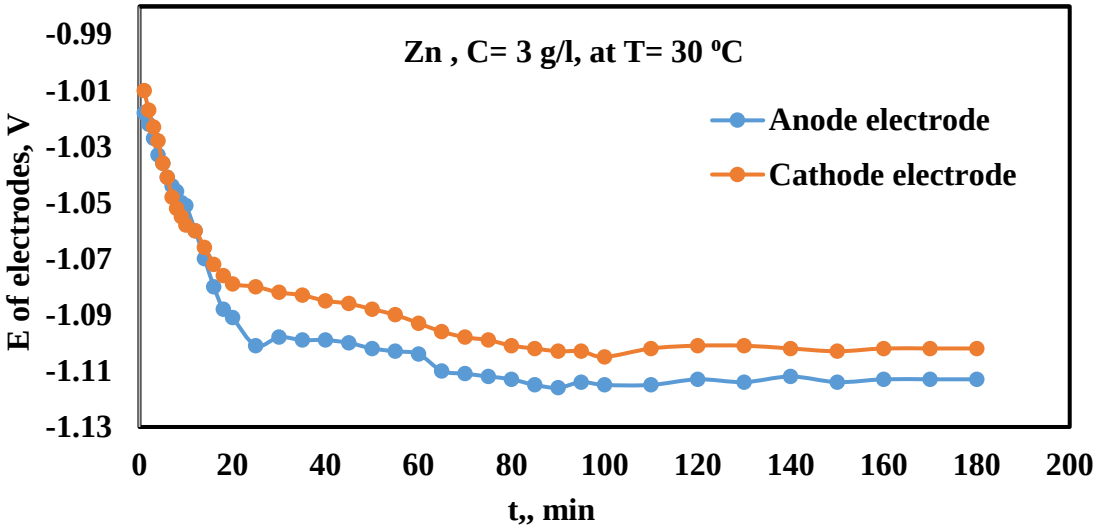

Figure 4.31 Electrode potentials of Zn at C= 6 g/l

Figures 4.32 and 4.33 illustrate the of microorganism concentration effect on the potential of Zinc electrode in MO and water solutions, respectively. Those figures show that an increase in bacteria concentration from 3 to 10 g/l results in a slight shift in Zn electrode potential in MO chamber to more positive. While in water solution increasing MO concentration gives rise to a prominent shift in Zn electrode potential into more positive. The cell currents (galvanic) increase as the potential differences between the two chambers increase as shown in Fig. 4.34. The MO chamber shows more negative potential than the water chamber. Consequently, as a general trend, the corrosion caused by concentration cell effect is higher in cathode chamber (Figure 4.35).

Figure 4.34 shows the MO concentration effect on the current density. It can be noted that increase MO concentration from 3 to 10 g/l increases the current density because of the bacteria oxidation and increased potential difference. A biofilm layer is created on the conductor surface of anode because of microorganism. Biofilm provides electron transfer

to the conductor (anode electrode). Therefore, biofilm formation and biofilm growth within the conductor (anode) will increase the power made in microorganism fuel cells (Karra 2013) (Figure 4.35).

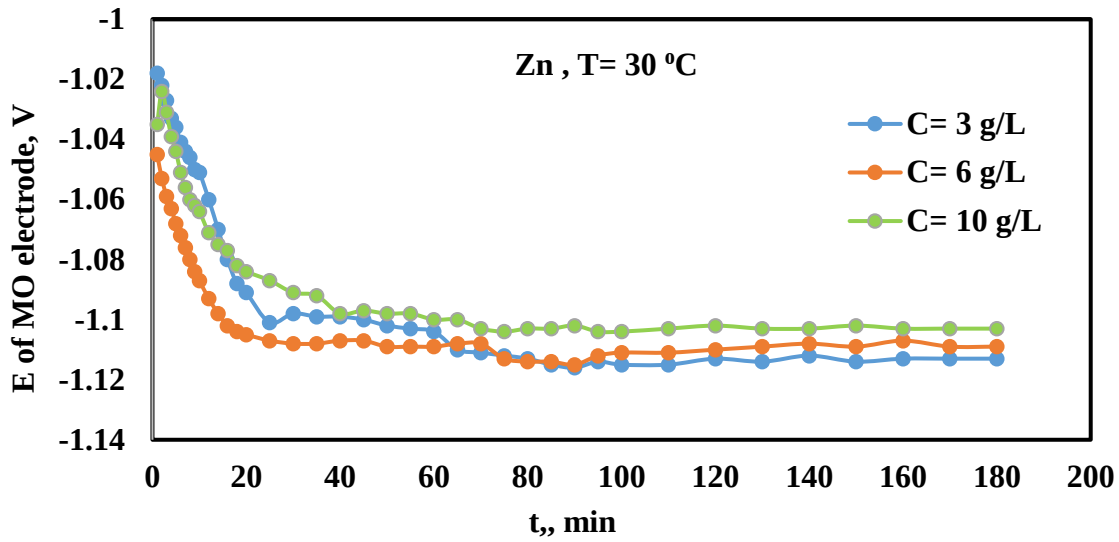

Figure 4.32 MO concentration effect on Zinc electrode potential in MO chamber

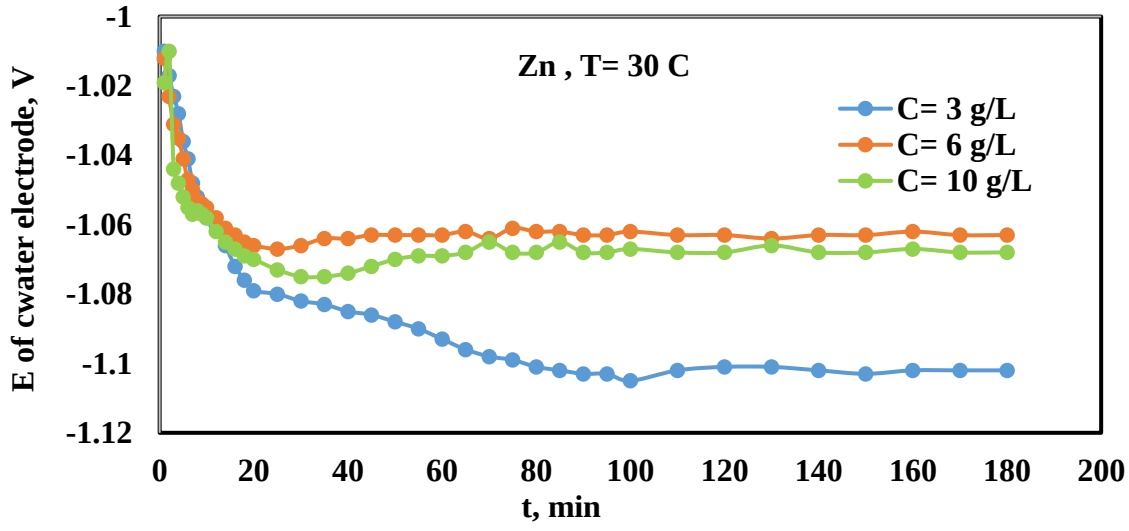

Figure 4.33 The effect of MO concentration on Zinc electrode potential in water compartment

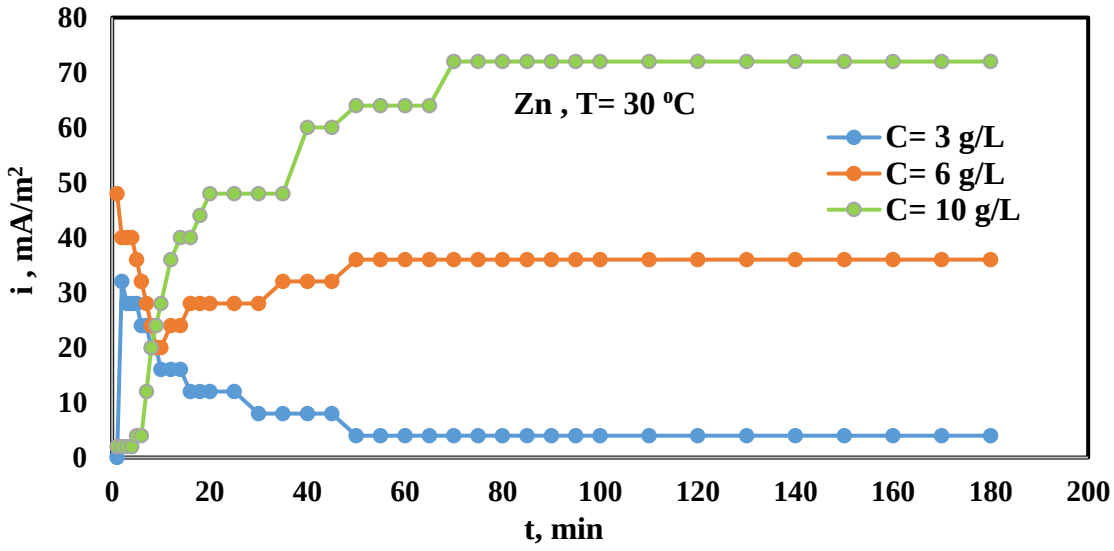

Figure 4.34 The effect of MO concentration on the current density of Zn electrodes

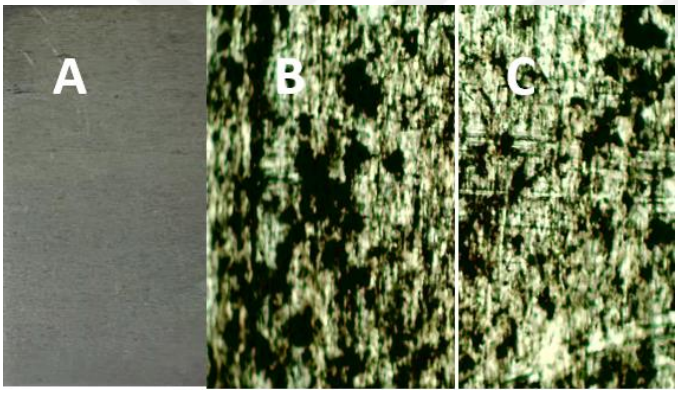

Figure 4.35 Microscopic image of (a) clear zinc electrode, (b) corroded Zn electrode in water compartment, (c) corroded Zn electrode in MO compartment at C= 3 g/l (500x zoom)

4.3.2 Effect of air pumping

Comparing Table 4.11 with Table 4.12 indicates that when pumping the air in water compartment, the corrosion rate of zinc electrodes in both compartments increases appreciably compared to the case of in the absence of air pumping. Table 4.12 shows the air pumping effect at different MO concentrations on the corrosion rate of zinc electrodes at 30ºC and 2g/l sodium acetate. It shows that increasing MO concentration increases the corrosion rate of electrodes in both chambers (cathode and anode) as shown in Figure

4.36 The corrosion rate in anode chamber is less than in cathode chamber as explained above in Zn electrode.

Table 4.12 The effect of air pumping in cathode chamber at different MO concentrations on the corrosion rate of zinc electrodes

MO Concentration with air pump 2.51 l/min	Zn corrosion rate in anode chamber gmd	Zn corrosion rate in cathode chamber gmd
Yeast 3 g/l	6.19	20.03
Yeast 6 g/l	15.38	25.92
Yeast 10 g/l	16.53	39.42

Figures 4.37a and 4.37b show a comparison of the zinc electrode potential in the MO and water compartments through the use of an air pumping in the water compartment. The result shows that air pumping into the water compartment shifts the electrode potential in water solution to more positive and shifts the electrode potential in MO compartment slightly to more positive since the high DO concentration in cathode chamber raise the electrode potential and for the anode chamber, the passage of oxygen across the salt bridge affects the active bacteria, shifting the potential to more positive.

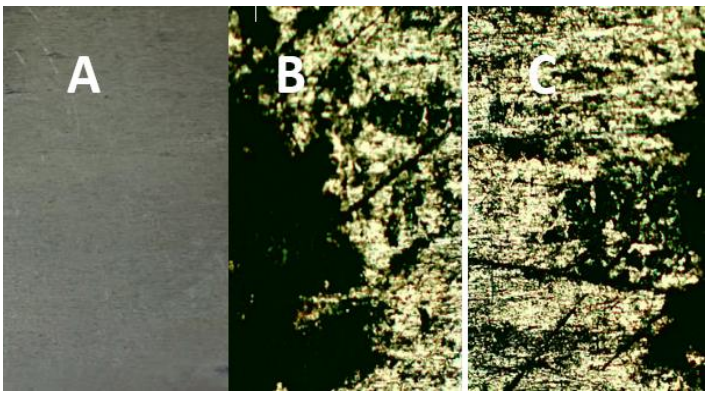

Figure 4.36 Microscopic image (a) clear stainless-steel electrode, (b) corroded Zn electrode in water compartment, (c) corroded Zn electrode in MO compartment at air pumping into the water compartment at C= 3 g/l (500x zoom)

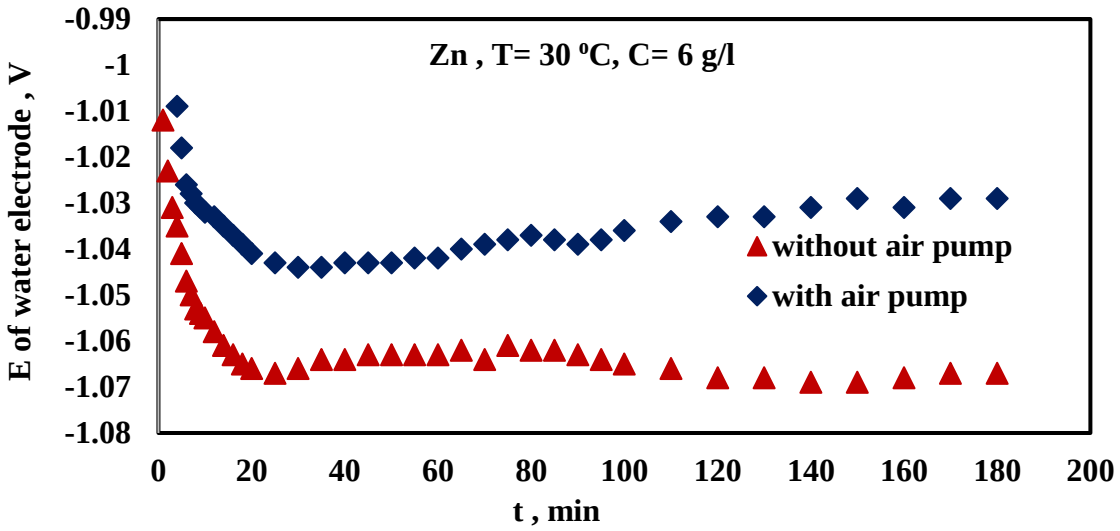

Figure 4.37 a) The air pumping effect in the water solution on the potential of the water electrode at 6 g/l of MO concentration

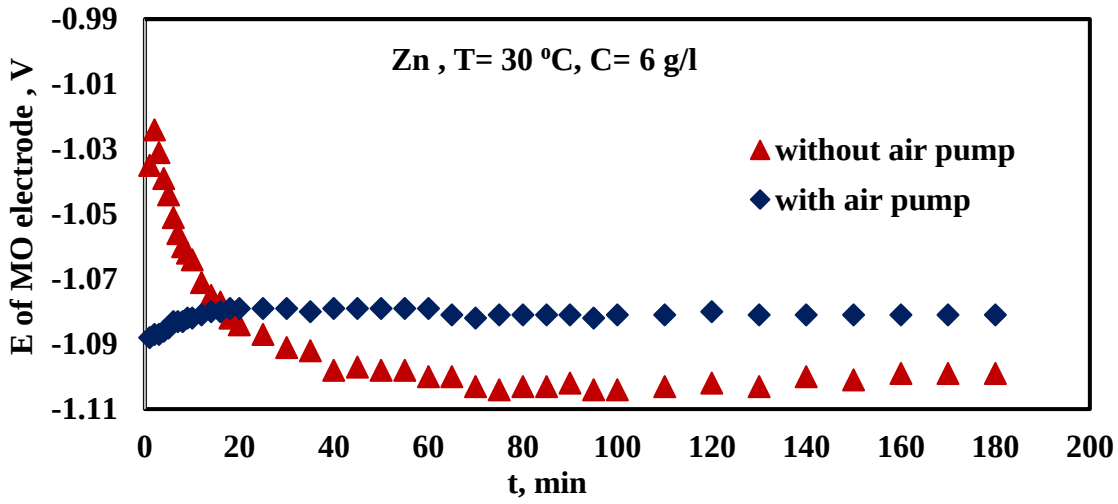

b) The effect of air pumping in the water solution on the potential of the MO electrode at 6 g/l of MO concentration

4.3.4 Effect of flow velocity

Table 4.13 shows different agitation velocity effect on the corrosion rate of zinc electrodes in both cathode and anode compartments at different MO concentrations at 2 g/l of sodium acetate. The results showed that at 3 g/l of MO concentration, increasing the agitation speed leads to increase in the electrode corrosion rate in the water compartment. The reason is agitation velocity increases the arrival of O_2 to the surface

and removes zinc oxide layer from the surface enhancing the corrosion. Zinc has the advantage of forming a film on the metal surface, which is produced by oxidation (patina) over time, this film layer significantly slows the corrosion of Zn itself (Kareta 2022). It is to be noted that the CR in the water chamber is much higher than in the MO chamber, indicating that the flow in water chamber enhanced the corrosion rate in both chambers (Figure 4.38).

Table 4.13 Agitation speed effect on the corrosion rate (CR) of zinc electrodes in cathode and anode compartments at different MO concentrations

MO Concentration	Speed, rpm in cathode chamber	Zn corrosion rate in anode chamber gmd	Zn corrosion rate in cathode chamber with agitation, gmd
Yeast 3 g/l	150	6.23	29.03
	300	9.23	26.34
	450	22.88	37.30
Yeast 10 g/l	150	6.32	33.52
	300	15.96	37.5
	450	23.65	44.65

Table 4.14 Measured DO concentration in two compartments at different agitation velocity at T= 30 ºC, 3 g/l MO concentration

Agitation speed (rpm)	DO conc. in MO solution mg/l	DO conc. in water solution mg/l
0	0.22	6.1
150	0.28	6.5
300	0.31	6.9
450	0.42	7.1

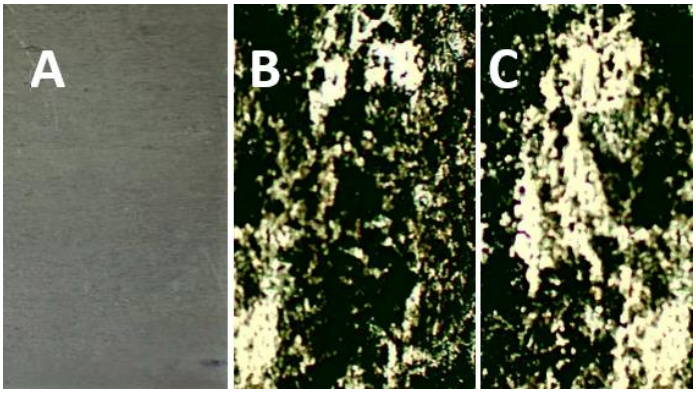

Figure 4.38 Microscopic image of (a) clear stainless-steel electrode, (b) corroded Zn electrode in the water compartment, (c) corroded Zn electrode in the MO compartment at 300 rpm agitation velocity in water compartment at C= 3 g/l (500x zoom)

Figures 4.39 and 4.40 show the effect of different agitation velocity in water chamber on zinc electrode potential in MO and water chambers, respectively. It is notable that when increasing agitation speed from 150 to 450 rpm in the water chamber, the potential of electrode in the MO compartment shifts slightly to a more positive value. In water compartment, it shifts to a much more positive value because of the lower DO concentration in the MO compartment compared with the water compartment (Table 4.14). In the cathode compartment, the potential under flow conditions is more positive than stationary condition because of the arrival of more O_2 to the cathode surface (Hamad and Hasan 2015).

Figure 4.41 shows the effect of agitation velocity in the water chamber on the cell current. Increasing speed from 150 to 450 rpm leads to an increase in the current density. Increasing speed leads to increase the oxygen transport to the cathode surface which increase the potential difference between the two chambers. This causes an increase in the oxidation reactions in the MO compartment and O_2 reduction reaction in the water compartment which results in an increase in the cell current. This agrees with the observations from the literature (Salam et al. 2020, Abdul-Wahid et al. 2021).

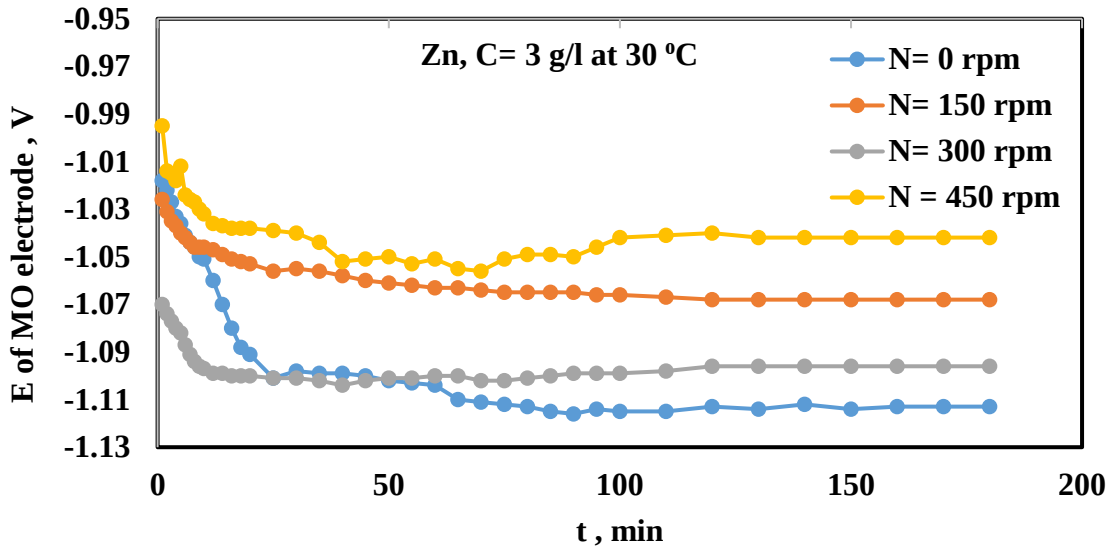

Figure 4.39 Effect of different agitation velocity in the water compartment on the Zn electrode potential of the MO compartment at 3 g/l of MO concentration

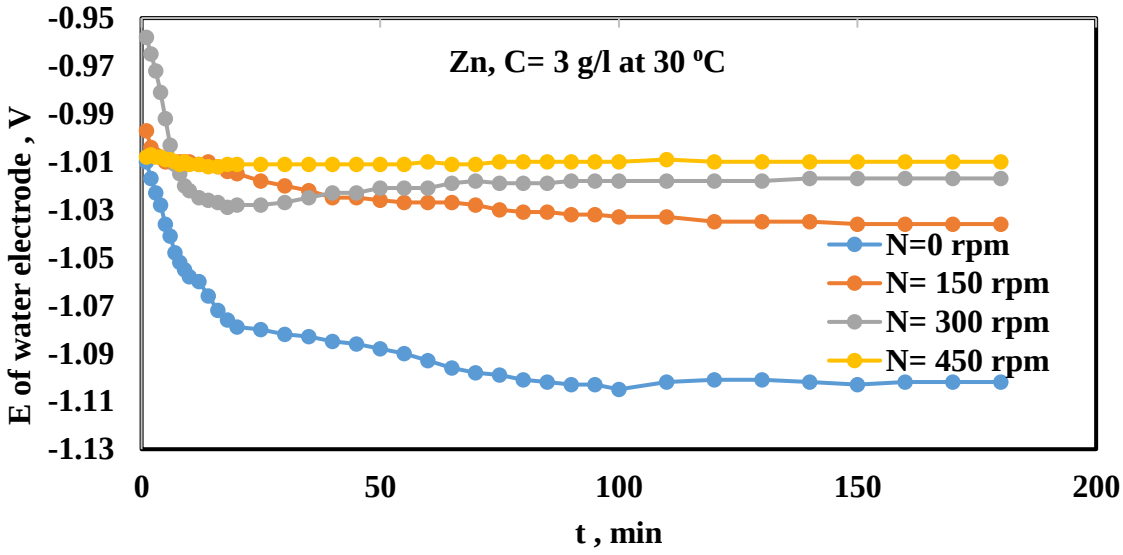

Figure 4.40 Effect of different agitation velocity in the water chamber on the zinc electrode potential of the water chamber at 3 g/l of MO solution

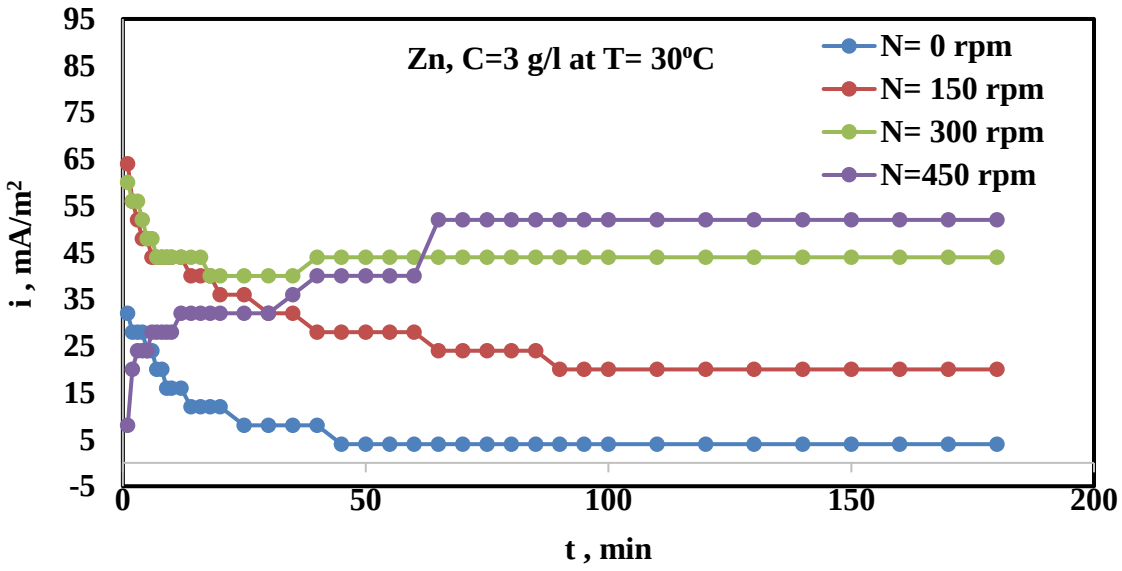

Figure 4.41 The effect of different agitation velocity in the water compartment on current density of zinc electrode at 3 g/l of MO concentration

4.3.4 Joint effect of air pumping and agitation velocity

Table 4.15 shows the CR values in both cathode and anode chambers at different MO concentration for under joint effect of agitation velocity and air pumping into the water compartment. The results show that increasing the agitation velocity with air pumping in the water compartment cause a considerable increase in CR of Zn electrode in the water compartment (Figure 4.42). It can be seen that the increase of CR with the agitation in presence of air is not uniform. This can be attributed to the high dispersion of air bubbles in the solutions which play two conflicting roles. The first is that the dispersion of air bubbles increases the concentration of O_2 in the solution which enhances the CR in water chamber and, thus, in the MO chamber. The second role is reduction of the solution electrical conductivity which reduces the CR value and the corrosion current especially when the bubble touches the electrode surface.

Table 4.15 The effect of the agitation velocity and air pumping in water compartment on the corrosion rate of zinc electrodes in both cathode and anode chambers at different MO concentrations

MO Concentration	Speed, rpm in cathode chamber	Zn corrosion rate in anode chamber gmd	Zn corrosion rate in cathode chamber gmd
Yeast 3 g/l	150	5.19	35.96
	300	28.30	44.76
	450	23.46	46.15
Yeast 10 g/l	150	6.8	55.23
	300	43.26	51.73
	450	45.87	62.79

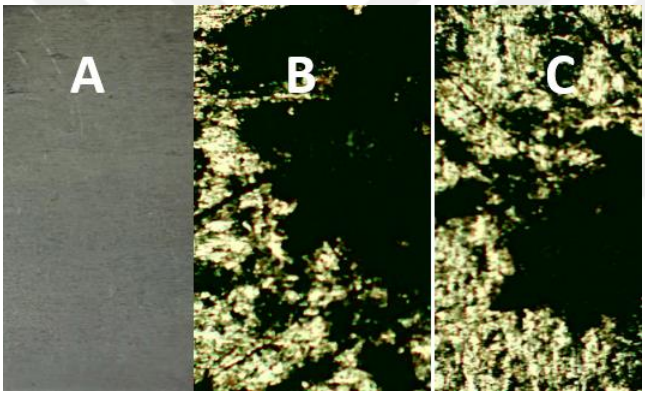

Figure 4.42 Microscopic image of (a) clear stainless-steel electrode, (b) corroded Zn electrode in the water compartment, (c) corroded Zn electrode in the MO compartment at 300 rpm agitation velocity and air pumping in the water compartment at C= 3 g/l (500x zoom)

Figure 4.43 shows the effect of the agitation velocity and pumping of air in the water chamber on cell current density at 3 g/l MO concentration. This figure shows that an increase in the agitation velocity with air pumping leads to an increase in current density because of the increase in the potential difference and increased oxidation and reduction reactions in both compartments. The maximum steady-state current density values are 4, 32, 12, and 92 mA/m^2 at 0-450 rpm, respectively.

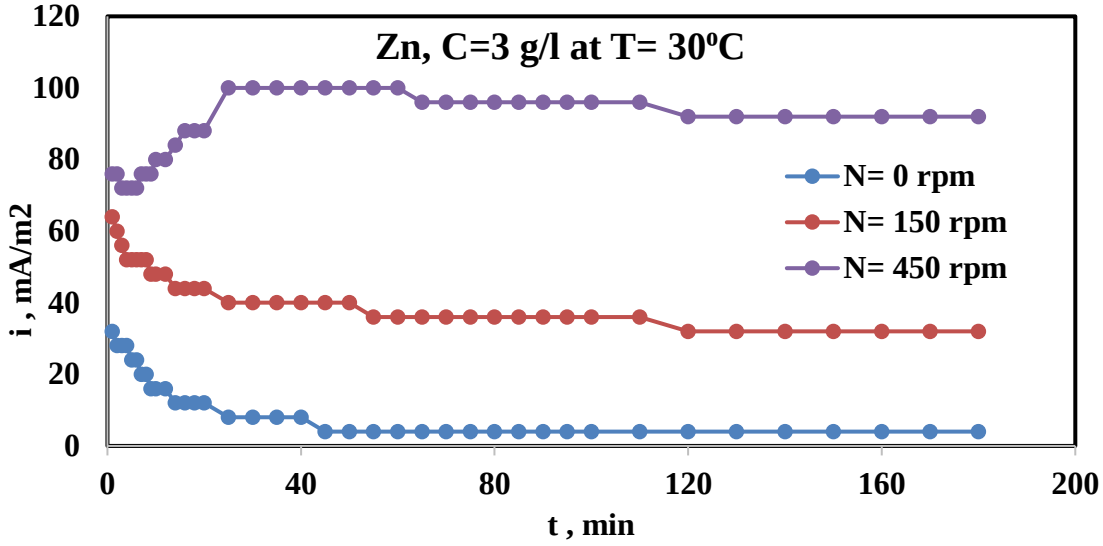

Figure 4.43 Effect of the agitation velocity and air pumping in the water compartment on the current density of zinc electrodes

4.4 Comparison Among the Copper, Stainless steel and Zinc Electrodes

4.4.1 Microorganism concentration effect

Figure 4.44 shows the comparison between corrosion rates of three electrodes at different MO concentrations. The corrosion rate of stainless steel is zero at low MO concentration and it is lower than copper and zinc electrodes because SS has high corrosion resistance. Figures 4.45 and 4.46 show the potential of three electrodes (anode and cathode chambers) at the microorganism's concentration of 3 g/l. It can be noted that there is a large difference between zinc potential and copper and stainless-steel electrodes. This is because zinc is more active and weaker in neutral and acidic solutions, thus its corrosion rate is high, and it is not recommended for microbial fuel cell. SS has the lowest corrosion rate in MFC medium and thus it is successful from corrosion point of view.

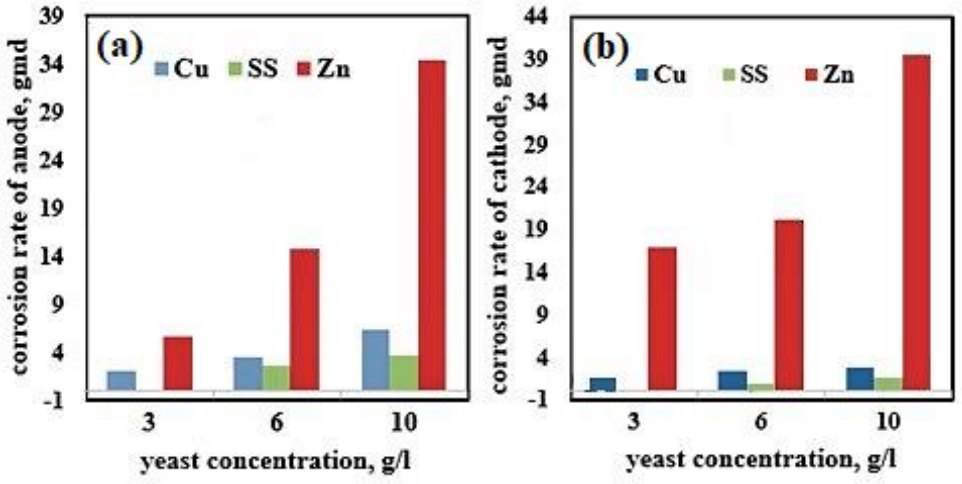

Figure 4.44 The comparison between corrosion rates of three electrodes at different MO concentrations, (a) CR in the anode (b) CR in the cathode

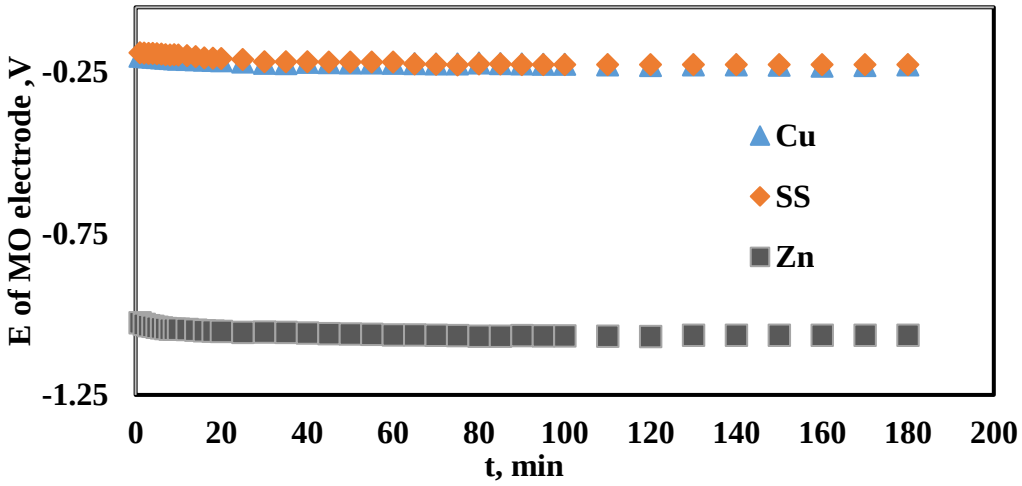

Figure 4.45 The potential of the MO electrode for three electrodes at the microorganism's concentration of 3 g/l

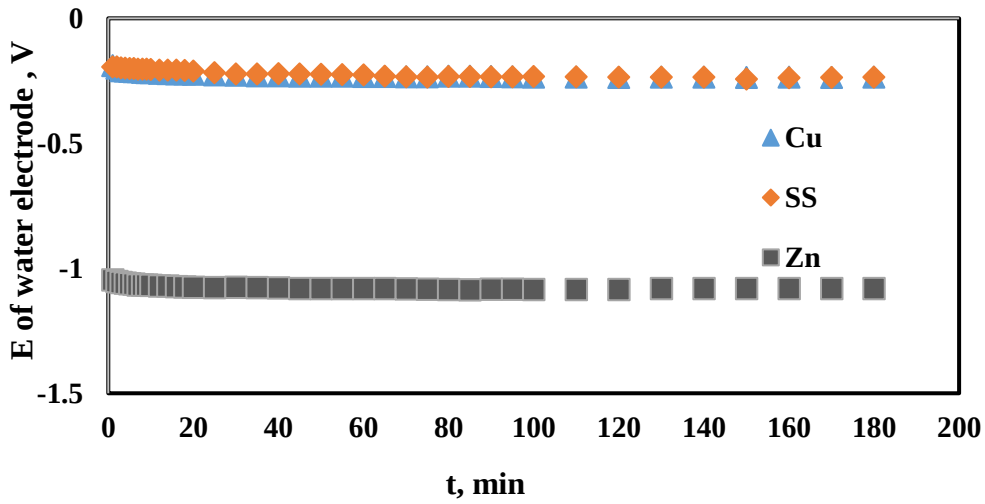

Figure 4.46 The potential of the water electrode for three electrodes at the concentration of microorganisms 3 g/l

Figure 4.47 shows the current density flowing in cell between three different electrodes at the microorganism's concentration of 10 g/l. The steady state current density of these electrode is 16, 4, and 70 mA/m^2 for copper, stainless steel and zinc respectively. Therefore, the highest current is provided by Zn, but a major part of this current is produced by the corrosion of Zn in both compartments. The SS produced the lowest current density indicating the high corrosion resistance.

In MFC, the produced current is dependent on several factors such as the adhesion of biofilm on the electrode surface, the thickness of that film, the electrochemical and corrosion properties of the electrode, and the ability of the microorganism for the oxidation (Salam et al. 2020, Kalia and Kumar 2017). Accordingly, this difference in the values of produced current for the three electrodes is ascribed to those reasons.

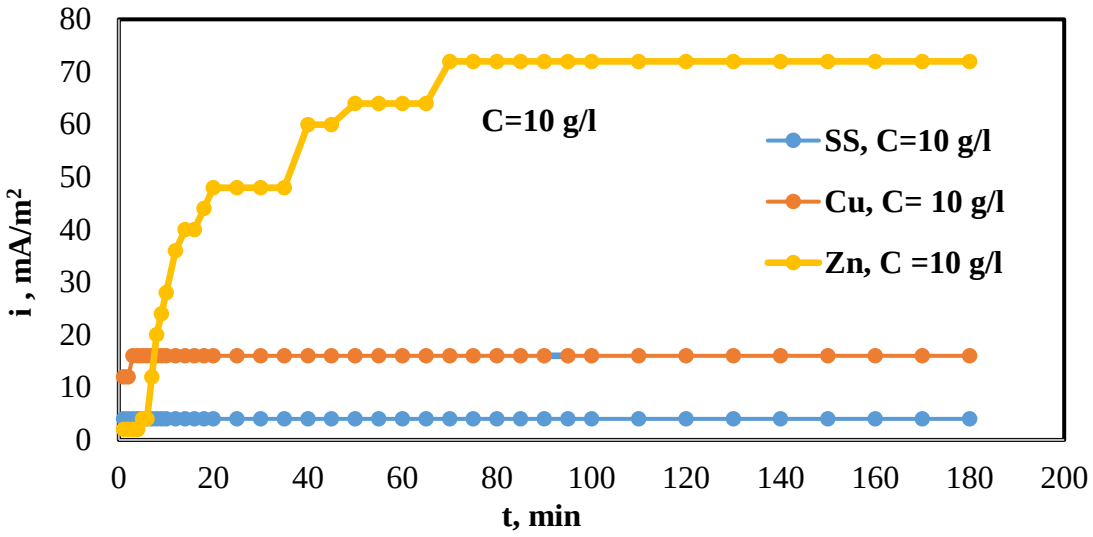

Figure 4.47 The current density for three electrodes at the microorganism's concentration of 10 g/l

4.4.2 Air pumping effect

Figure 4.48 shows a comparison between the corrosion rate of three electrodes under air pumping in the water compartment at 3g/l MO concentration. It can be seen in the presence of aeration; SS results the lowest CR and Zn results the highest for all MO concentrations (Figures A.3 and A.4).

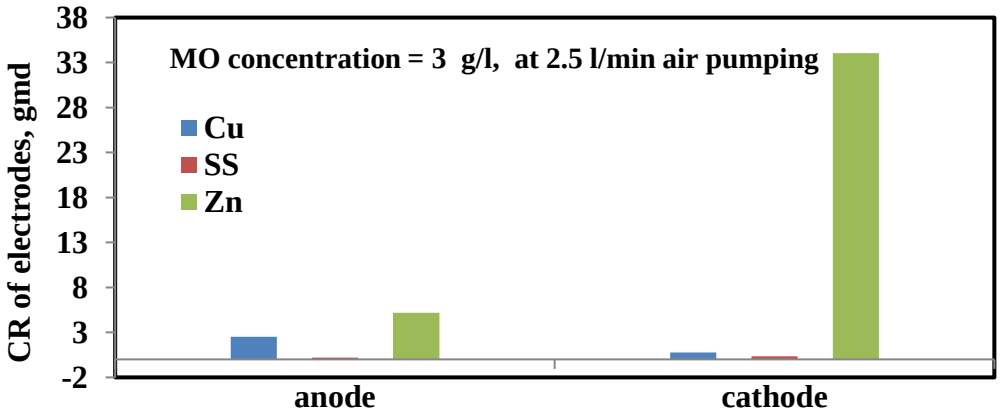

Figure 4.48 The comparison of the corrosion rate of three electrodes at 2.51 l/min of air pumping in the water compartment at 3 g/l MO concentration

4.4.3 Effect of agitation velocity

When comparing the corrosion rate of three electrodes at different agitation velocities in the water compartment according to Tables 4.4, 4.9 and 4.6, the stainless steel shows the lowest corrosion rate among the experimented electrodes for the whole range of velocities (Figure A-5 and A-6). Figure 4.49 shows the current density of Cu, SS, and Zn electrodes at the agitation velocity of 150 rpm. According to this figure, the lowest current was obtained with SS electrodes due to the low corrosion rate and the highest current was obtained with Zn electrodes due to the high corrosion rate. This difference depends on the nature of the electrode surface, its conductivity, and its porosity, as well as the corrosion of the electrode.

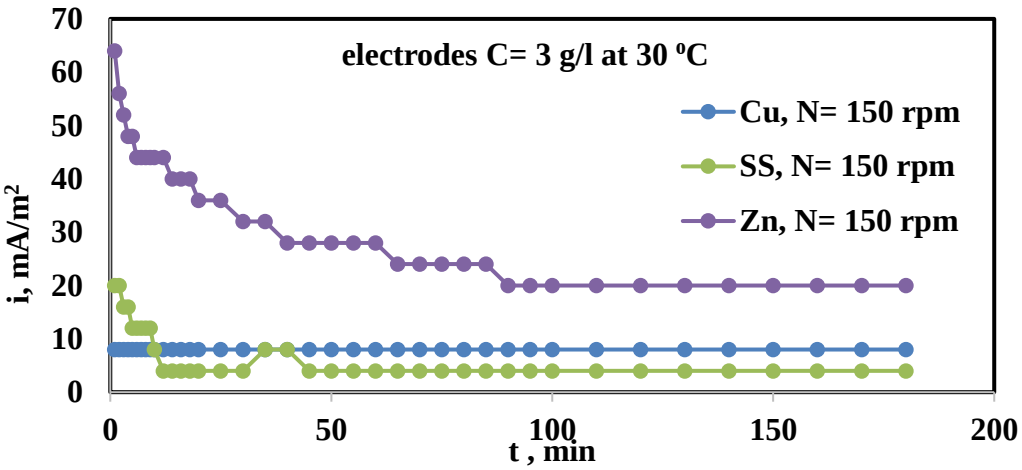

Figure 4.49 Current density vs. time for three electrodes at 150 rpm of agitation velocity and at 3 g/l of MO concentration

4.4.4 Joint effect of air pumping and flow velocity

According to Tables 4.6, 4.10 and 4.15, the stainless-steel shows low corrosion rate compared to zinc and copper electrodes at different agitation speeds. Increasing the agitation velocity (150, 300 and 450 rpm) at air pumping in the water compartment increase the corrosion rate of Cu, SS, and Zn electrodes in both compartments (anode and cathode (Figure A.7 and A.8).

5. CONCLUSIONS AND RECOMMENDATION

5.1 Conclusions

The major conclusions that are deduced from the experimental work of corrosion behavior of electrode materials (stainless steel, copper and zinc) used in microbial fuel cells (MFC) under different operating conditions are as follows:

1. The selection of the electrode material (metals properties) is crucial for the performance of MFCs in terms of corrosion resistant, bacterial adhesion, electron transfer and electrochemical efficiency. Overall, the stainless steel is a successful electrode from corrosion standpoint in MFC, but the energy generated by such electrodes is low, followed by copper.
2. Zinc is not suitable electrode to be used in MFC neither in the MO (anode) compartment nor in the water (cathode) compartment because it exhibits high corrosion rate in both compartments.
3. The microorganism concentration increases the corrosion rate of electrodes in both anode and cathode compartments in MFC due to the metabolism and concentration cell effect.
4. The biofilms that attached to the surfaces are useful for providing longer time of contact between the bacteria and surface but at the same time, it can cause a considerable corrosion rate of anode electrodes by biological corrosion.
5. The current produced in the MFC cell is a result of two contributions. Part of this current is bio-current generated by MO and part is due to the corrosion of electrodes.
6. The air pumping in the water compartment increases the corrosion rate of electrodes in both MO and water compartments and increases the cell current.
7. The agitation velocity of catholyte increases the corrosion rate of electrodes in both MO and water compartments. It increases the cell current too.
8. In general, the potential in the MO compartment is more positive than in water compartment due to the MO activity which increases the CR in this compartment and increases the cell current

9. Stainless steel and copper exhibited higher potential in both compartments (comparing with zinc electrode) leading to high corrosion resistance.
10. The zinc electrode is the best electrode in the output current but high corrosion rate was obtained according to the results.

5.2 Recommendations for Future Work

The recommendations for further investigations are as follows:

1. Investigate the corrosion rate of the SS and Cu by using another type of microorganism.
2. Extending the work to understand the mechanisms associated with corrosion of electrodes and the effect of metals ions on the microorganism's activity.
3. Study the effect temperature and salt concentrations of the corrosion rate of electrode and produced current of MFC.
4. Investigation of the effect of substrate type and concentration on the corrosion rate of electrodes.
5. Use of another method for determining the corrosion rate of electrodes in MFC such as polarization technique.

REFERENCES

Aghababaie, M., Farhadian, M., Jeihanipour, A. and Biria, D., 2015. Effective factors on the performance of microbial fuel cells in wastewater treatment–a review. Environmental Technology Reviews, 4(1), pp.71-89.

Ahmad, Z., 2006. Principles of corrosion engineering and corrosion control. Elsevier.

Babanova, S., Jones, J., Phadke, S., Lu, M., Angulo, C., Garcia, J., Carpenter, K., Cortese, R., Chen, S., Phan, T. and Bretschger, O., 2020. Continuous flow, large-scale, microbial fuel cell system for the sustained treatment of swine waste. Water Environment Research, 92(1), pp.60-72.

Baday, A.A., ElShazly, Y.M. and Nosier, S.A., 2017. Corrosion rate determination of vessel walls agitated by double impeller and gas sparging. Corrosion Reviews, 35(1), pp.53-62.

Beech, I.B. and Sunner, J., 2004. Biocorrosion: towards understanding interactions between biofilms and metals. Current opinion in Biotechnology, 15(3), pp.181-186.

Bennetto, H.P., Stirling, J.L., Tanaka, K. and Vega, C.A., 1983. Anodic reactions in microbial fuel cells. Biotechnology and bioengineering, 25(2), pp.559-568.

Bergel, A., Féron, D. and Mollica, A., 2005. Catalysis of oxygen reduction in PEM fuel cell by seawater biofilm. Electrochemistry Communications, 7(9), pp.900-904.

Bibb, M., 1985. Bacterial corrosion in the South African power industry. Biologically induced corrosion, pp.96-101.

Blatter, M., Delabays, L., Furrer, C., Huguenin, G., Cachelin, C.P. and Fischer, F., 2021. Stretched 1000-L microbial fuel cell. Journal of Power Sources, 483, p.229130.

Booth, G.H., 1964. Sulphur bacteria in relation to corrosion. Journal of Applied Bacteriology, 27(1), pp.174-181.

Borenstein, S.W., 1994. Microbiologically influenced corrosion handbook, Wood head Pub. Ltd., Cambridge.

Bouwman, L., Van Houtven, D., Pant, D., Gallego, Y.A. and Vanbroekhoven, K., Vito NV, 2020. Carbon Based Electrode with Large Geometric Dimensions. U.S. Patent Application 16/753,027.

Brennenstuhl, A.M. and Doherty, P.E., 1990. The economic impact of microbiologically influenced corrosion at Ontario Hydro s nuclear plants. Microbiologically Influenced Corrosion and Biodeterioration, University of Tennessee, Knoxville, TN, p.7.

Buyanov, V. (2011). BP: statistical review of world energy 2011. Economic Policy, 4, 38–55.

Christgen, B., 2011. Electricity generation from wastewater using microbial fuel cells: a study of electrode and membrane materials (Doctoral dissertation, Newcastle University).

Clauwaert, P., Rabaey, K., Aelterman, P., De Schamphelaire, L., Pham, T.H., Boeckx, P., Boon, N. and Verstraete, W., 2007. Biological denitrification in microbial fuel cells. Environmental science & technology, 41(9), pp.3354-3360.

Clauwaert, P., P. Aelterman, L. De Schamphelaire, M. Carballa, K. Rabaey,W. Verstraete. 2008. "Minimizing Losses in Bio Electrochemical Systems: The Road to Applications." Applied Microbiology and Biotechnology 79(6):901–913.

Coker, A.K., 2007. Ludwig's applied process design for chemical and petrochemical plants, vol. 1. GPP, Ed.) Elsevier, Oxford, United Kingdom.Kim, J. R., Cheng, S., Oh, S.-E., & Logan, B. E., 2007, Power generation using different cation, anion, and ultrafiltration membranes in microbial fuel cells. Environmental Science & Technology, 41(3), 1004–1009

Costerton, J.W. ed., 2007. The biofilm primer. Berlin, Heidelberg: Springer Berlin Heidelberg.

Çek, N., 2016. Parçacıklar ve Enerji Kaynakları. LAP LAMBERT Academic Publishing.

Dai, X., Wang, H., Ju, L.K., Cheng, G., Cong, H. and Newby, B.M.Z., 2016. Corrosion of aluminum alloy 2024 caused by Aspergillus niger. International Biodeterioration & Biodegradation, 115, pp.1-10.

Darowicki, K., Bohdanowicz, W. and Walaszkowski, J., 2001. Pro-ecological aspects of application of cathodic protection. Polish Journal of Environmental Studies, 10(5), pp.325-330..

Das, I., Ghangrekar, M.M., Satyakam, R., Srivastava, P., Khan, S. and Pandey, H.N., 2020. On-site sanitary wastewater treatment system using 720-L stacked microbial fuel cell: case study. Journal of Hazardous, Toxic, and Radioactive Waste, 24(3), p.04020025.

Deval, A. S., Parikh, H. A., Kadier, A., Chandrasekhar, K., Bhagwat, A. M., & Dikshit, A. K., 2017, Sequential microbial activities mediated bioelectricity production from distillery wastewater using bio-electrochemical system with simultaneous waste remediation. International Journal of Hydrogen Energy, 42(2), 1130–1141.

Donlan, R.M., 2002. Biofilms: microbial life on surfaces. Emerging infectious diseases, 8(9), p.881.

Drapcho, C.M., Nghim, N.P. and Walker, T., 2008. Biofuels engineering process technology. McGraw-Hill Education.

Erable, B., Féron, D., Bergel, A., 2012. Microbial catalysis of the oxygen reduction reaction for microbial fuel cells: A review. ChemSusChem, 5(6), 975-987.

Ersan, K., Irfan, A.R. and Tukek, S., 2010. Effect of humidification of gases on first home constructed PEM fuel cell stack potential. Gazi University Journal of Science, 23(1), pp.61-70.

Estrada-Arriaga, E.B., Hernández-Romano, J., García-Sánchez, L., Garcés, R.A.G., Bahena-Bahena, E.O., Guadarrama-Pérez, O. and Chavez, G.E.M., 2018. Domestic wastewater treatment and power generation in continuous flow air-

cathode stacked microbial fuel cell: effect of series and parallel configuration. Journal of environmental management, 214, pp.232-241.

Flemming, H.C., 1996. Biofouling and microbiologically influenced corrosion (MIC)-an economical and technical overview. Microbial deterioration of materials.

Fontana, M.G. and Greene, N.D., 2018. Corrosion engineering. McGraw-hill.

Fornero, J.J., Rosenbaum, M. and Angenent, L.T., 2010. Electric power generation from municipal, food, and animal wastewaters using microbial fuel cells. Electroanalysis: An International Journal Devoted to Fundamental and Practical Aspects of Electroanalysis, 22(7-8), pp.832-843.

Gadkari, S., Fontmorin, J.M., Yu, E. and Sadhukhan, J., 2020. Influence of temperature and other system parameters on microbial fuel cell performance: Numerical and experimental investigation. Chemical Engineering Journal, 388, p.124176.

Gerdon, A.E., 2020. Connecting Chemistry to Social Justice in a Seminar Course for Chemistry Majors. Journal of Chemical Education, 97(12), pp.4316-4320.

Ge, Z. and He, Z., 2016. Long-term performance of a 200-liter modularized microbial fuel cell system treating municipal wastewater: treatment, energy, and cost. Environmental Science: Water Research & Technology, 2(2), pp.274-281.

Gong, K., Wu, M., Xie, F. and Liu, G., 2020. Effect of dissolved oxygen concentration on stress corrosion cracking behavior of pre-corroded X100 steel base metal and the welded joint in wet–dry cycle conditions. Journal of Natural Gas Science and Engineering, 77, p.103264.

Gray, J.R., 2004. Conductivity analyzers and their application. Environmental instrumentation and analysis handbook, pp.491-510.

H. N. Wagh, 2017, STUDY OF EFFECT OF AGITATION BY MFC, International Journal of Advanced Research in Science and Engineering, 6(3), 591-595.

Hall-Stoodley, L., Costerton, J.W. and Stoodley, P., 2004. Bacterial biofilms: from the natural environment to infectious diseases. Nature reviews microbiology, 2(2), pp.95-108.

Hamad, M.F., Kader, H.D.A. and Hasan, B.O., 2015. Galvanic Corrosion of Carbon Steel–Copper in Aerated H2SO4 Under Agitation Conditions. corrosion and materials, 1(5), p.6.

Hamed, M. S., Majdi, H. S., & Hasan, B. O., 2020. Effect of Electrode Material and Hydrodynamics on the Produced Current in Double Chamber Microbial Fuel Cells. https://doi.org/10.1021/acsomega.9b04451.

Hamilton, W.A. 2003. Microbially influenced corrosion as a model system for the study of metal microbe interactions: a unifying electron transfer hypothesis. Biofouling, 19(1), 65-76.

Harshitha, G., Sahoo, A., & Sethy, R., 2019, Bioelectricity generation from different biomass 87 feed at anode chamber and to study process parameters in microbial fuel cells. Biocatalysis and Agricultural Biotechnology, 20(June), 101191. https://doi.org/10.1016/j.bcab.2019.101191

Hamilton, W.A., 2003. Microbially influenced corrosion as a model system for the study of metal microbe interactions: a unifying electron transfer hypothesis. Biofouling, 19(1), pp.65-76.

Hasan, B.O., 2014. Galvanic corrosion of carbon steel–brass couple in chloride containing water and the effect of different parameters. Journal of Petroleum Science and Engineering, 124, pp.137-145.

He, W.; Dong, Y.; Li, C.; Han, X.; Liu, G.; Liu, J.; Feng, Y., 2019, Field tests of cubic-meter scale microbial electrochemical system in a municipal wastewater treatment plant. Water Res, 155, 372–380.

He, Y.-R., F. Du, Y.-X. Huang, L.-M. Dai, W.-W. Li, H.-Q. Yu. 2016. "Preparation of Microvillus-like Nitrogen-Doped Carbon Nanotubes as the Cathode of a Microbial Fuel Cell." Journal of Materials Chemistry A 4(5):1632–1636.

Heidersbach, R., 2018. Metallurgy and corrosion control in oil and gas production. John Wiley & Sons

Hiegemann, H.; Littfinski, T.; Krimmler, S.; Lübken, M.; Klein, D.; Schmelz, K.-G.; Ooms, K.; Pant, D.; Wichern, M., 2019, Performance and inorganic fouling of a submergible 255 L prototype microbial fuel cell module during continuous long-term operation with real municipal wastewater under practical conditions. Bioresour. Technol. 294, 122227.

Hisham, N. S. N., S. M. Zain, S. Jusoh, N. Anuar, F. Suja, A. Ismail, N. E. A. Basri. 2013. "Microbial Fuel Cells Using Different Types of Wastewater for Electricity Generation and Simultaneously Removed Pollutant." Journal of Engineering Science and Technology 8(3):317–326. Ieropoulos, I., Greenman, J., and Melhuish, C. 2003

Hussein A. M., 2006, Corrosion under two phase flow kerosene / water simulated by turbulently agitated systems, M. Sc. Thesis, Chem. Eng. Dept, Nahrain University.

Ilhan-Sungur, E., Ozuolmez, D., Çotuk, A., Cansever, N., Muyzer, G., 2017. Isolation of a sulfide-producing bacterial consortium from cooling-tower water: evaluation of corrosive effects on galvanized steel. Anaerobe 43, 27–34.

Ilhan-Sungur, E., Unsal-Istek, T., Cansever, N., 2015. Microbiologically influenced corrosion of galvanized steel by Desulfovibrio sp. and Desulfosporosinus sp. in the presence of Ag–Cu ions. Mater. Chem. Phys. 162, 839–851.

Israa K Abdul-Wahid, Saleem M Obyed, Basim O Hasan, 2020, The Use of Different Electrode Materials for Electricity Production in a Microbial Fuel Cell Using a Klebsiella oxytoca Microorganism Under Different Operating Conditions, Recent Innovations in Chemical Engineering, 14, 3 (246-258).

Jack, R.F.; Ringelberg, D.B.; White, D.C., 1992 Differential corrosion rates of carbin steel by combinations of Bacillus sp., Hafnia alvei, and Desulfovibrio gigas established by phospholipid analysis of electrode biofilm. Corr. Sci., 33: 1843-1853.

Jia, R., Unsal, T., Xu, D., Lekbach, Y. and Gu, T., 2019. Microbiologically influenced corrosion and current mitigation strategies: a state of the art review. International biodeterioration & biodegradation, 137, pp.42-58.

Jones-Meehan, J.; Walch, M.; Little, B.J.; Ray, R.I.; Mansfeld, F.B., 1994, Biofouling and Biocorrosion in Industrial Water Systems. Lewis, Boca Raton, Fla., p. 107.

Juzeliūnas, E., Ramanauskas, R., Lugauskas, A., Leinartas, K., Samulevičienė, M., Sudavičius, A., Juškėnas, R., 2007. Microbially influenced corrosion of zinc and aluminium – two-year subjection to influence of Aspergillus niger. Corrosion Sci. 49,4098–4112.

Kakooei, S., Ismail, M.C., Ariwahjoedi, B. 2012. Mechanisms of Microbiologically Influenced Corrosion: A Review. World Applied Sciences Journal, 17(4), 524-531.

Kalia, V. C., & Kumar, P. , 2017, Microbial applications. In Microbial Applications (Issue October). https://doi.org/10.1007/978-3-319-52666-9.

Karmakar, M. and Ray, R.R., 2011. Current trends in research and application of microbial cellulases. Research Journal of Microbiology, 6(1), p.41.

Karra, U., Manickam, S. S., McCutcheon, J. R., Patel, N., Li, B., 2013, "Power generation and organics removal from wastewater using activated carbon nanofiber (ACNF) microbial fuel cells (MFCs)", International Journal of Hydrogen Energy, 38: 1588-1597.

Kato Marcus, A., C. I. Torres, B. E. Rittmann. 2007. "Conduction-based Modeling of the Biofilm Anode of a Microbial Fuel Cell." Biotechnology and Bioengineering 98(6):1171–1182.

Kumar, R., Singh, L., Wahid, Z.A. and Din, M.F.M., 2015. Exoelectrogens in microbial fuel cells toward bioelectricity generation: a review. International Journal of Energy Research, 39(8), pp.1048-1067.

Kim, Jong Jip, and Yu Mi Young., 2013, "Study on the passive film of type 316 stainless steel." Int. J. Electrochem. Sci 8.10: 11847-11859.

Kryachko, Y., Hemmingsen, S.M., 2017. The role of localized acidity generation in microbially influenced corrosion. Curr. Microbiol. 74, 870–876.

Lee, H., Seo, J., Kim, M.S., Lee, C., 2017. Inactivation of biofilms on RO membranes by copper ion in combination with norspermidine. Desalination 424, 95–101

Liang, P.; Duan, R.; Jiang, Y.; Zhang, X.; Qiu, Y.; Huang, X., 2018, One-year operation of 1000-L modularized microbial fuel cell for municipal wastewater treatment. Water Res. , 141, 1–8.

Little, B.; Wagner P., 1994, Indicators for sulfate-reducing bacterium microbiologially influenced corrosion. In: G.G. Geesey, Z. Lewandowski and H.C. Flemming (eds.) Biofouling and Biocorrosion in Industrial Water Systems, 2nd ed, CRC Press Inc., Boca Raton, FL, , pp. 213-230.

Logan, B. E., Hamelers, B., Rozendal, R., Schröder, U., Keller, J., Freguia, S., Aelterman, P., Verstraete, W., & Rabaey, K. 2006, Microbial fuel cells:

methodology and technology. Environmental Science & Technology, 40(17), 5181–5192.

Logan, B. E., Regan, J. M. 2006. “Electricity-Producing Bacterial Communities in Microbial Fuel Cells.” TRENDS in Microbiology 14(12):512–518

Logan, B.E., 2010, Scaling up microbial fuel cells and other bioelectrochemical systems. Appl. Microbiol. Biotechnol. 85(6), 1665.

Lu, M.; Chen, S.; Babanova, S.; Phadke, S.; Salvacion, M.; Mirhosseini, A.; Chan, S.; Carpenter, K.; Cortese, R.; Bretschger, O. , 2017, Long-term performance of a 20-L continuous flow microbial fuel cell for treatment of brewery wastewater. J. Power Sources, 356, 274–287.

Lyon W., 1996, “Standard Handbook of Petroleum and Natural Gas Engineering”, vol.1, Gulf Company, Houston, Texas.

Mahato, B. K., C. Y. Cha, L. W. Shemilt. 1980. “Unsteady State Mass Transfer Coefficients Controlling Steel Pipe Corrosion under Isothermal Flow Conditions.” Corrosion Science 20(3):421–441

Manam, N.S., Harun, W.S.W., Shri, D.N.A., Ghani, S.A.C., Kurniawan, T., Ismail, M.H., Ibrahim, M.H.I., 2017. Study of corrosion in biocompatible metals for implants: a review. J. Alloy. Comp. 701, 698–715.

Mand, J., Park, H.S., Jack, T.R., Voordouw, G. 2014. The role of acetogens in microbial influenced corrosion of steel. Frontiers in Microbiology, 5.

Marwa E.M. Ali and Basim O. Hasan, 2020, Galvanic corrosion of carbon steel under concentration cell formation in MgCl2 solution as an inorganic pollutant and the effect of flow velocity, Corros Rev, 38(3): 287–298.

Marwa S. Hamed, Hasan Sh. Majdi, and Basim O. Hasan,2020, Effect of Electrode Material and Hydrodynamics on the Produced Current in Double Chamber Microbial Fuel Cells ACS Omega **,** 5 (18), 10339-10348.

Mashkour, M., & Rahimnejad, M., 2015, Effect of various carbon-based cathode electrodes on the performance of microbial fuel cell. Biofuel Res. J, 2(4), 296–300.

Melchers, R. E., 2005, "The Effect of Corrosion on the structure reliability of Steel Offshore Structures", Corrosion Science, Vol. 47, No.10, Pp.2391-2410, 2005.

MIN, M. A., Chala, G. T., & Saravanan, R., 2018. Influence of Aluminum Mesh electrode on Performance of a Microbial Fuel Cell (MFC). International Journal of Engineering and Technology, 7(3), 176-180.

Mohan, S. V., & Chandrasekhar, K., 2011a, Self-induced bio-potential and graphite electron accepting conditions enhances petroleum sludge degradation in bio-electrochemical system with simultaneous power generation. Bioresource Technology, 102(20), 9532– 9541.

Mohan, S. V., & Chandrasekhar, K., 2011b. Solid phase microbial fuel cell (SMFC) for harnessing bioelectricity from composite food waste fermentation: influence of electrode assembly and buffering capacity. Bioresource Technology, 102(14), 7077–7085.

Mook, W.T., Chakrabarti, M.H., Aroua, M.K., Khan, G.M.A., Ali, B.S., Islam, M.S. and Hassan, M.A., 2012. Removal of total ammonia nitrogen (TAN), nitrate and total organic carbon (TOC) from aquaculture wastewater using electrochemical technology: a review. Desalination, 285, pp.1-13.

Muhammad Waqas, Mohammad Rehan, Asad S. Aburiazaiza, Abdul-Sattar Nizami, 2018, Chapter 17 - Wastewater Biorefinery Based on the Microbial Electrolysis Cell: Opportunities and Challenges Progress and Recent Trends in Microbial Fuel Cells, Elsevier,2018, Pages 347-374,

Musa A. Y., A. A. H. Kadhum, A. B. Mohamad, M. S. Takriff, S. K. Kamarudin, and A. R. Daud, 2011, "Determination of Mild Steel Corrosion Rate under Turbulent Flow in Highly Acidic Solution", journal of applied science, No.13, vol. 11, pp.2464-2466.

Natarajan, D., Van Nguyen, T., 2004, Effect of electrode configuration and electronic conductivity on current density distribution measurements in PEM fuel cells. J. Power Sources 135(1), 95.

Nicole Kareta, 2022, Zinc for Corrosion Protection, spotlight metals, (https://www.spotlightmetal.com/zinc-for-corrosion-protection-a-931563/)

Norsworthy, R., 2014. Understanding corrosion in underground pipelines: basic principles. In Underground Pipeline Corrosion (pp. 3-34). Woodhead Publishing.

Nurettin, Ç. E. K. , 2017. Examination of zinc electrode performance in microbial fuel cells. Gazi University Journal of Science, 30(4), 395-402.

Ogugbue, C. J., E. E. Ebode, S. Leera. 2015. "Electricity Generation from Swine Wastewater Using Microbial Fuel Cell." Journal of Ecological Engineering 16(5).

Oliveira, V., Carvalho, T., Melo, L., Pinto, A., & Simões, M., 2016, Effects of hydrodynamic stress and feed rate on the performance of a microbial fuel cell. Environmental Engineering and Management Journal, 15(11), 2497–2504. https://doi.org/10.30638/eemj.2016.273

Pant, D., Singh, A., Van Bogaert, G., Olsen, S. I., Nigam, P. S., Diels, L., & Vanbroekhoven, K., 2012. Bioelectrochemical systems (BES) for sustainable energy production and product recovery from organic wastes and industrial wastewaters. Rsc Advances, 2(4), 1248–1263.

Potter, M. C., 1911. "Electrical Effects Accompanying the Decomposition of Organic Compounds." Proceedings of the Royal Society of London. Series B, Containing Papers of a Biological Character 84(571):260–276.

Poulson B.,1993, "Advances in Understanding Hydrodynamic Effect on Corrosion", Corrosion Science, No.1- 4, vol.35, pp.655-665.

R. N. Miller, W. C. Herron, A. G. Krigens, J. L. Cameron, and B. M. Terry, 1964, Microorganisms Cause Corrosion in Aircraft Fuel Tanks, Mater. Protect. 3(9), 60-67.

Rabaey, K., Boon, N., Siciliano, S. D., Verhaege, M., & Verstraete, W. (2004). Biofuel cells select for microbial consortia that self-mediate electron transfer. Appl. Environ. Microbiol., 70(9), 5373–5382.

Rahimnejad, M., A. Adhami, S. Darvari, A. Zirepour, S.-E. Oh. 2015. "Microbial Fuel Cell as New Technology for Bioelectricity Generation: A Review." Alexandria Engineering Journal 54(3):745–756.

Revie R.W. and H. H. Uhlig, 2008, "Corrosion and Corrosion Control an Introduction to Corrosion Science and Engineering" fourth edition, John Wiley & Sons, Inc., Hoboken New Jersey.

Revie, R.W. ed., 2011. Uhlig's corrosion handbook (Vol. 51). John Wiley & Sons.

Rhoads, A., Beyenal, H. and Lewandowski, Z., 2005. Microbial fuel cell using anaerobic respiration as an anodic reaction and biomineralized manganese as a cathodic reactant. Environmental science & technology, 39(12), pp.4666-4671.

Rismani-Yazdi, H., Carver, S.M., Christy, A.D., Tuovinen, O.H.: , 2008, Cathodic limitations in microbial fuel cells: an overview.J. Power Sources 180(2), 683 .

Richard A. Hays, , 2021, for the Director, Corrosion Policy & Oversight (DCPO), (DASD) [Materiel Readiness].

Robert G., Kelly and J. R. Scully, D. W. Shoesmith, and R. G. Buchheit, 2003, "Electrochemical Techniques in Corrosion Science and Engineering", Marcel Dekker, Inc. New York.

Roberge, P.R., 2019. Handbook of corrosion engineering. McGraw-Hill Education.

Rossi, R.; Jones, D.; Myung, J.; Zikmund, E.; Yang, W.; Gallego, Y.A.; Pant, D.; Evans, P.J.; Page, M.A.; Cropek, D.M, 2019, Evaluating a multi-panel air cathode through electrochemical and biotic tests. Water Res. , 148, 51–59

Santoro, C., Guilizzoni, M., Correa Baena, J. P., Pasaogullari, U., Casalegno, A., Li, B., Babanova, S., Artyushkova, K., & Atanassov, P. , 2014. The effects of carbon electrode surface properties on bacteria attachment and start up time of microbial fuel cells. Carbon, 67, 128–139. https://doi.org/10.1016/j.carbon.2013.09.071

Schuster, S.M., 2009. Biotechnology: Applying the genetic revolution by David P. Clark and Nanette J. Pazdernik.

Scotto, V., and M. E. Lai. 2016, "The ennoblement of stainless steels in seawater: a likely explanation coming from the field." Corrosion science 40.6 (1998): 1007-1018.

Sengodu, P. and Deshmukh, A.D., 2015. Conducting polymers and their inorganic composites for advanced Li-ion batteries: a review. RSC advances, 5(52), pp.42109-42130.

Shripad T. Revankar, Pradip Majumdar , 2014 ,Fuel Cells: Principles, Design, and Analysis, Book.

Tao, Q., Luo, J., Zhou, J., Zhou, S., Liu, G., & Zhang, R., 2014, . Effect of dissolved oxygen on nitrogen and phosphorus removal and electricity production in

microbial fuel cell. Bioresource Technology, 164, 402–407. https://doi.org/10.1016/j.biortech.2014.05.002

U. R. Evans, The Corrosion and Oxidation of Metals, Edward Arnold, London (1960).

Uhlig HH., 2011, The corrosion handbook, 3rd ed., New York: John Wiley and Sons.

Usher, K.M., Kaksonen, A.H., Cole, I., Marney, D., 2014. Critical review: microbially influenced corrosion of buried carbon steel pipes. Int. Biodeterior. Biodegrad. 93,84–106

Vânia B. Oliveira, Joana Vilas Boas, Alexandra M.F.R. Pinto,, 2018, Chapter 15 - Kinetics and Mass Transfer Within Microbial Fuel Cells,,Progress and Recent Trends in Microbial Fuel Cells, Elsevier, Pages 313-326,

Vasconcelos JMT, Alves SS, Barata JM., 1995, Mixing in gas-liquid contactors agitated by multiple turbines. Chem Eng Sci; 50: 2343–2354.

Veerachamy, S., Yarlagadda, T., Manivasagam, G. and Yarlagadda, P.K., 2014. Bacterial adherence and biofilm formation on medical implants: a review. Proceedings of the Institution of Mechanical Engineers, Part H: Journal of Engineering in Medicine, 228(10), pp.1083-1099.

Venzlaff, H., Enning, D., Srinivasan, J., Mayrhofer, K.J.J., Hassel, A.W., Widdel, F., Stratmann, M. 2013. Accelerated cathodic reaction in microbial corrosion of iron due to direct electron uptake by sulfate-reducing bacteria. Corrosion Science, 66(0),88-96.

Venkata Mohan, S.; Velvizhi, G.; Vamshi Krishna, K.; Lenin Babu, M., 2014, Microbial catalyzed electrochemical systems: A bio-factory with multi-facet applications. Bioresour. Technol. 165, 355–364

Vilajeliu-Pons, A.; Puig, S.; Salcedo-Dávila, I.; Balaguer, M.; 2017, Colprim, J. Long-term assessment of six-stacked scaled-up MFCs treating swine manure with different electrode materials. Environ. Sci. Water Res. Technol., 3, 947–959.

Vroom, J.M., Grauw, K.J.D., Gerritsen, H.C., Bradshaw, D.J., Marsh, P.D., Watson, G.K., Birmingham, J.J., Allison, C., 1999. Depth penetration and detection of pH gradients in biofilms by two-photon excitation microscopy. Appl. Environ. Microbiol. 65, 3502–3511.

Wang, A.-J.; Wang, H.-C.; Cheng, H.-Y.; Liang, B.; Liu, W.-Z.; Han, J.-L.; Zhang, B.; Wang, S.-S., 2020, Electrochemistry-stimulated environmental bioremediation: Development of applicable modular electrode and system scale-up. Environ. Sci. Ecotechnol. , 3, 100050.

Wang, H.Y., Bernarda, A., Huang, C.Y., Lee, D.J., Chang, J.S., 2011, Micro-sized microbial fuel cell: a mini-review. Bioresour.Technol. 102(1), 235.

Warren P. Iverson., Microbial Corrosion of Metals. 2008.

Winston Revie, R., H. H. Uhlig. 2008. “Corrosion and Corrosion Control: An Introduction to Corrosion Science and Engineering.” :28–34.

Wu, S.; Li, H.; Zhou, X.; Liang, P.; Zhang, X.; Jiang, Y.; Huang, X. , 2016, A novel pilot-scale stacked microbial fuel cell for efficient electricity generation and wastewater treatment. Water Res. , 98, 396–403.

Xu, D., Gu, T., 2014. Carbon source starvation triggered more aggressive corrosion against carbon steel by the Desulfovibrio vulgaris biofilm. Int. Biodeterior. Biodegrad. 91, 74–81

Xu, D., Jia, R., Li, Y., Gu, T., 2017a. Advances in the treatment of problematic industrial biofilms. World J. Microbiol. Biotechnol. 33, 97.

Xu, D., Li, Y., Gu, T., 2012a. A synergistic D-tyrosine and tetrakis hydroxymethyl phosphonium sulfate biocide combination for the mitigation of an SRB biofilm. World J. Microbiol. Biotechnol. 28, 3067–3074.

Xu, D., Li, Y., Gu, T., 2016. Mechanistic modeling of biocorrosion caused by biofilms of sulfate reducing bacteria and acid producing bacteria. Bioelectrochemistry 110,52–58

Yang, J., Yang, H., Yu, H., Wang, W., Zeng, X. 2017, "Corrosion Behavior of Additive Manufactured Ti-6Al-4V Alloy in NaCl Solution", Metallurgical and Materials Transactions A, 48: 3583-3593.

Yu, Z., Zhang, J., Zhao, X., Zhao, X., Duan, J., Song, X. , 2014, "Effects of Microorganism on Corrosion Performance of Zinc in Natural Seawater", International Journal of Electrochemical Science, 9: 7587-7595.

Yuvraj C, Aranganathan V. , 2017, MFC—an approach in enhancing electricity generation using electroactive biofilm of dissimilatory iron-reducing (DIR) Bacteria. Arabian J Sci Eng. 2017; 42:2341–7.

Zhang, Y., Liu, M., Zhou, M., Yang, H., Liang, L. and Gu, T., 2019. Microbial fuel cell hybrid systems for wastewater treatment and bioenergy production: synergistic effects, mechanisms and challenges. Renewable and Sustainable Energy Reviews, 103, pp.13-29.

Zhou, E., Li, H., Yang, C., Wang, J., Xu, D., Zhang, D., Gu, T., 2018. Accelerated corrosion of 2304 duplex stainless steel by marine Pseudomonas aeruginosa biofilm. Int. Biodeterior. Biodegrad. 127, 1–9.

Zhou, M., Yang, J., Wang, H., Jin, T., Hassett, D.J. and Gu, T., 2014. Bioelectrochemistry of microbial fuel cells and their potential applications in bioenergy. Bioenergy Research: Advances and Applications, pp.131-152.

Zuo, R. "Biofilms: strategies for metal corrosion inhibition employing microorganisms", Applied Microbiology and Biotechnology, 76: 1245-1253, (2007).

Zvandasara, T., 2010. Influence of hydrodynamics on carbon steel erosion-corrosion and inhibitor efficiency in simulated oilfield brines (Doctoral dissertation, University of Glasgow).

APPENDIX

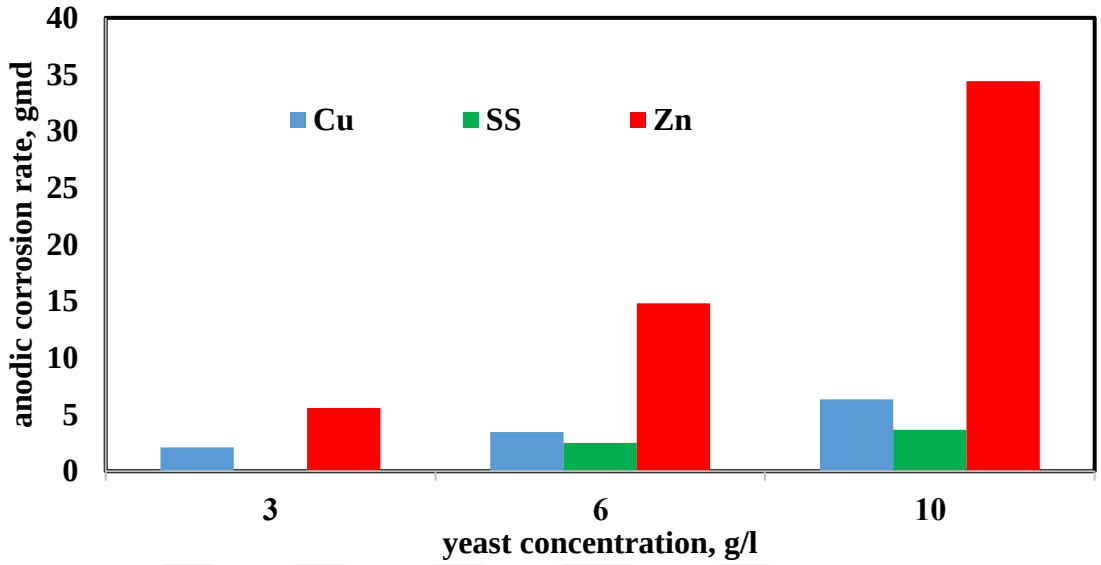

The value of corrosion rate of electrodes at different MO concentrations in anode chamber

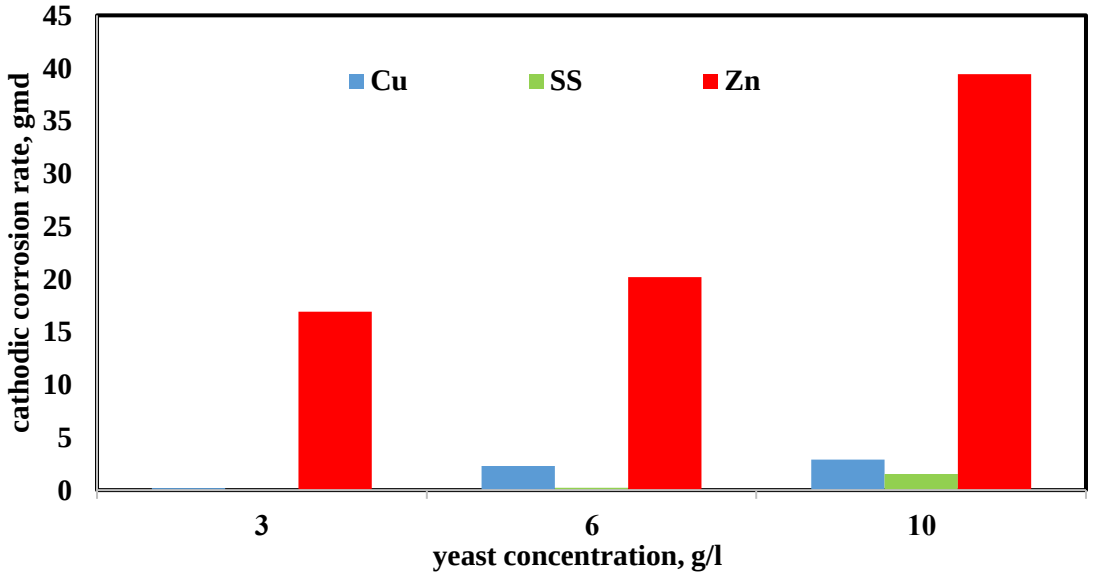

The value of corrosion rate of electrodes in cathode chamber at different MO concentrations

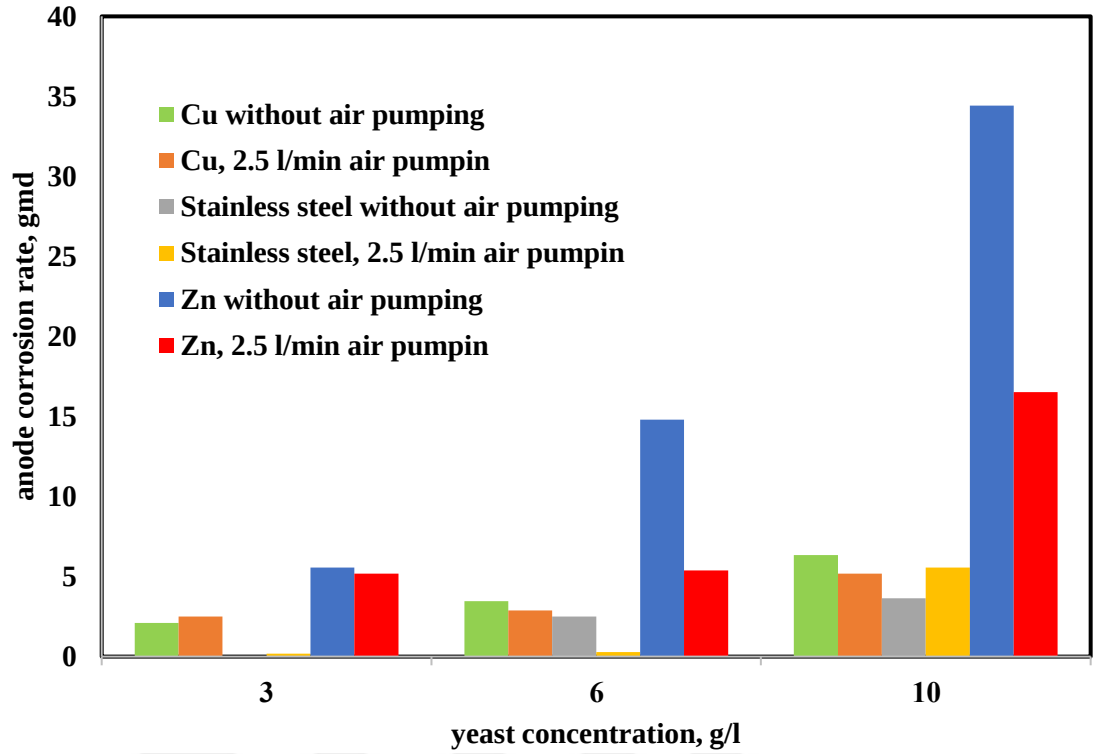

The value of corrosion rate of electrodes in the anode compartment at air pumping into the cathode chamber with different MO concentrations

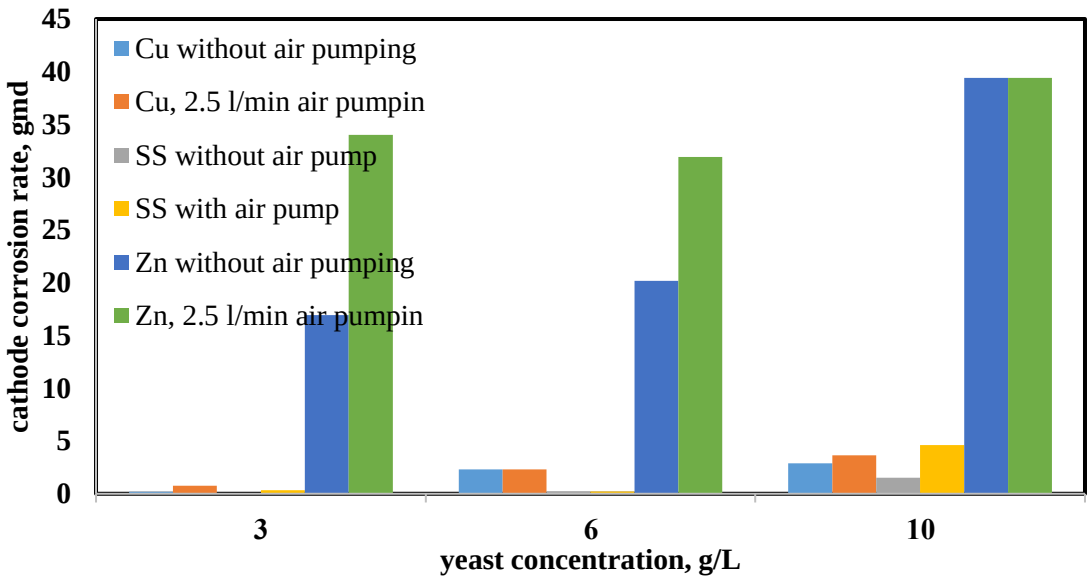

The value of corrosion rate of electrodes in the cathode compartment at air pumping into the cathode chamber with different MO concentrations

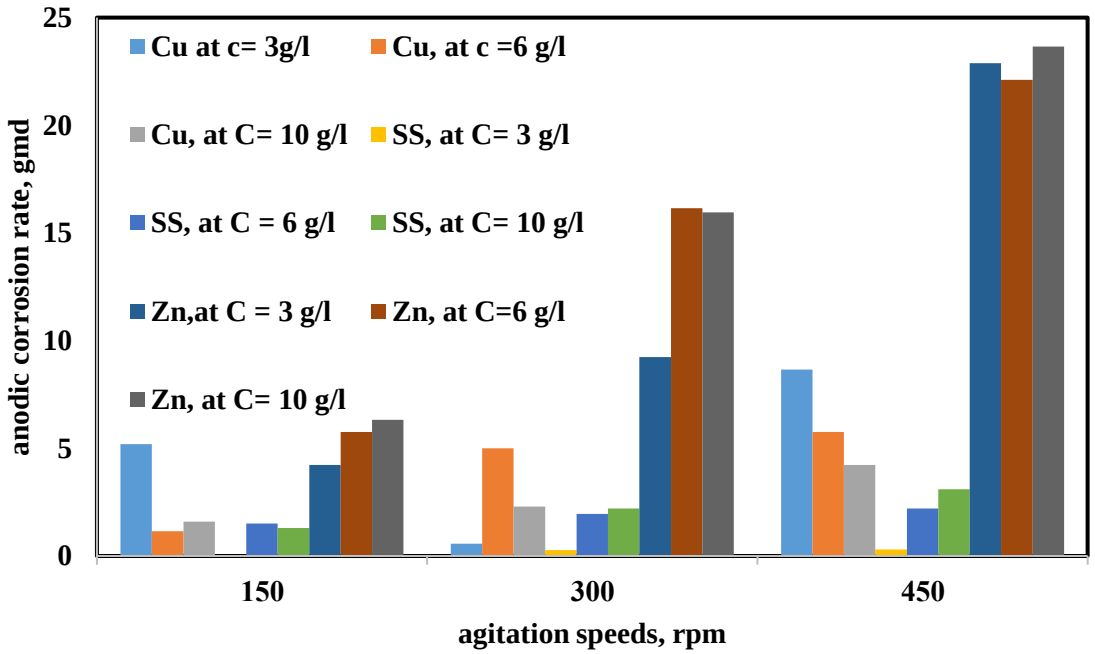

The value of corrosion rate of electrodes in the anode compartment at different agitation speeds in the cathode chamber with different MO concentrations

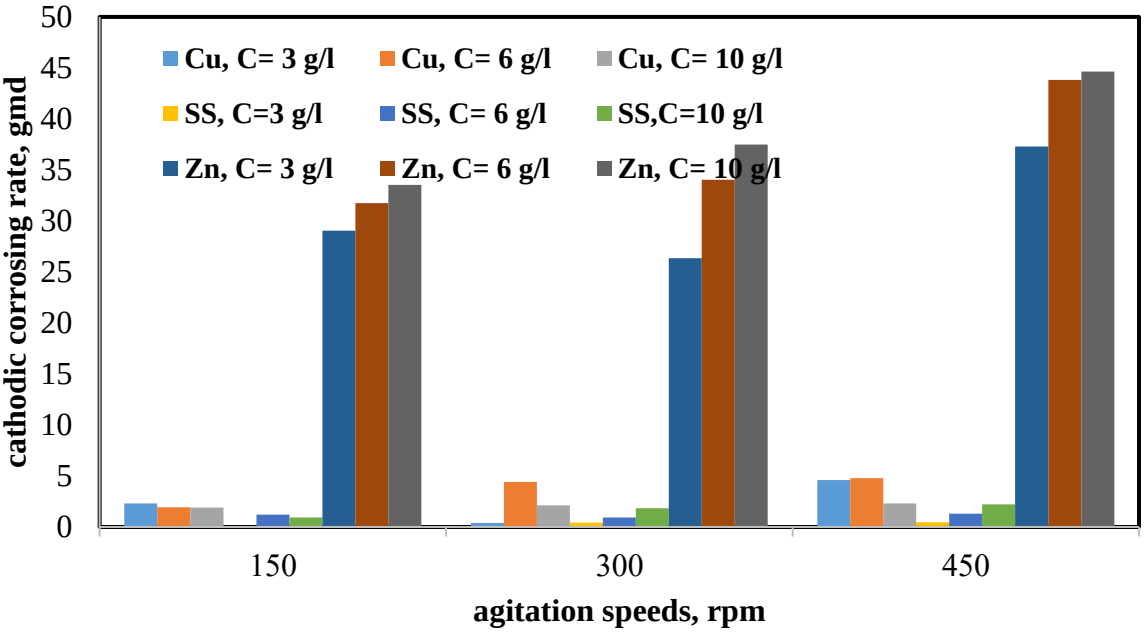

The value of corrosion rate of electrodes in the cathode compartment at different agitation speeds in the cathode chamber with different MO concentrations

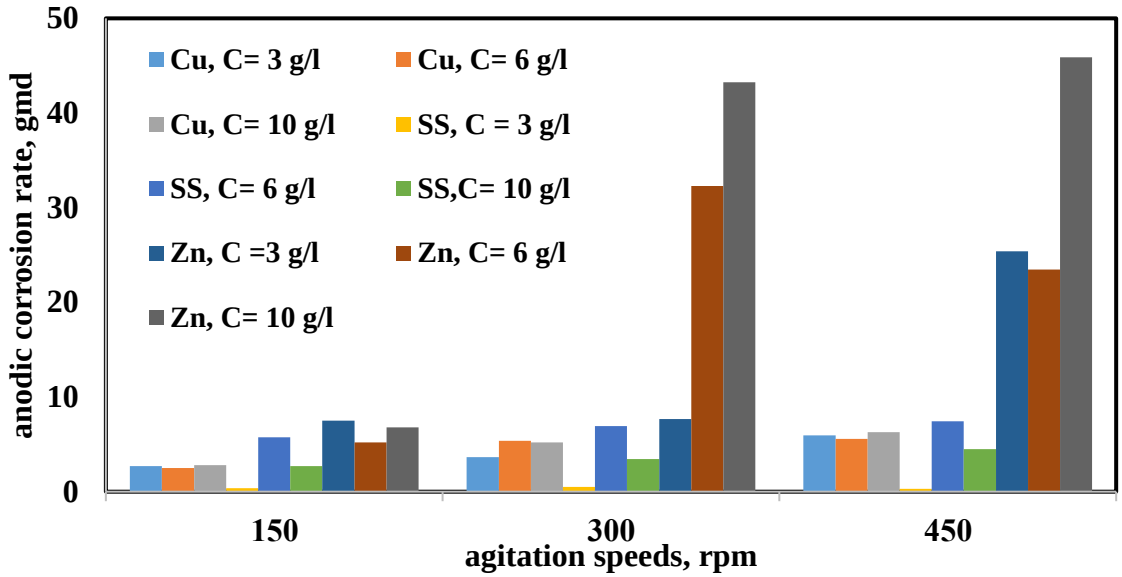

The value of corrosion rate of electrodes in the anode compartment at different agitation speeds and air pumping in the cathode chamber with different MO concentrations

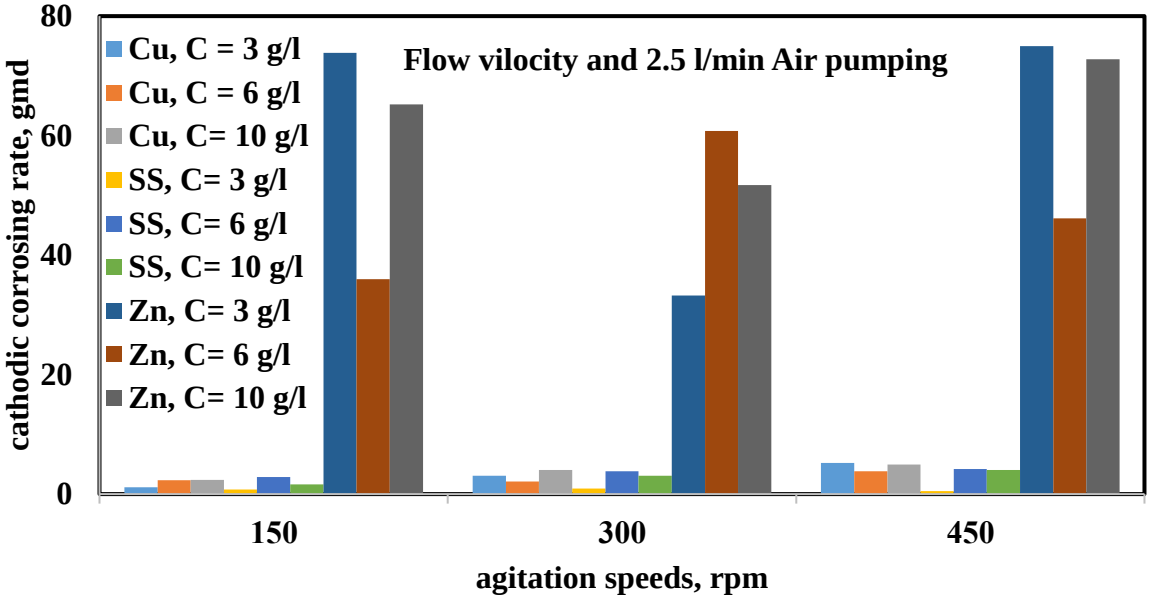

The value of corrosion rate of electrodes in the cathode compartment at different agitation speeds and air pumping in the cathode chamber with different MO concentrations